Environmental Science & Technology

pubs.acs.org/est

Article

Toxicological Mechanism of Individual Susceptibility to Formaldehyde-Induced Respiratory Effects

Mingming Tian, Pu Xia, Lu Yan, Xiao Gou, John P. Giesy, Jiayin Dai, Hongxia Yu, and Xiaowei Zhang*

Cite This: https://doi.org/10.1021/acs.est.1c07945

Read Online

ACCESS | Metrics & More | Article Recommendations | Supporting Information

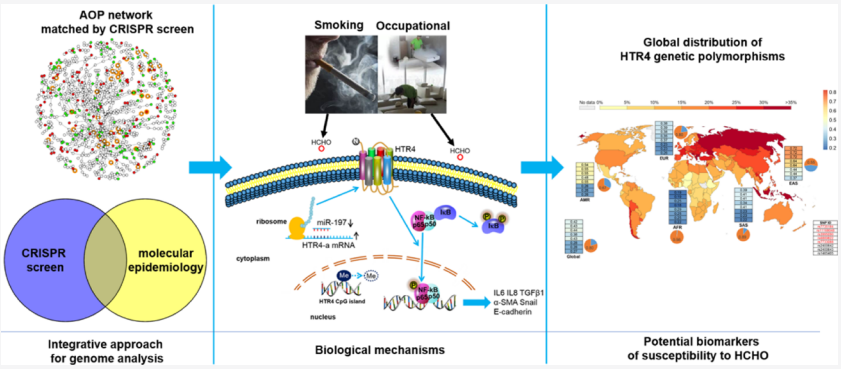

ABSTRACT: Understanding the mechanisms of individual susceptibility to exposure to environmental pollutants has been a challenge in health risk assessment. Here, an integrated approach combining a CRISPR screen in human cells and epidemiological analysis was developed to identify the individual susceptibility to the adverse health effects of air pollutants by taking formaldehyde (FA) and the associated chronic obstructive pulmonary disease (COPD) as a case study. Among the primary hits of CRISPR screening of FA in human A549 cells, HTR4 was the only gene genetically associated with COPD susceptibility in global populations. However, the association between HTR4 and FA-induced respiratory toxicity is unknown in the literature. Adverse outcome pathway (AOP) network analysis of CRISPR screen hits provided a potential mechanistic link between activation of HTR4 (molecular initiating event) and FA-induced lung injury (adverse outcome). Systematic toxicology tests (in vitro and animal experiments) were conducted to reveal the HTR4-involved biological mechanisms underlying the susceptibility to adverse health effects of FA. Functionality and enhanced expression of HTR4 were required for susceptibility to FA-induced lung injury, and FA-induced epigenetic changes could result in enhanced expression of HTR4. Specific epigenetic and genetic characteristics of HTR4 were associated with the progression and prevalence of COPD, respectively, and these genetic risk factors for COPD could be potential biomarkers of individual susceptibility to adverse respiratory effects of FA. These biomarkers could be of great significance for defining subpopulations susceptible to exposure to FA and reducing uncertainty in the next-generation health risk assessment of air pollutants. Our study delineated a novel toxicological pathway mediated by HTR4 in FA-induced lung injury, which could provide a mechanistic understanding of the potential biomarkers of individual susceptibility to adverse respiratory effects of FA.

KEYWORDS: *CRISPR screen, formaldehyde, lung injury, COPD, genetic susceptibility, air pollutants, AOP network*

INTRODUCTION

Understanding the biological mechanisms underlying individual susceptibility to chemical exposure is the foundation of accurate assessments of health risks.[1−3] Heterogeneity in the individual responses to adverse effects of pollutants can bring uncertainty in the current risk assessment.[2,3] It has long been recognized that certain subpopulations are more susceptible to adverse health outcomes than others, and genetic variations could contribute to a significant portion of susceptibility variability.[1,2,4] Many genetic variations in environmentally responsive genes can influence the toxicokinetics or toxicodynamics of toxic chemicals and thus confer resistance or susceptibility to adverse effects of toxic pollutants.[3,5] It is essential to identify susceptible subpopulations to reduce uncertainty and utilize individualistic benchmark values that are protective and beneficial to achieve the next-generation risk assessment of chemical exposure.[3,4] However, current knowledge of the biological mechanisms underlying the genetic susceptibility to environmental pollutants

Received: December 6, 2021
Revised: April 7, 2022
Accepted: April 7, 2022

is still very limited for the identification of susceptible subpopulations.[1,2,4]

Integrated approaches for genome analysis are required to uncover the molecular mechanisms underlying the genetic susceptibility to adverse effects of toxic pollutants.[4,6] Conventional approaches of molecular epidemiology, such as genome-wide association studies, can demonstrate associations between diseases and genetic variations.[7,8] However, due to a lack of mechanistic evidence, these approaches may fail to identify key genetic variations, which can determine the susceptibility of individual humans to adverse effects of pollutants.[2,8,9] Functional genomic approaches, such as CRISPR screening, can reveal the direct links between a specific gene and the corresponding loss of function, which confers resistance or susceptibility to chemical exposure.[2,10] By measuring the abundance of single-gene knockout cells exposed to toxic chemicals, specific genes whose loss of functions facilitate cellular resistance or susceptibility to toxic effects can be screened out in the CRISPR screen. Therefore, the key genes involved in the susceptibility to adverse effects of pollutants could be identified by the CRISPR screening approach. Here, we proposed that an integrated approach combining CRISPR screening and molecular epidemiology analysis could provide a mechanistic understanding of the genetic susceptibility of individual humans to adverse effects of toxicant pollutants.[1,4,6]

Air pollutants are important environmental risk factors for adverse health outcomes in the human respiratory system, such as cigarette smoke for chronic obstructive pulmonary disease (COPD) and PM2.5 for asthma.[9,11] Formaldehyde (FA) is a widespread air pollutant that can be detected in both indoor[12,13] and outdoor[12] air. Due to volatilization from manufactured products, including flooring and furniture, greater concentrations of FA can occur in indoor environments, especially in some occupational environments.[13,14] Great concentrations of FA also exist in tobacco smoke, and thus, smokers are the subpopulations who suffer from exposure to high doses of FA.[15−17] Exposure to FA was shown to result in inflammatory and fibrotic responses in the lung airways of mice and humans[18−21] and airway hyperresponsiveness in human bronchi.[22,23] However, the biological mechanism underlying the genetic susceptibility to FA-induced lung injury is unclear. Although associations between genetic variations and heterogeneity in the responses of individuals to FA have been observed in some epidemiologic studies, the mechanisms underlying the linkages are poorly understood.[22,24] In addition, exposure to FA via inhalation increased the risk of COPD,[12,21,23,25−29] especially for occupational exposure.[25−27] For example, it has been previously shown that occupational exposure to FA could lead to chronic bronchitis, which is a progressional stage of COPD.[25−27,29] Approximately 600 million people suffer from COPD globally,[11] and the pathological features of COPD are similar to those of FA-induced lung injury, including inflammation of lung airways, fibrosis of airway walls, and severe airflow obstruction.[11,30] Here, we hypothesized that susceptibility to injury of lung tissue due to exposure to FA was related to specific genetic risk factors of COPD.[1,24]

Here, we developed a novel research strategy integrating genome analysis and molecular epidemiology analysis to identify the toxicological molecular mechanism of an air pollutant FA, which could explain the genetic susceptibility to adverse health outcomes in the human population. Specifically, a CRISPR screen in human pulmonary alveolar epithelial cells (A549 cells) was combined with molecular epidemiology analysis to identify the primary genetic factors that were involved in the vulnerability of A549 cells to adverse respiratory effects of FA. Adverse outcome pathway (AOP) network analysis of CRISPR screen hits provided mechanistic links between the primary genetic factors (molecular events) and FA-induced adverse health outcomes.[31,32] Subsequently, systematic toxicological tests (in vitro cellular tests of cytotoxicity, inflammation and fibrotic effects, and epigenetic regulation; mice lung functional and pathological tests) were performed to provide a mechanistic understanding of the primary genetic factors required to facilitate susceptibility to FA-induced lung injury. Finally, the present study also provided specific genetic risk factors for COPD as potential biomarkers for individual susceptibility to lung injury caused by exposure to FA.

METHODS

Cell Culture, Cellular Viability, and Glutathione Assay. Human type II pulmonary alveolar epithelial A549 cells (ATCC, Manassas, VA) were maintained in Dulbecco's modified Eagle's medium (DMEM, Gibco) supplemented with 10% fetal bovine serum (Gibco) in a humidified atmosphere of 5% CO_2 at 37 °C. HTR4 knockout (KO) A549 cells, HTR4 overexpression (OV) A549 cells, and wild-type (WT) A549 cells transfected with nontargeting (NT) sgRNA or empty vector (EV) of pLenti-puro plasmid (GeneScript; the detailed methods for creation of these cell lines are available in the Supporting Information) were also maintained in the same culture conditions as that of wild-type A549 cells. A549 cells were seeded into 96-well plates at a density of 1×10^4 cells per well. After attachment for 24 h, cells were treated with 4800, 2400, 1200, 600, 300, 150, and 0 μM formaldehyde (FA, Sigma) for another 24 h. To examine cellular viability, 20 μL of Cell Titer 96 AQueous One Solution Reagent (Promega) was added to each well followed by 1 h incubation at 37 °C. The optical density of each well was detected using a microplate reader (BioTek) set to 490 nm. For pretreatment with forskolin (Sigma) followed by FA treatment, after cell attachment for 24 h, the cells were treated with 10 μM forskolin for 3 h. For the cellular glutathione (GSH) assay, the methods for seeding cells and exposure to FA were the same as those for the bioassay of cell viability, and wild-type A549 cells were treated with FA for 24 h. Levels of cellular GSH were measured using a GSH-Glo Glutathione Assay kit (Promega).

Genome-Scale Knockout A549 Cells. Construction of genome-scale knockout A549 cells was performed as previously described.[10] Plasmids came from the Genome-Scale CRISPR Knockout (GeCKO) version 1 library (Broad Institute of MIT and Harvard, Cambridge, MA), and these plasmids were merged into lentiviral vectors to transfect A549 cells. Lentiviral packages were conducted by cotransfection of GeCKO library plasmids together with two viral packaging plasmids, pVSVg and psPAX2 (Addgene), into HEK293T cells (ATCC, Manassas, VA) when the cells reached 80−90% confluency. Opti-MEM (Thermo Scientific), Lipofectamine 2000 (Thermo Scientific), and PLUS reagent (Thermo Scientific) were used to promote the plasmids to enter HEK293T cells, and the procedures were performed according to the manufacturer's recommendation. After 6 h, the media were replaced with fresh D10 media (DMEM supplemented with 10% fetal bovine serum). 60 h post transfection, the media were removed and centrifuged at 24,000 rpm for 2 h at 4 °C to collect lentiviruses. The titer of the virus was 2.2×10^8 IFU/mL (Lenti-X p24 Rapid Titer Kit, TaKaRa), and 20 μl of lentivirus and 8 μg/mL polybrene (Sigma) were added to 1×10^6 A549 cells per well of a 12-well

https://doi.org/10.1021/acs.est.1c07945
Environ. Sci. Technol. XXXX, XXX, XXX−XXX

plate. The volume of the virus was optimized to ensure a multiplicity of infection of 0.3 and to make most cells receive at most one genetic perturbation. Four plates were centrifuged at 2000 rpm for 2 h at 37 °C. After incubation for 24 h, the medium was changed, and the cells were transferred to 175 cm^2 flasks to filter out the cells not transfected using puromycin (0.5 μg/mL, Sigma) treatment for 10 days. A total of 3×10^7 cells were collected for genomic DNA extraction (Blood and Cell Culture DNA Midi Kit, Qiagen) and analysis for quality control of the transduction efficiency of the GeCKO library by deep sequencing using HiSeq X-Ten as described below. Sequencing of single clones from genome-scale knockout A549 cells was performed to evaluate the transduction of a single sgRNA plasmid and the loss-of-function of the corresponding gene, and the detailed protocols are available in the Supporting Information.

CRISPR-Cas9 Screening Using FA. A total of 5×10^7 cells (genome-scale knockout A549 cells) were seeded in two 225 cm^2 flasks with or without 150 μM FA treatments for 10 days. Exposure to 150 μM FA (in the CRISPR screen) mimicked occupational exposure to a high dose of FA (see the third paragraph in the Discussion). Each flask was passaged at a ratio of 1:2 every 3 days, and the medium was changed every day. After exposure, the genomic DNA of the remaining cells was extracted using a Blood and Cell Culture DNA Midi Kit (Qiagen). The concentrations of genomic DNA were detected by a Qubit dsDNA assay (Thermo Scientific). Nested PCR was used to amplify sgRNA inserts, and the procedures were described in a previous study.[10] Barcodes of sequencing were added to the second PCR, and products of the second PCR were pooled, purified, and sequenced on a HiSeq X-Ten (Illumina). Primers (GeneScript) of the nested PCR are given in Table S1.

AOP Network Analysis of CRISPR Screen Hits. The procedures of AOP network analysis of CRISPR screen hits were performed according to previous studies.[31] The log fold change (Log FC) of a gene was the Log FC of the sgRNA with the second largest absolute Log FC (read counts of the sgRNA in treatment vs control). Log FC of a Gene Ontology (GO) was the sum Log FC of the matched genes with the top three largest absolute Log FCs. Log FC of a key event (KE) was the Log FC of the GO annotated to that KE.

Measurements of Protein Expression. In this study, the protein expression of several genes (HTR4, p-p65, E-cadherin, α-SMA, and Snail) was detected by using western blotting. In addition, the distribution of the p-p65 protein in A549 cells was evaluated by using immunofluorescence. The production of cytokines (IL6, IL8, and TGFβ1) from A549 cells was determined by using an enzyme-linked immunosorbent assay. The detailed protocols for these methods are available in the Supporting Information.

Real-Time Quantitative Polymerase Chain Reaction. Total RNA containing small RNA was extracted from A549 cells using the RNeasy Plus Mini Kit (Qiagen). First-strand cDNA was synthesized using 1 μg total RNA by a reverse transcription system (TransScript). SYBR Green qPCR mix (Thermo Scientific) was used to detect the expression of proinflammatory cytokines and fibrosis and EMT biomarkers. The primers (GeneScript) for these genes are shown in Table S2. Expression of HTR4 transcripts was detected using a TaqMan Fast Advanced Master Mix (Thermo Scientific). Reverse transcription of microRNA (miRNA) was carried out using specific stem-loop primers (Thermo Scientific), and the primers and probes of qPCR were included in TaqMan Small RNA Assays (ID 002420 for miR-16-1-3p, ID 000439 for miR-103a-3p, ID 000377 for let-7a-5p, ID 000497 for miR-197-3p, and ID 462237_mat for miR-4660, Thermo Scientific). Detailed methods for the transfection of RNA oligoribonucleotides (mimics and inhibitors of miRNA, see Table S3) into A549 cells are available in the Supporting Information. GAPDH (GeneScript) and U6 (ID 001973, Thermo Scientific) were selected as housekeeping genes for mRNA and miRNA quantification, respectively. Conditions for PCR were consistent with the instructions of the manufacturer (StepOnePlus Real-Time PCR System, Thermo Scientific). The data were analyzed using ddCt in StepOne Software v2.3.

Bisulfite Sequencing PCR for Methylation Analysis. After cell attachment for 24 h, WT A549 cells were treated with FA (150 μM or 300 μM) for 24 h. Treatment with 5 or 10 μM hypomethylating agent, 5-aza-2′-deoxycytidine (5-aza, Sigma), was used as a positive control for FA treatment of WT A549 cells. Then, the expression of HTR4 was analyzed using western blotting and real-time qPCR as previously described. Genomic DNA was extracted from WT A549 cells using a QIAamp DNA Mini Kit (Qiagen). The concentrations of genomic DNA were detected by a Qubit dsDNA assay (Thermo Scientific). One microgram of genomic DNA for each sample was treated with EpiTect Fast Bisulfite Conversion Kits (Qiagen). Purified DNA was PCR-amplified with specific bisulfate sequencing primers (GeneScript; Table S4), and PCRs were carried out using Taq DNA polymerase (DBI Bioscience). Target PCR products (435 bp) were cloned into the pMD18-T vector (TaKaRa). After transformation to competent *Escherichia coli* cells, 20 positive clones were selected randomly to be sequenced. Sequencing data were analyzed using the BiQ analyzer. Methylation of each CpG site was represented by the mean of the value (0 to 1) of the corresponding site in 20 positive clones.

Evaluation of FA-Induced Mice Lung Injury. Wild-type ($HTR4^{+/+}$) and $HTR4^{+/-}$ C57BL/6 mice (KOCMP-23817-htr4) were purchased from Cyagen Biosciences. $HTR4^{-/-}$ mice were generated by $HTR4^{+/-} \times HTR4^{+/-}$ breeders. All mice (male) were 8−9 weeks of age (weight: 23.1−26.4 g) at the time of FA exposure. Experiments with animals were conducted in accordance with regulations of the Institutional Animal Care and Use Committee (IACUC) of Nanjing University. For subacute exposure, the concentration of FA in the air in the exposure chamber was 22.0 ppm (20.6−23.5 ppm). The mice were exposed via inhalation of either FA or phosphate-buffered saline (PBS) (negative control) for 14 consecutive days at 2 h/day. Subchronic exposure mimicked exposure to FA in the occupational environment; the concentration of FA in the high-dose group was 4.0 ppm (3.1−4.7 ppm),[13] and it was 0.40 ppm (0.29−0.48 ppm) in the low-dose group.[14] The mice were administered FA or PBS by inhalation for 5 weeks at 4 h/day. For both subacute and subchronic exposure, there were 6 mice in each group for each treatment. During the exposures, samples of air in exposure chambers were collected every 20 min, concentrations of FA were measured by a PPM-400th analyzer (PPM Technology), and the variations of FA concentrations came from the instrumental error. The detailed protocols for exposure of animals are available in the Supporting Information. After the exposure experiments, the lung functions of the mice were measured, inflammatory cells and cytokines in bronchoalveolar lavage fluid (BALF) were analyzed, and histological analysis of lung airway tissues was performed by hematoxylin and eosin (H&E) or Masson's trichrome staining and

https://doi.org/10.1021/acs.est.1c07945
Environ. Sci. Technol. XXXX, XXX, XXX−XXX

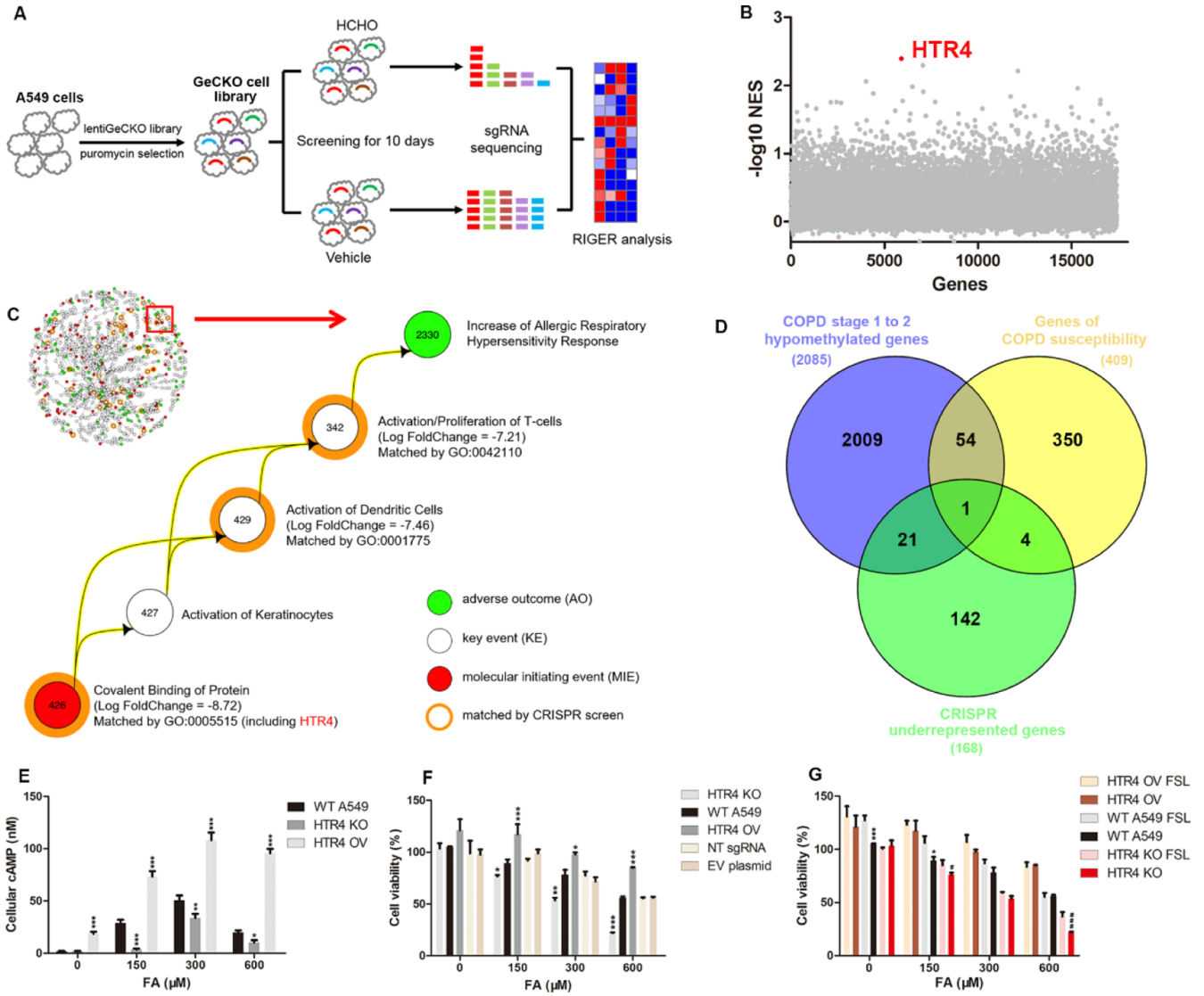

Figure 1. Gene profiles from CRISPR screening and identification of the key role of HTR4 in human A549 cells. (A) Workflow of CRISPR screening using formaldehyde (FA; HCHO). (B) Ranking all the knockout genes according to their NES, each dot represents a gene, and HTR4 (red dot) was ranked no. 1. (C) AOP network matched by CRISPR screen using FA, edges in yellow represent an extracted AOP starting from an MIE and ending in an AO. (D) Venn diagram of the three genes clusters (2085 hypomethylated genes obtained from reanalysis of methylation data set in GSE111396, 409 genes associated with chronic obstructive pulmonary disease (COPD) susceptibility retrieved from DisGeNET database, and 168 underrepresented genes of CRISPR screening), HTR4 is the only one common gene of the three clusters. (E) Cyclic AMP (cAMP) was measured in wild-type (WT), HTR4 knockout (KO), and HTR4 overexpression (OV) A549 cells treated with increasing doses of FA. (F) Dose−response pattern of five A549 cell lines against the cytotoxicity of FA. The five cell lines included HTR4 KO, WT, HTR4 OV A549 cells, and wild-type A549 cells transfected with nontargeting (NT) sgRNA or empty vector (EV) plasmid. (G) Dose−response pattern of three A549 cell lines against the cytotoxicity of FA. Pretreatment of 10 μM forskolin (FSL) was used to raise levels of intracellular cAMP in A549 cells. For panels (E−G), the FA exposure was for 24 h, the bars represented means with SEMs ($n = 4$). For panel (E,F), $^{*}p < 0.05$, $^{**}p < 0.01$, and $^{***}p < 0.001$ compared with wild-type A549 cells by two-way ANOVA test followed by Bonferroni post-tests. For panel (G), $^{*}p < 0.05$ and $^{***}p < 0.001$ compared with wild-type A549 cells with pretreatment of FSL by two-way ANOVA test followed by Bonferroni post-tests, $^{\#}p < 0.05$ and $^{\#\#\#}p < 0.001$ compared with HTR4 KO cells with pretreatment of FSL by a two-way ANOVA test followed by Bonferroni post-tests.

immunohistochemistry of p-p65. The detailed protocols for these methods are also available in the Supporting Information.

Measurement of Intracellular cAMP. Three types of A549 cells (wild-type, HTR4 knockout, and HTR4 overexpression, 1×10^4 cells per well) were seeded into 96-well poly-d-lysine-coated, white, clear-bottom plates (BD Bioscience). After attachment for 24 h, the cells were exposed to 0, 150, 300, and 600 μM FA for 24 h. The cAMP-Glo assay was used to measure cellular cAMP, and the procedures were performed according to the manufacturer's instructions (Promega). The luminescence of cells was detected by a microplate reader using optical filters in the "lum" mode (BioTek, Synergy H4).

Epidemiology Analysis. The genes associated with COPD susceptibility were obtained by retrieving the DisGeNET database.[33] The methylation data set of GSE111396[34] was reanalyzed to obtain the differentially methylated genes in the lungs of COPD patients. The common genes among the three genes sets (the genes identified by CRISPR screening, the genes associated with COPD susceptibility, and the differentially methylated genes in the lungs of COPD) were identified as key

https://doi.org/10.1021/acs.est.1c07945
Environ. Sci. Technol. XXXX, XXX, XXX−XXX

genes. Related previous studies and databases were retrieved to obtain COPD prevalence, HTR4 genetic variants, and their allele frequencies. The detailed methods for these analyses are available in the Supporting Information.

Statistical Analysis. In the CRISPR screen, if a sgRNA knocked out a gene required for cellular resistance to FA, the gene knockout cells would be more sensitive to FA than wild-type cells. The sgRNAs for that gene would be underrepresented in surviving cells compared with their representations in untreated cells, and that gene was termed an underrepresented gene. The underrepresented genes in CRISPR screening were identified by using RNAi Gene Enrichment Ranking (RIGER) at the options of "Second Best Rank" and "Signal to Noise".[10,35] The underrepresented genes (RIGER p value < 0.01) were ranked according to normalized enrichment scores (NES) calculated in RIGER. Kyoto Encyclopedia of Genes and Genomes (KEGG) pathway enrichment of human genes was performed by using g:Profiler software[36] in accordance with the recommendation of g:Profiler, and "all known genes" were selected for statistical domain scope. A cutoff of that adjusted p value less than 0.01 was applied. Bar plots represent means with SEMs. One-way ANOVA or two-way ANOVA with Bonferroni posttests was used for statistical significance analysis (GraphPad Prism). The difference was considered statistically significant when the p value was less than 0.05. Correlation analysis between allele frequencies of single nucleotide polymorphisms (SNPs) and COPD prevalence was carried out with a two-tailed test (GraphPad Prism).

RESULTS

Genome-Scale Knockout Human A549 Cells. The genome-scale CRISPR knockout (GeCKO) sgRNA library was transduced into A549 cells using packaged lentivirus. The GeCKO library consists of 64,751 sgRNA plasmids targeting 18,080 genes with an average of 3−4 sgRNAs per gene.[10] The plasmid library was qualified, and 98.3% of the sgRNAs were covered at an abundance of more than 10 reads (Figure S1). More than 97.7% of genes (17,678 genes) in the GeCKO library were knocked out in A549 cells (Figure S2A). The remaining genes (402 genes) were evaluated using Gene Ontology analysis, which identified roles in basic cellular functions (Figure S2B), suggesting that these genes may be essential for cell growth and viability. In addition, 10 single clones were randomly selected from the cell library, and only one sgRNA was detected in each clone by deep sequencing. All the genes targeted by these sgRNAs were modified (Table S5).

Identification and Characterization of HTR4 Associated with Susceptibility to FA. Exposure of WT A549 cells to 150 μM FA induced significant depletion of intracellular GSH (a decrease of 15.6−22.4%, Figure S3A) and caused cell death in 10% of A549 cells (Figures 1A and S3B). The underrepresented genes were ranked according to their NES, which were determined by RIGER analysis (Figures 1A and S3C, Table S6). HTR4 had the lowest NES among the genes with loss attenuated cellular resistance to FA (Figures 1B and S3D), suggesting that the loss of function of HTR4 was the primary genetic factor determining the vulnerability of A549 cells to FA. A total of 168 underrepresented genes (RIGER p value < 0.01, Table S6) were enriched in thirteen KEGG pathways, as determined using g:Profiler software (Figure S4C).[36] To compare the candidate genes for FA resistance identified in the CRISPR screen with existing data for genes associated with COPD, we pulled data from the DisGeNET database and reanalyzed the methylation data set of GSE111396 to identify genes potentially related to COPD pathogenesis in the lungs of nonsmokers and ex-smokers. A total of 409 genes were retrieved from the DisGeNET database (Table S7), and genetic variations of the 409 genes were associated with COPD susceptibility. A total of 2085 hypomethylated genes (Table S8) in the lungs of nonsmokers and ex-smokers who belonged to COPD stage 1−2 were identified through reanalysis of the methylation data set. There were five common genes between the 168 underrepresented genes of the CRISPR screen and the 409 genes associated with COPD susceptibility (Figure 1D). Among the five common genes, only HTR4 was differentially methylated (hypomethylation) (Figure 1D), identified as a potential pathogenesis-related gene. In the AOP network matched by CRISPR screen hits (the 168 underrepresented genes), only the present AOP was a respiratory toxicity-related AOP, in which a respiratory disease (allergic respiratory hypersensitivity response, a pathological feature of COPD) was the adverse outcome (AO) (Figure 1C). Interestingly, HTR4 was included in the molecular initiating event (MIE, covalent binding of protein) of the AOP, and the HTR4-cAMP signaling pathway was enriched by the genes in the MIE (Figures S4D and S5), indicating a potential AOP that started from activation of HTR4 and ended in FA-induced lung injury. Therefore, HTR4, an important genetic risk factor for COPD, linked the susceptibility to FA-induced lung injury to the prevalence and development of COPD. In addition, the HTR4-cAMP signaling pathway was the only common pathway after enrichment analysis (Figures S4 and S5), suggesting that the HTR4-cAMP signaling pathway was related to COPD progression and the toxic effects of FA.

Activation of HTR4-cAMP signaling was essential for maintaining the viability of A549 cells after exposure to FA (Figure S5). There were six transcript variants of HTR4 in humans,[37] and to evaluate which transcript variants were present in A549 cells, we used TaqMan real-time qPCR to measure the mRNA of six transcript variants of HTR4 (Table S9). In A549 cells exposed to FA or the vehicle, only an HTR4 transcript variant (HTR4-a) was detected (Figure S3E). To construct HTR4-null cells and HTR4-overexpressing cells, all six transcript variants of HTR4 were knocked out (Table S10), and HTR4-a was overexpressed in wild-type A549 cells (Figures S3F,G,H and S6). Levels of the HTR4 protein (Figure S3F) and mRNA (Figure S3G) were higher in wild-type (WT) and HTR4-overexpressing (OV) A549 cells treated with 300 μM FA than in those treated with the vehicle. Activation of HTR4-cAMP signaling was assessed by determining intracellular cAMP levels. WT A549 cells exposed to FA up to 600 μM had higher levels of cAMP than those exposed to the vehicle (Figure 1E). FA-exposed HTR4 knockout (KO) cells, in contrast, had lower levels of cAMP than FA-exposed WT cells, whereas FA-exposed HTR4 OV cells had higher levels of cAMP than FA-exposed WT cells (Figure 1E), suggesting that the FA-induced increase in intracellular cAMP was mediated by HTR4. In addition, WT A549 cells and those cells transfected with the NT sgRNA or EV plasmid had similar viability when exposed to FA or the vehicle (Figure 1F). In contrast, FA-exposed KO cells had lower viability than FA-exposed WT cells, whereas FA-exposed OV cells had higher viability than FA-exposed WT cells (Figure 1F). Finally, forskolin (FSL, a known cAMP rising agent) pretreatment relieved the decrease in cellular viability, especially in FA-exposed KO cells, where the FA-induced increase in intracellular cAMP was suppressed because of loss-of-function HTR4 (Figure 1E,G).

https://doi.org/10.1021/acs.est.1c07945
Environ. Sci. Technol. XXXX, XXX, XXX−XXX

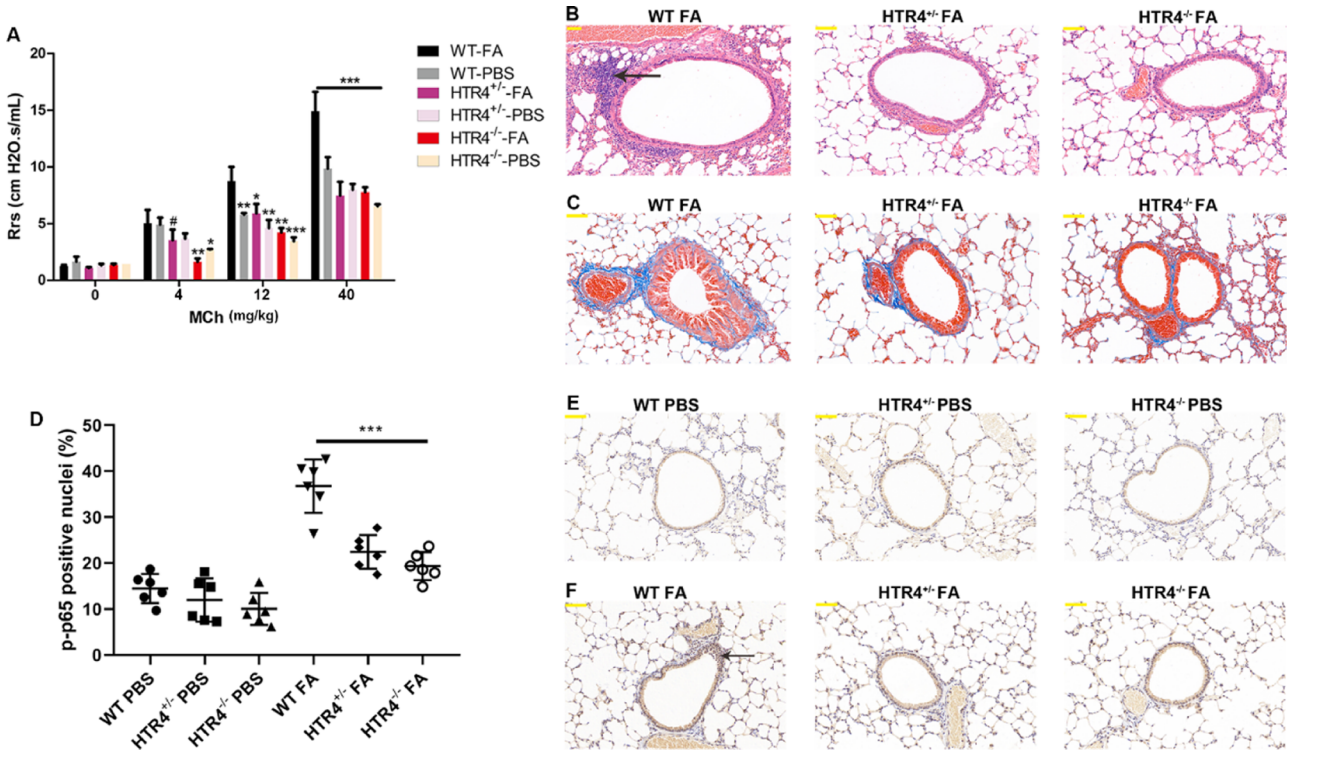

Figure 2. Different severity of lung injury caused by subacute exposure to FA in wild-type mice and HTR4 mutant ($HTR4^{+/-}$ or $HTR4^{-/-}$) mice. (A) Resistance of the respiratory system (Rrs) of mice ($n = 6$) following methacholine (MCh) gradient treatment. Bar plot represents the mean with SEM, $^{*}p < 0.05$, $^{**}p < 0.01$, and $^{***}p < 0.001$ compared with wild-type (WT) mice exposed to FA by a two-way ANOVA test followed by Bonferroni post-tests, $\#p < 0.05$ compared with $HTR4^{-/-}$ mice exposed to FA by two-way ANOVA test followed by Bonferroni post-tests. Panel (B) is hematoxylin and eosin (H&E) staining, and panel (C) is Masson trichrome staining for histopathology analysis of lung airway sections of WT, $HTR4^{+/-}$ and $HTR4^{-/-}$ mice. The black arrow in panel (B) points position with inflammatory cells infiltration. (D) Percentage of p-p65 positive nuclei in mice airway cells after immunohistochemistry analysis ($n = 6$). Three random views were taken from each section and total numbers of cells were used for calculation. The bars represent means with SEMs, $^{***}p < 0.001$ compared with WT mice exposed to FA by one-way ANOVA test followed by Dunnett's multiple comparisons test. Panels (E,F) are immunohistochemistry analyses of the p-p65 protein in lung airways, and the black arrow indicates aggregation of airway cells with p-p65 positive nuclei. For panels (B,C), yellow scale bars represent 100 μm, for panels (E,F), yellow scale bars represent 120 μm. For panels (B,C,E,F), all histological images were representative, and 6 images for each treatment were evaluated.

HTR4 and Susceptibility to FA-Induced Lung Injury. The resistance of the respiratory system (Rrs) of each mouse continued to rise with increasing doses of methacholine (MCh) after subacute exposure to FA (Figures 2A and S7). Exposure to FA aggravated airway hyperresponsiveness (AHR) in WT mice, but this reaction was alleviated in HTR4-null mice. After inhalation of FA, the Rrs of WT mice were 1.5−2.0 times or 1.9−3.1 times that of $HTR4^{+/-}$ or $HTR4^{-/-}$ mice, respectively (Figure 2A). WT mice exposed to FA via inhalation exhibited massive inflammatory cell infiltration near the bronchia, but very little infiltration was observed in the airways of $HTR4^{+/-}$ and $HTR4^{-/-}$ mice (Figures 2B and S8A). Both significant thickening of walls and excessive deposition of collagen were observed in the airways of WT mice exposed to FA, whereas only slight collagen deposition around the bronchia was observed in the lungs of $HTR4^{+/-}$ and $HTR4^{-/-}$ mice (Figures 2C and S8B). The Ashcroft score for airway fibrosis in the lungs of WT mice exposed to FA was approximately 4.0; in contrast, the scores were less than 3.0 for $HTR4^{+/-}$ and $HTR4^{-/-}$ mice (Figure S8C). The immunohistochemical analysis for phosphorylated RELA (p-p65, Ser 536) showed that the number of airway cells with p-p65-positive nuclei was higher (more than 2-fold) in the lungs of WT mice after inhalation of FA, while a limited increase was observed in the lungs of $HTR4^{+/-}$ and $HTR4^{-/-}$ mice (Figure 2D−F). In addition, exposure to FA induced increasing populations of neutrophils, eosinophils, lymphocytes, and macrophages in BALF from WT mice (Figure S9A). Little population growth of each kind of immune cell was measured in BALF from $HTR4^{-/-}$ mice after inhalation of FA although the counts of total cells increased. Changes in the concentrations of two cytokines, IL6 and TGFβ1, in BALF were consistent with the results of histopathology analysis (Figure S9B,C).

For subchronic exposure (Figure S7), the Rrs of WT mice was 1.3−1.6 times or 1.1−1.2 times that of $HTR4^{-/-}$ mice in the high-dose group or in the low-dose group, respectively (Figure 3A). Both exposure to the high dose and low dose of FA induced an increase in immune cells in BALF from WT mice. For the high dose groups, a significant decrease (approximately 1.5-fold) in each kind of immune cell was observed in BALF from $HTR4^{-/-}$ mice compared with that of WT mice. In the low-dose groups, only the counts of macrophages and neutrophils decreased in BALF from $HTR4^{-/-}$ mice compared with those of WT mice (Figure 3B). In addition, after exposure to FA, noticeable inflammatory cell infiltration and collagen deposition were observed surrounding the lung airways of WT mice. However, mild inflammation and fibrotic responses of $HTR4^{-/-}$ mice were observed only in those mice that were exposed to the high dose of FA (Figures 3C,D and S8D).

Effects of HTR4 Expression on Cellular NF-κB Activation, Inflammation, and Fibrotic Responses. Differential protein levels of nuclear phosphorylated RELA (p-p65

https://doi.org/10.1021/acs.est.1c07945
Environ. Sci. Technol. XXXX, XXX, XXX−XXX

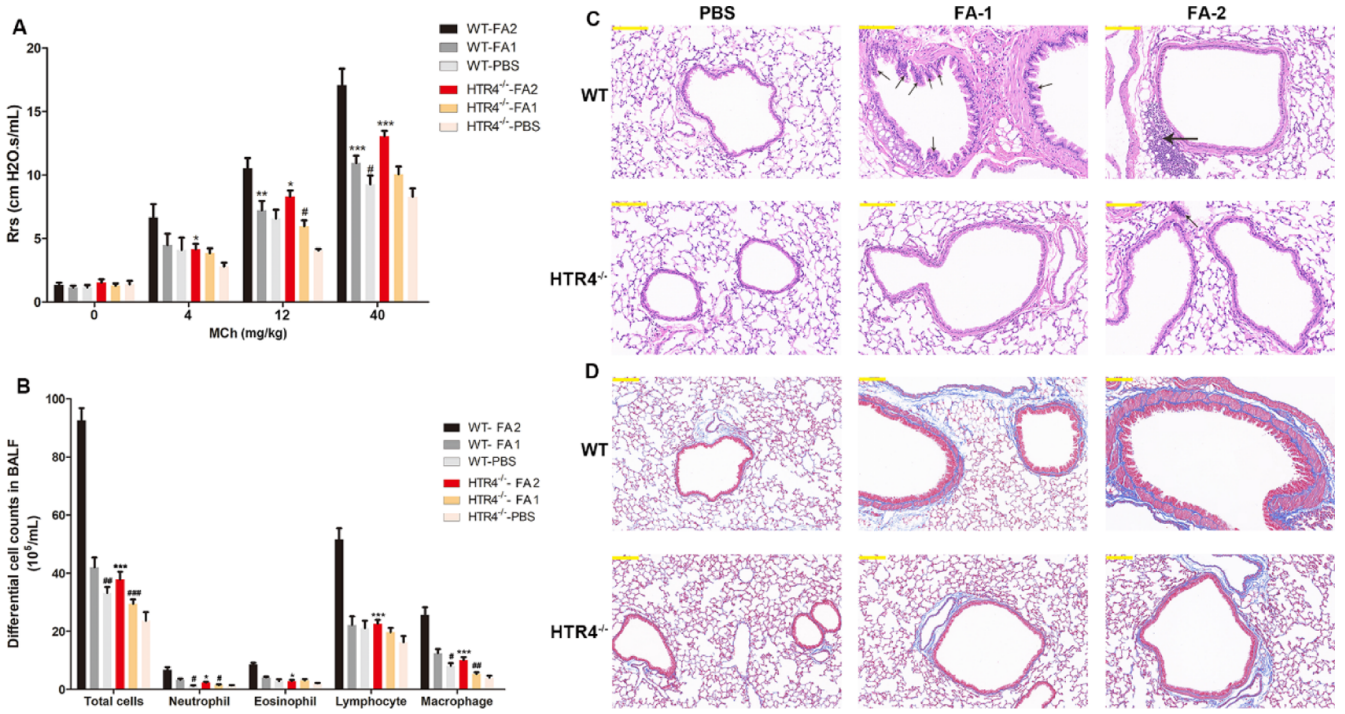

Figure 3. Different severity of lung injury caused by subchronic exposure to FA of wild-type mice and HTR4$^{-/-}$ mice. (A) Resistance of the respiratory system (Rrs) of mice challenged by FA or PBS for 5 weeks ($n = 6$). Rrs was measured following methacholine (MCh) gradient treatment. The bar plot represented the mean with SEM, $^{*}p < 0.05$, $^{**}p < 0.01$, and $^{***}p < 0.001$ compared with wild-type (WT) mice exposed to a high dose of FA (FA2) by two-way ANOVA test followed by Bonferroni post-tests, $^{\#}p < 0.05$ compared with WT mice exposed to a low dose of FA (FA1) by a two-way ANOVA test followed by Bonferroni post-tests. (B) Counts of immune cells in bronchoalveolar lavage fluid (BALF) from WT or HTR4$^{-/-}$ mice challenged by inhalation of FA or PBS for 5 weeks. The bar plot represented the mean with SEM ($n = 6$ mice), $^{*}p < 0.05$ and $^{***}p < 0.001$ compared with WT mice exposed to high dose of FA (FA2) by a two-way ANOVA test followed by Bonferroni post-tests, $^{\#}p < 0.05$, $^{\#\#}p < 0.01$, and $^{\#\#\#}p < 0.001$ compared with WT mice exposed to low dose of FA (FA1) by a two-way ANOVA test followed by Bonferroni post-tests. (C,D) Histology of lung airway sections of wild-type (WT) and HTR4$^{-/-}$ (KO) mice challenged by FA (FA-1, low dose: 0.29−0.48 ppm; FA-2, high dose: 3.1−4.7 ppm) or PBS inhalation for 5 weeks. Panel (C) is H&E staining, and panel (D) is Masson trichrome staining. The black arrow points to positions with inflammatory cells infiltration. Yellow scale bars represent 100 μm. All histological images were representative, and 6 images for each treatment were evaluated.

and Ser 536) among different groups were reflected in the relative potency (ReP) of nuclear p-p65 compared to that of WT A549 cells exposed to the vehicle. In the three A549 cell lines (WT, HTR4-KO, and OV), the total levels of p-p65 and the ReP of nuclear p-p65 were higher with increasing concentrations of FA (Figures 4A,B,D, S10A,B, and S15A). Moreover, the total levels of p-p65 and the ReP of nuclear p-p65 in the three cell lines exposed to the same concentration of FA followed the order OV > WT > KO (Figures 4A,B,D and S10A,B).

Differential production of two inflammatory cytokines (interleukin 6 and interleukin 8) was observed in the three cell lines exposed to 0, 150, or 300 μM FA. The concentrations of interleukin (IL) 6 and IL8 were higher in cellular supernatants of WT and HTR4-OV cell lines exposed to FA compared with those of the cells exposed to the vehicle (Figure 4C). In contrast, in HTR4-null cells, after exposure to FA, there were no significant effects on the concentrations of cytokines in the supernatants. Under the same treatment conditions, the levels of cytokines released by HTR4-OV cells were always greater than those released by WT and HTR4-null cells (Figure 4C). Similar changes in the abundances of mRNAs for IL6 and IL8 were also detected in all three cell lines (Figure S10C,D).

HTR4 was essential in the fibrotic response of airway epithelial cells to FA exposure, including the differential expression of transforming growth factor beta 1 (TGFβ1), a fibrogenic marker, and three epithelial−mesenchymal transition (EMT) biomarkers, Snail, E-cadherin, and α-SMA. TGFβ1 was released by the three A549 cell lines with or without exposure to FA, in the decreasing order OV > WT > KO (Figure 4E). Although the increased release of TGFβ1 from WT and HTR4-null A549 cells exposed to 300 μM FA compared to the control was limited to approximately 80 pg/mL, the increased secretion of TGFβ1 by HTR4 OV cells exposed to 300 μM FA compared to the control was approximately 200 pg/mL. Western blotting showed higher protein levels of Snail and α-SMA and lower protein levels of E-cadherin in FA-exposed cells than in vehicle-exposed cells (both WT and HTR4 OV cells; Figures 4F and S15). The protein expression of Snail and α-SMA in the three A549 cell lines exposed to the same treatment was OV > WT > KO. In contrast, E-cadherin, a marker of the epithelial phenotype, was expressed in the order OV < WT < KO (Figures 4F and S15). Similar differences in the mRNA expression of these genes were observed (Figure S11).

Epigenetic Regulation of Expression of HTR4. Methylation of the CpG island in the HTR4 genomic sequence (−2000 base from transcription start site to +466 base) was evaluated, and there are 47 CpG sites in the CpG island. Among the 47 CpG sites, hypomethylation of 8 sites was measured after treatment with FA (150 or 300 μM) or 5-aza-2′-deoxycytidine (5-aza, 5 μM), which is known to demethylate DNA (Figure 5A−C). HTR4-a was upregulated in WT A549 cells exposed to FA or 5-aza, and the expression of HTR4-a was similar between cells treated with FA (300 μM) and 5-aza (5 μM) (Figure 5D,E).

https://doi.org/10.1021/acs.est.1c07945
Environ. Sci. Technol. XXXX, XXX, XXX−XXX

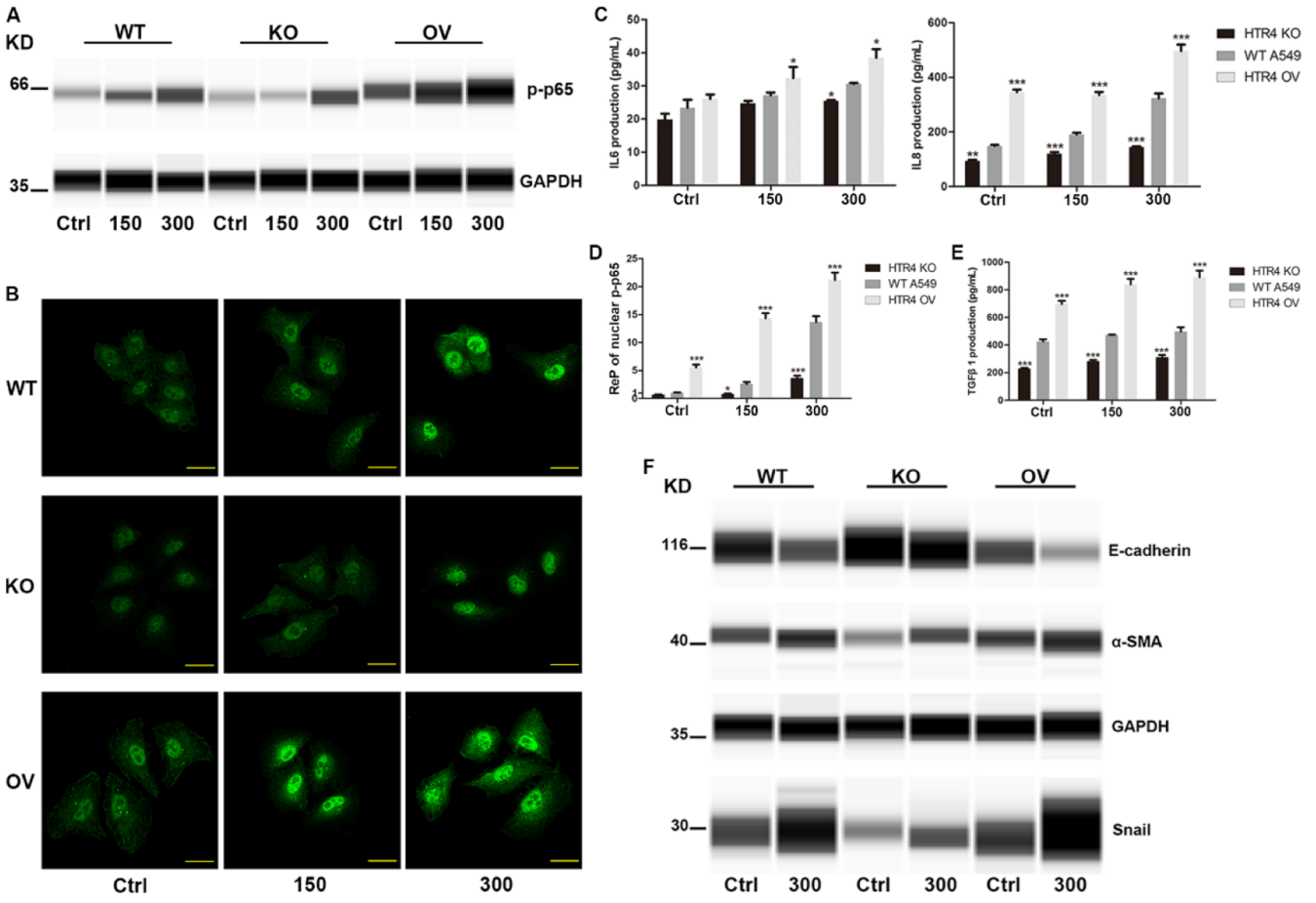

Figure 4. Differential responses to FA exposure in wild-type (WT), HTR4 knockout (KO), and overexpression (OV) A549 cells. (A) Representative western blotting analysis of phosphorylated p65 (p-p65) in A549 cells exposed to 0 (Ctrl), 150, and 300 μM FA. (B) Representative immunofluorescence analysis of p-p65 in three A549 cell lines, yellow scale bars represent 20 μm. (C) Release of proinflammatory cytokines (IL6 and IL8) from A549 cells exposed to 0 (Ctrl), 150, and 300 μM FA. (D) Relative potency (ReP) of nuclear p-p65 compared to that of WT A549 cells exposed to the vehicle, the data were obtained from quantification of the fluorescence intensity of the immunofluorescence analysis of p-p65. € Release of TGFβ1 from A549 cells exposed to 0, 150, and 300 μM FA, respectively. (F) Representative western blotting analysis of three epithelial−mesenchymal transition (EMT) biomarkers (E-cadherin, α-SMA, and Snail) in A549 cells exposed to 0 (Ctrl) or 300 μM FA. For all panels, exposure to FA was for 24 h, bar plot represented mean with SEM (n = 4), *p < 0.05, **p < 0.01, and ***p < 0.001 compared with WT cells by a two-way ANOVA test followed by Bonferroni post-tests.

Four out of the five examined microRNAs, including miR-16-1, miR-103a, let-7a, and miR-197, were expressed at lower levels with increasing concentrations of FA to which the cells were exposed (Figure 5F). Then, WT A549 cells were transfected with 25 nM inhibitors or mimics of these four microRNAs (Table S3, Figure S12), after which the expression of HTR4-a was detected using RT-qPCR (TaqMan). HTR4-a mRNA expression was higher in cells treated with the inhibitor of miR-197, and HTR4-a mRNA expression was lower after treatment with the mimic of miR-197 (Figure 5G). In contrast, treatments with an inhibitor or mimic of miR-103a, let-7a or miR-16-1 had no significant effect on the expression of HTR4-a. The sequence of miR-197 matched the coding sequence (CDS) of HTR4-a, which suggested that miR-197 can mediate the cleavage of HTR4-a mRNA (Figure 5I). WT A549 cells pretransfected with the miR-197 mimic and exposed to FA had higher expression of HTR4-a than WT A549 cells pretransfected but exposed to the vehicle (Figure 5H).

Genetic Polymorphisms of HTR4 and COPD Prevalence. Alternative (ALT) allele frequencies of the eight HTR4 SNPs were associated with the prevalence of COPD globally (two-tailed p < 0.05) (Figures 6 and S13), and the r values were similar to that of the positive reference variant rs4905179. The ALT allele frequencies of the eight SNPs of HTR4 (Tables S11 and S12) are shown in Figure 6. The worldwide prevalence of COPD varied from 5.4 to 15.0% in 10 major regions (Table S13).

DISCUSSION

Here, loss-of-function HTR4 was identified as the primary genetic factor that determined the vulnerability of A549 cells to FA by CRISPR screening. Specifically, the expression of HTR4 and an increase in intracellular cAMP were required for the cellular resistance of A549 cells to FA-induced cell death, and the FA-induced rise in cAMP levels was mediated by HTR4. In vivo studies suggested that injury to mouse lungs caused by inhalation of FA, including increased AHR, airway inflammation, and fibrosis, was also mediated by HTR4. In vitro studies showed that enhanced expression of HTR4 was required for facilitating FA-induced NF-κB activation, inflammation, and fibrotic responses in A549 cells. In addition, FA-induced epigenetic changes, including hypomethylation of the CpG island in the HTR4 genome and suppression of miR-197-3p, were important causes of enhanced expression of HTR4 in A549

https://doi.org/10.1021/acs.est.1c07945
Environ. Sci. Technol. XXXX, XXX, XXX−XXX

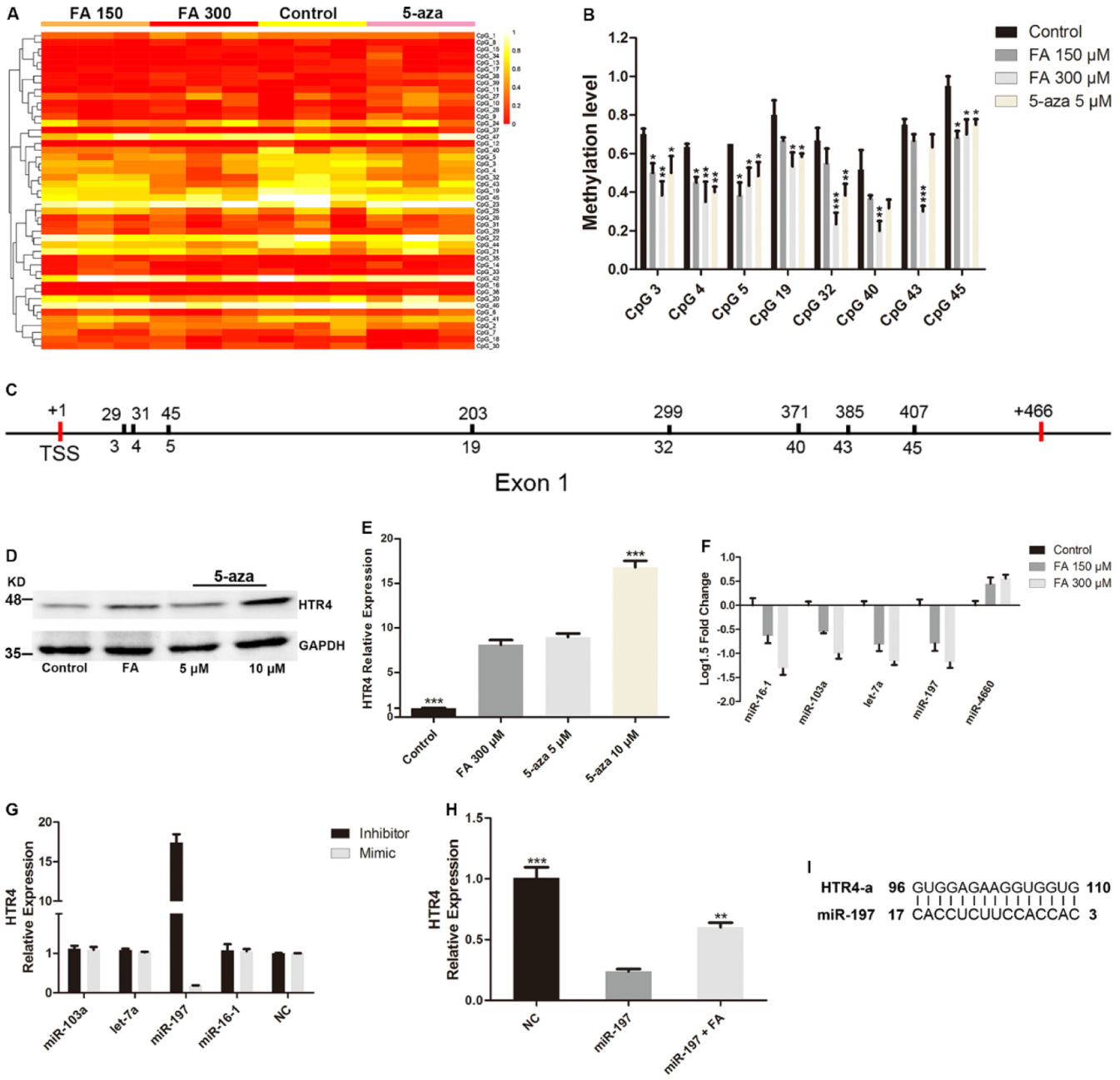

Figure 5. Evaluation of the roles of methylation of CpG island and microRNAs on the expression of HTR4. (A) Methylation profile of 47 CpG sites in the CpG island of HTR4. The methylation level of each CpG site was represented using red, yellow, or white colors in a heatmap. 1 indicated full methylation and 0 indicated absolute demethylation ($n = 3$ independent experiments). (B) Bar plots of methylation levels of the 8 CpG sites (CpG 3, 4, 5, 19, 32, 40, 43, and 45) (means with SEMs, $n = 3$, $^{*}p < 0.05$, $^{**}p < 0.01$, and $^{***}p < 0.001$ compared with untreated control by a two-way ANOVA test followed by Bonferroni post-tests). (C) Location of 8 CpG sites in HTR4 genomic sequence, TSS represented transcription start site. (D) Representative western blotting analysis of the HTR4 protein in WT A549 cells exposed to 300 μM FA or 5 μM or 10 μM 5-aza-2′-deoxycytidine (5-aza). (E) Expression of HTR4-a mRNA in WT A549 cells. $^{***}p < 0.001$ compared with FA treatment by a one-way ANOVA test. (F) Fold change of expression of five microRNAs in WT A549 cells exposed to FA. (G) Expression of HTR4-a mRNA in WT A549 cells transfected with 25 nM of mimic or inhibitor of four microRNAs(see Table S3). NC represented mimic or inhibitor of nontargeting microRNA. The expression was relative to the expression of HTR4-a mRNA in cells transfected with NC. GAPDH was the housekeeping gene. (H) Expression of HTR4-a mRNA in WT A549 cells pretransfected with a mimic of miR-197 and then exposed to 300 μM FA. $^{**}p < 0.01$ and $^{***}p < 0.001$ compared with cells only pretransfected with a mimic of miR-197 by a one-way ANOVA test. For panels (E−H), the bar plot represented the mean with SEM ($n = 4$). I Sequence of mature miR-197-3p matched with CDS of HTR4-a. For all panels, treatment of FA or 5-aza was for 24 h.

cells exposed to FA. Furthermore, HTR4 was prioritized when linking the susceptibility to toxic effects of FA to genetic risk factors for COPD. Finally, the ALT allele frequencies of the eight HTR4 SNPs were associated with the worldwide prevalence of COPD.

CRISPR screening can identify the direct links between specific genes and the biological phenotypes responding to chemicals exposure. Some toxicological bioassay approaches have been raised, such as proteomics, metabolomics, and combinational chemistry. These approaches exhibit advances

https://doi.org/10.1021/acs.est.1c07945
Environ. Sci. Technol. XXXX, XXX, XXX−XXX

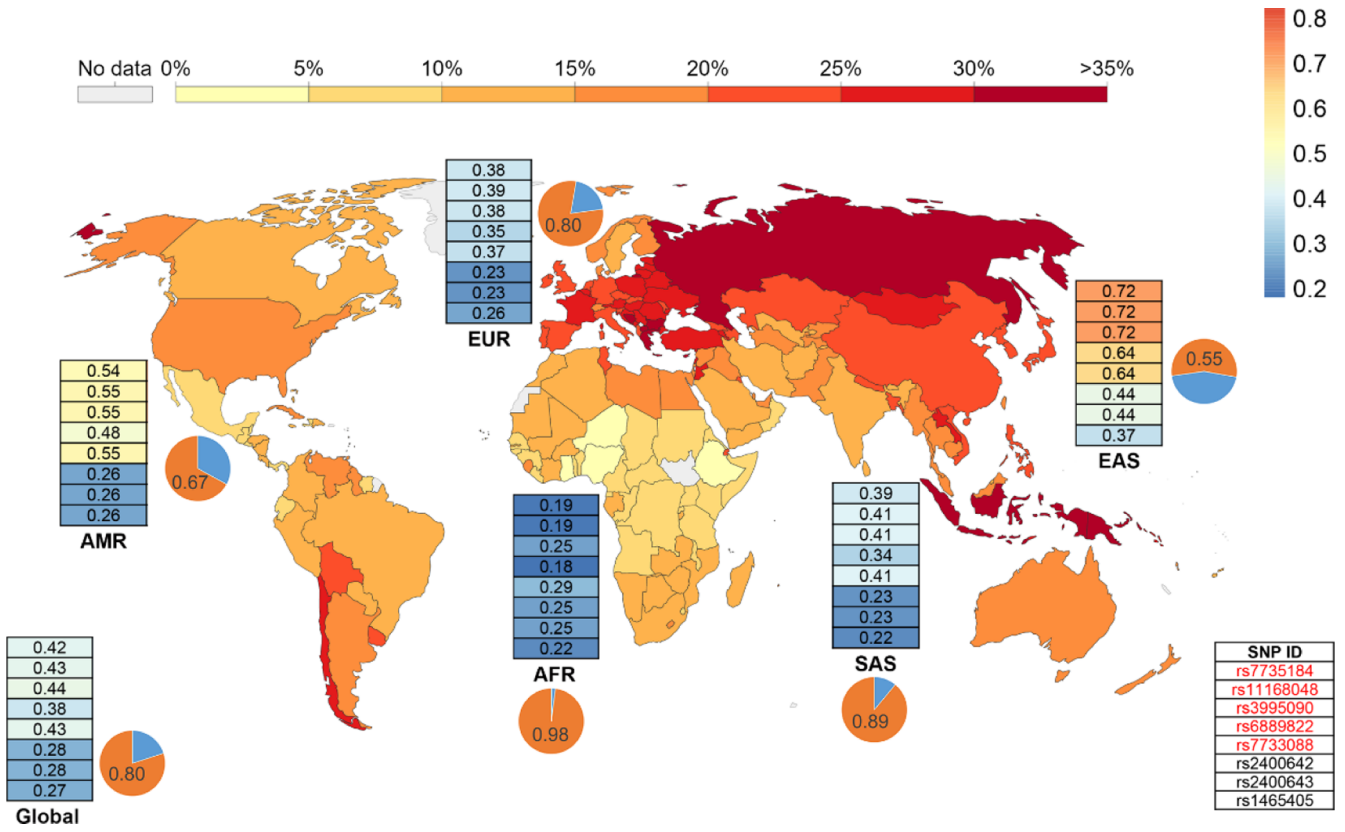

Figure 6. Distribution and the allele frequencies of representative variants for HTR4 in global populations. The background map represented the distribution of daily smokers (the color gradient from yellow to red indicates the increased percentages of the prevalence of daily smoking in different countries). The allele frequencies of 5 variants (SNP ID in red font) and 3 eQTLs (SNP ID in black font) are shown in a single-column table for each population. The color gradient from blue to red indicates the increase of allele frequencies. Pie charts depict the allele frequencies of rs4905179 located in SERPINA1 in different populations. Orange color and blue color denote the frequency of reference and alternative allele, respectively. SNP, single nucleotide polymorphism; eQTLs, expression quantitative trait loci; EAS, East Asian; EUR, European; AFR, African; SAS, South Asian; and AMR, Ad Mixed American.

and strengths in predicting the toxic potency of environmental pollutants and in exploring the toxicological mechanisms, by measuring the molecular products.[38,39] These molecular products are related to the functions of specific genes, and abundance changes of molecular products are associated with changes in biological phenotypes. However, these associations are not direct connections.[10] These approaches may fail to identify direct links between specific genes and the biological phenotypes responding to chemicals exposure.[40] By directly measuring the changes in biological phenotypes (e.g., cellular viability or other toxicity endpoints), CRISPR screening can uncover the direct connections between specific genes and the corresponding loss of functions which confer resistance or susceptibility to chemicals exposure.[2,40] Here, CRISPR screening was used to identify the primary genetic factors which confer resistance or susceptibility to FA exposure to human lung airway cells. Detailed statements for the features of the CRISPR screen are available in the Supplementary texts for the CRISPR screen of the Supporting Information.

The identification of the HTR4-mediated pathway significantly enriched the toxicological molecular mechanism of FA-induced lung injury under occupational exposure levels. The depletion of glutathione in FA-exposed in vitro cells[41] and in vivo tissues[18,42−44] has been previously documented; however, the underlying molecular mechanisms are poorly understood. Here, CRISPR screening was carried out in human alveolar epithelial A549 cells at 150 μM FA, which induced cell death in 10% of A549 cells. In addition, a significant depletion of intracellular GSH was observed when A549 cells were exposed to FA at no less than 150 μM (Figure S3A). Several underrepresented genes (e.g., GSTM4 and GCLC, Table S6) associated with glutathione metabolism were identified in the CRISPR screen and enriched in a KEGG pathway (glutathione metabolism, Figure S4C), suggesting that exposure to 150 μM FA disturbed glutathione metabolism in A549 cells. A significant decrease in GSH in epithelial cells of rat airways was observed when rats were exposed to FA at no less than 4.0 ppm.[13,42] Thus, based on similar cytotoxic effects (depletion of intracellular GSH), exposure to 150 μM FA (in the CRISPR screen) may mimic in vivo exposure to 4.0 ppm FA. In addition, FA (4.0 ppm) in the occupational environment was an initial threshold for increased risk of human cancers, such as leukemia[13,45] and nasopharyngeal carcinoma,[13,46] as well as, occupational exposure to 4.0 ppm FA significantly increased the risks of COPD and irreversible functional impairments of human lungs.[25,26,29] Therefore, exposure to 150 μM FA (in the CRISPR screen) mimicked occupational exposure to a high dose of FA, an exposure that may contribute to increased risks of human cancers and COPD.

Functionality and enhanced expression of HTR4 were required for susceptibility to injury to the lung caused by exposure to FA. Here, the results of the CRISPR screen suggested that the loss of function of HTR4 was the primary genetic factor determining the vulnerability of A549 cells to FA,

https://doi.org/10.1021/acs.est.1c07945
Environ. Sci. Technol. XXXX, XXX, XXX−XXX

according to the ranking of the normalized enrichment scores (NES). AOP network analysis of CRISPR screen hits identified a mechanistic linking between HTR4 and FA-induced lung injury and suggested that activation of HTR4-cAMP signaling might be essential for MIE (covalent binding of protein), providing important clues for the biological mechanisms underlying susceptibility to FA-induced lung injury. Subsequently, activation of HTR4-cAMP signaling was essential for cellular resistance to FA-induced cell death of A549 cells. The functionality of HTR4 contributed to the severity of FA-induced impairment of function and airway pathological changes in the lungs of mice exposed to FA. Wild-type mice exposed to FA suffered from exacerbation of respiratory resistance, inflammation, and fibrosis of the airways compared with HTR4-null mice. By measuring several biomarkers of airway inflammation and fibrosis,[47−49] an in vitro study revealed that enhanced expression of HTR4 was a key molecular event in mediating NF-κB activation, inflammation, and fibrotic responses of airway cells induced by exposure to FA. Therefore, it can be concluded that HTR4 plays a crucial role in determining susceptibility to FA-induced lung injury in vitro and in vivo.

Epigenetic differences in A549 cells following exposure to FA promoted the expression of HTR4 through transcriptional and posttranscriptional regulation. Only small amounts of transcripts and proteins of HTR4 were expressed in the lung cells of humans.[37] In this study, A549 cells (WT and HTR4-OV) exposed to FA exhibited higher expression of HTR4. Exposure to FA can induce the hypomethylation of genomic DNA in human lung cells.[50] This effect resulted in less methylation of CpG islands.[51,52] The CpG island of HTR4 is located in the first exon of the transcript variant b (HTR4-b). Only an HTR4 transcript variant (HTR4-a) was detected in this study. HTR4-a and HTR4-b are generated by alternative splicing of the HTR4 gene, sharing the same transcription start site (TSS).[51,53] Transcription of HTR4-a can be promoted by FA-induced hypomethylation of the CpG island near the TSS.[37,53] It may be a limitation of this study that some methylation intervention methods with better specificity than 5-aza were not used. On the other hand, exposure to FA altered the abundance of some miRNAs in human lung cells.[54] Based on the results of previous studies[55,56] and predictions from two databases, miRBase and miRWalk, five microRNAs, miR-16-1-3p, miR-103a-3p, let-7a-5p, miR-197-3p, and miR-4660, can target HTR4-a. In the present study, among these five miRNAs associated with the expression of HTR4-a, treatment of cells with mimic or inhibitor of only miR-197-3p resulted in a lower or higher expression of HTR4-a in human A549 cells. Exposure to FA caused suppression of miR-197-3p, which resulted in enhanced expression of HTR4, possibly by reducing the miRNA-mediated cleavage of HTR4-a mRNA. To the best of our knowledge, this is the first study to investigate the epigenetic mechanism underlying FA-induced enhanced expression of HTR4. Our findings suggested that because of suppression of miR-197-3p and hypomethylation of the CpG island in the HTR4 genome, the expression of HTR4 was promoted in A549 cells exposed to FA. When HTR4 was upregulated or overexpressed in A549 cells, some biological effects caused by exposure to FA, including activation of NF-κB, inflammation, and fibrotic responses, were augmented.[19,20] At the same exposure to FA, these effects were attenuated by HTR4 knockout. Therefore, we suggest that enhanced expression of HTR4 caused by epigenetic changes facilitated activation of NF-κB, inflammation, and fibrotic responses in A549 cells after exposure to FA (Figure S14). More types of human lung cells, such as immune cells,[57] may be used to validate the biological mechanisms uncovered in this study, and further studies are ongoing.

HTR4 genetic and epigenetic characteristics within individuals were associated with the prevalence and progression of COPD. First, previous studies demonstrated that HTR4 was a potential genetic risk factor for COPD.[58,59] Activation and enhanced expression of HTR4 increased the production of inflammatory cytokines from human airway cells[60] and were associated with the development of human airway inflammation.[61] The present study showed that functionality and enhanced expression of HTR4 were required for facilitating FA-induced lung injury. Three expression quantitative trait locus (eQTLs) of HTR4 (rs2400642, rs2400643, and rs1465405, Table S11) were retrieved from the GTEx database by using a cutoff of which the absolute value of normalized effect size (NES) was greater than 0.38.[62] The effect of ALT alleles of these three eQTLs could increase the expression of HTR4 relative to the reference alleles. Therefore, ALT alleles of the 3 eQTLs of HTR4 could be related to exacerbation of human airway inflammation. ALT alleles of the other five SNPs of HTR4 were associated with impairment of human lung function (Table S12). Both the impairment of lung function and airway inflammation were the main pathological features of COPD.[63] ALT allele frequencies of the eight HTR4 SNPs were associated with the prevalence of COPD globally. On the other hand, A549 cells treated with FA had lower expression of miR-197 and hypomethylation of the HTR4 CpG island, which resulted in higher expression of HTR4. In the lungs of COPD patients, miR-197 was downregulated, and miR-197 was inversely correlated with airflow obstruction.[64] The reanalysis of the methylation data set of GSE111396 showed that hypomethylation of the HTR4 gene was observed in the lungs of nonsmokers and ex-smokers, who belonged to COPD stage 1−2. This molecular epidemiological evidence further strengthened the linkages between the increased expression of HTR4 and the progression of COPD.

The present study provided mechanistic evidence for the identification of potential biomarkers of genetic susceptibility to exposure to FA by inhalation. Biomarkers of genetic susceptibility are of great significance for defining susceptible subpopulations.[65,66] Exposure to FA by inhalation was associated with an increased risk of COPD.[12,25−29] The specific epigenetic and genetic changes of HTR4 that were associated with the progression and prevalence of COPD included a decreased abundance of miR-197 and hypomethylation of HTR4 genomics, 3 eQTLs (Table S11), and 5 SNPs (Table S12) of HTR4. ALT alleles of the 5 SNPs of HTR4 were associated with impairment of human lung functions, and the other genetic and epigenetic changes of HTR4 were related to enhanced expression of HTR4. Here, functionality and enhanced expression of HTR4 were required to facilitate susceptibility to FA-induced lung injury. Therefore, these specific epigenetic and genetic changes in HTR4 could be potential biomarkers for genetic susceptibility to FA-induced lung injury. Thus, individuals with these biomarkers could be susceptible to lung injury caused by exposure to FA, and lung injury likely promoted the prevalence and progression of COPD. It is well known that tobacco smoke is the primary environmental risk factor for COPD.[11] FA is a major oxidation byproduct of tobacco smoking,[15,17] and inhalation of FA from tobacco smoke is an important contribution to FA exposure.[67]

https://doi.org/10.1021/acs.est.1c07945
Environ. Sci. Technol. XXXX, XXX, XXX−XXX

For smokers, the concentrations of FA in mainstream tobacco smoke were excessively high; even if dilution inspiration was taken into consideration, FA exposures on a per puff basis were in a range of 1.5−19.5 ppm/puff.[15] In addition, indoor smoking was associated with higher levels of FA in indoor air.[15,16] It is possible that individuals with specific genetic or epigenetic changes in HTR4 would be more vulnerable to lung injury caused by exposure to FA from tobacco smoke, especially smokers.[68] The distributions of daily smokers and ALT allele frequencies of the HTR4 SNPs are shown in Figure 6. For the East Asian population, both the percentages of daily smokers and the ALT allele frequencies were top-ranked, suggesting the high prevalence of lung injury caused by exposure to FA in tobacco smoking in the East Asian population. This was consistent with the high prevalence of COPD in China and Japan (Table S13).

In vitro and in vivo data in this study illustrated that HTR4 played a crucial role in determining susceptibility to FA-induced lung injury. By uncovering the genetic risk factors for COPD (specific genetic and epigenetic changes of HTR4) as potential biomarkers of genetic susceptibility to respiratory effects of FA, the present study also suggested that individuals with these biomarkers could be susceptible to lung injury caused by exposure to FA, and this lung injury likely promoted the risk of COPD. The integrative approach for genome analysis, combining the advantage of the CRISPR screen (toxicological mechanisms) and the strength of molecular epidemiology (genes associated with the susceptibility), provided a solution for uncovering the mechanisms underlying the susceptibility to adverse effects of environmental pollutants. By using this approach, this study provided a paradigm for the identification of individual susceptibility to exposure to air pollutants and provided mechanistic evidence for accurately assessing the health risks of environmental chemicals and decision-making.

■ ASSOCIATED CONTENT

Supporting Information

The Supporting Information is available free of charge at https://pubs.acs.org/doi/10.1021/acs.est.1c07945.

Detailed protocols for the methods, supplementary texts for the CRISPR screen, Figures S1−-S15, and Tables S1−−S13 (PDF)

■ AUTHOR INFORMATION

Corresponding Author

Xiaowei Zhang − *State Key Laboratory of Pollution Control & Resource Reuse, School of the Environment, Nanjing University, Nanjing 210023, People's Republic of China;* orcid.org/0000-0001-8974-9963; Email: zhangxw@nju.edu.cn

Authors

Mingming Tian − *State Key Laboratory of Pollution Control & Resource Reuse, School of the Environment, Nanjing University, Nanjing 210023, People's Republic of China*

Pu Xia − *State Key Laboratory of Pollution Control & Resource Reuse, School of the Environment, Nanjing University, Nanjing 210023, People's Republic of China;* orcid.org/0000-0002-1186-378X

Lu Yan − *State Key Laboratory of Pollution Control & Resource Reuse, School of the Environment, Nanjing University, Nanjing 210023, People's Republic of China*

Xiao Gou − *State Key Laboratory of Pollution Control & Resource Reuse, School of the Environment, Nanjing University, Nanjing 210023, People's Republic of China*

John P. Giesy − *Department of Veterinary Biomedical Sciences and Toxicology Centre, University of Saskatchewan Saskatoon, Saskatoon SK S7N 5B3, Canada; Zoology Department, Center for Integrative Toxicology, Michigan State University, East Lansing, Michigan 48824, United States; Department of Environmental Science, Baylor University, Waco, Texas 76798, United States*

Jiayin Dai − *Key Laboratory of Animal Ecology and Conservation Biology, Institute of Zoology, Chinese Academy of Sciences, Beijing 100101, People's Republic of China;* orcid.org/0000-0003-4908-5597

Hongxia Yu − *State Key Laboratory of Pollution Control & Resource Reuse, School of the Environment, Nanjing University, Nanjing 210023, People's Republic of China*

Complete contact information is available at: https://pubs.acs.org/10.1021/acs.est.1c07945

Author Contributions

M.T., P.X., and X.Z. conceived the study and designed the experiments; most of the experiments were conducted by M.T., and M.T. and P.X. completed data analysis. M.T. did the animal experiments with L.Y. and X.G. This paper was written by M.T. and X.Z. with the participation of P.X., J.P.G., H.Y., and J.D.

Notes

The authors declare no competing financial interest.

■ ACKNOWLEDGMENTS

This work is supported by the National Natural Science Foundation of China (grant no. 41977206), Jiangsu Environmental Protection Research Fund (2018001), and the National Key Research and Development Program of China (2019YFC1804004). X.W.Z. was supported by the Fundamental Research Funds for the Central Universities. Prof. Giesy was supported by the Canada Research Chair program and a Distinguished Visiting Professorship in the Department of Environmental Sciences at Baylor University, Waco, Texas, USA.

■ REFERENCES

(1) De Jong, K.; Vonk, J. M.; Imboden, M.; Lahousse, L.; Hofman, A.; Brusselle, G. G.; Probst-Hensch, N. M.; Postma, D. S.; Boezen, H. M. Genes and Pathways Underlying Susceptibility to Impaired Lung Function in the Context of Environmental Tobacco Smoke Exposure. *Respir. Res.* **2017**, *18*, 142.

(2) Shen, H.; Mchale, C. M.; Smith, M. T.; Zhang, L. Functional Genomic Screening Approaches in Mechanistic Toxicology and Potential Future Applications of Crispr-Cas9. *Mutat. Res. Rev. Mutat. Res.* **2015**, *764*, 31−42.

(3) Basu, N.; Goodrich, J. M.; Head, J. Ecogenetics of Mercury: From Genetic Polymorphisms and Epigenetics to Risk Assessment and Decision-Making. *Environ. Toxicol. Chem.* **2014**, *33*, 1248−1258.

(4) Mortensen, H. M.; Euling, S. Y. Integrating Mechanistic and Polymorphism Data to Characterize Human Genetic Susceptibility for Environmental Chemical Risk Assessment in the 21st Century. *Toxicol. Appl. Pharmacol.* **2013**, *271*, 395−404.

(5) Abdo, N.; Xia, M.; Brown, C. C.; Kosyk, O.; Huang, R.; Sakamuru, S.; Zhou, Y.-H.; Jack, J. R.; Gallins, P.; Xia, K.; Li, Y.; Chiu, W. A.; Motsinger-Reif, A. A.; Austin, C. P.; Tice, R. R.; Rusyn, I.; Wright, F. A. Population-Based in Vitro Hazard and Concentration-Response Assessment of Chemicals: The 1000 Genomes High-Throughput Screening Study. *Environ. Health Perspect.* **2015**, *123*, 458−466.

(6) Kasela, S.; Daniloski, Z.; Bollepalli, S.; Jordan, T. X.; Tenoever, B. R.; Sanjana, N. E.; Lappalainen, T. Integrative Approach Identifies Slc6a20 and Cxcr6 as Putative Causal Genes for the Covid-19 Gwas Signal in the 3p21.31 Locus. *Genome Biol.* **2021**, *22*, 242.
(7) Hunter, D. J. Gene-Environment Interactions in Human Diseases. *Nat. Rev. Genet.* **2005**, *6*, 287−298.
(8) Thomas, D. Gene-Environment-Wide Association Studies: Emerging Approaches. *Nat. Rev. Genet.* **2010**, *11*, 259−272.
(9) Gref, A.; Merid, S. K.; Gruzieva, O.; Ballereau, S.; Becker, A.; Bellander, T.; Bergström, A.; Bossé, Y.; Bottai, M.; Chan-Yeung, M.; Fuertes, E.; Ierodiakonou, D.; Jiang, R.; Joly, S.; Jones, M.; Kobor, M. S.; Korek, M.; Kozyrskyj, A. L.; Kumar, A.; Lemonnier, N.; Macintyre, E.; Ménard, C.; Nickle, D.; Obeidat, M. E.; Pellet, J.; Standl, M.; Sääf, A.; Söderhäll, C.; Tiesler, C. M. T.; Van Den Berge, M.; Vonk, J. M.; Vora, H.; Xu, C.-J.; Antó, J. M.; Auffray, C.; Brauer, M.; Bousquet, J.; Brunekreef, B.; Gauderman, W. J.; Heinrich, J.; Kere, J.; Koppelman, G. H.; Postma, D.; Carlsten, C.; Pershagen, G.; Melén, E. Genome-Wide Interaction Analysis of Air Pollution Exposure and Childhood Asthma with Functional Follow-Up. *Am. J. Respir. Crit. Care Med.* **2017**, *195*, 1373−1383.
(10) Xia, P.; Zhang, X.; Xie, Y.; Guan, M.; Villeneuve, D. L.; Yu, H. Functional Toxicogenomic Assessment of Triclosan in Human Hepg2 Cells Using Genome-Wide Crispr-Cas9 Screening. *Environ. Sci. Technol.* **2016**, *50*, 10682−10692.
(11) López-Campos, J. L.; Tan, W.; Soriano, J. B. Global Burden of Copd. *Respirology* **2016**, *21*, 14−23.
(12) Bentayeb, M.; Norback, D.; Bednarek, M.; Bernard, A.; Cai, G.; Cerrai, S.; Eleftheriou, K. K.; Gratziou, C.; Holst, G. J.; Lavaud, F.; Nasilowski, J.; Sestini, P.; Sarno, G.; Sigsgaard, T.; Wieslander, G.; Zielinski, J.; Viegi, G.; Annesi-Maesano, I.; Study, G. Indoor Air Quality, Ventilation and Respiratory Health in Elderly Residents Living in Nursing Homes in Europe. *Eur. Respir. J.* **2015**, *45*, 1228−1238.
(13) Nielsen, G. D.; Larsen, S. T.; Wolkoff, P. Re-Evaluation of the Who (2010) Formaldehyde Indoor Air Quality Guideline for Cancer Risk Assessment. *Arch. Toxicol.* **2017**, *91*, 35−61.
(14) Golden, R. Identifying an Indoor Air Exposure Limit for Formaldehyde Considering Both Irritation and Cancer Hazards. *Crit. Rev. Toxicol.* **2011**, *41*, 672−721.
(15) Godish, T. Formaldehyde Exposures from Tobacco-Smoke-a Review. *Am. J. Publ. Health* **1989**, *79*, 1044−1045.
(16) Paumgartten, F. J. R.; Gomes-Carneiro, M. R.; Amado Xavier De Oliveira, A. C. The Impact of Tobacco Additives on Cigarette Smoke Toxicity: A Critical Appraisal of Tobacco Industry Studies. *Cad. Saude Publica* **2017**, *33*, No. e00132415.
(17) Baker, R. R. The Generation of Formaldehyde in Cigarettes - Overview and Recent Experiments. *Food Chem. Toxicol.* **2006**, *44*, 1799−1822.
(18) Ye, X.; Ji, Z.; Wei, C.; Mchale, C. M.; Ding, S.; Thomas, R.; Yang, X.; Zhang, L. Inhaled Formaldehyde Induces DNA-Protein Crosslinks and Oxidative Stress in Bone Marrow and Other Distant Organs of Exposed Mice. *Environ. Mol. Mutagen.* **2013**, *54*, 705−718.
(19) Shi, Y.-Q.; Chen, X.; Dai, J.; Jiang, Z.-F.; Li, N.; Zhang, B.-Y.; Zhang, Z.-B. Selenium Pretreatment Attenuates Formaldehyde-Induced Genotoxicity in A549 Cell Lines. *Toxicol. Ind. Health* **2014**, *30*, 901−909.
(20) Zhang, X.; Zhao, Y.; Song, J.; Yang, X.; Zhang, J.; Zhang, Y.; Li, R. Differential Health Effects of Constant Versus Intermittent Exposure to Formaldehyde in Mice: Implications for Building Ventilation Strategies. *Environ. Sci. Technol.* **2018**, *52*, 1551−1560.
(21) Krzyzanowski, M.; Quackenboss, J. J.; Lebowitz, M. D. Chronic Respiratory Effects of Indoor Formaldehyde Exposure. *Environ. Res.* **1990**, *52*, 117−125.
(22) Mcgwin, G., Jr.; Lienert, J.; Kennedy, J. I., Jr. Formaldehyde Exposure and Asthma in Children: A Systematic Review. *Environ. Health Perspect.* **2010**, *118*, 313−317.
(23) Jude, J.; Koziol-White, C.; Scala, J.; Yoo, E.; Jester, W.; Maute, C.; Dalton, P.; Panettieri, R., Jr. Formaldehyde Induces Rho-Associated Kinase Activity to Evoke Airway Hyperresponsiveness. *Am. J. Respir. Cell Mol. Biol.* **2016**, *55*, 542−553.
(24) Zeng, X.; Vonk, J. M.; Van Der Plaat, D. A.; Faiz, A.; Paré, P. D.; Joubert, P.; Nickle, D.; Brandsma, C.-A.; Kromhout, H.; Vermeulen, R.; Xu, X.; Huo, X.; De Jong, K.; Boezen, H. M. Genome-Wide Interaction Study of Gene-by-Occupational Exposures on Respiratory Symptoms. *Environ. Int.* **2019**, *122*, 263−269.
(25) Malaka, T.; Kodama, A. M. Respiratory Health of Plywood Workers Occupationally Exposed to Formaldehyde. *Arch. Environ. Health* **1990**, *45*, 288−294.
(26) Neghab, M.; Soltanzadeh, A.; Choobineh, A. Respiratory Morbidity Induced by Occupational Inhalation Exposure to Formaldehyde. *Ind. Health* **2011**, *49*, 89−94.
(27) Yacoub, M.-R.; Malo, J.-L.; Labrecque, M.; Cartier, A.; Lemiere, C. Occupational Eosinophilic Bronchitis. *Allergy* **2005**, *60*, 1542−1544.
(28) Hulin, M.; Simoni, M.; Viegi, G.; Annesi-Maesano, I. Respiratory Health and Indoor Air Pollutants Based on Quantitative Exposure Assessments. *Eur. Respir. J.* **2012**, *40*, 1033−1045.
(29) Nowrin, K.; Sohal, S. S.; Peterson, G.; Patel, R.; Walters, E. H. Epithelial-Mesenchymal Transition as a Fundamental Underlying Pathogenic Process in Copd Airways: Fibrosis, Remodeling and Cancer. *Expet Rev. Respir. Med.* **2014**, *8*, 547−559.
(30) Clark, A.; Jit, M.; Warren-Gash, C.; Guthrie, B.; Wang, H. H. X.; Mercer, S. W.; Sanderson, C.; Mckee, M.; Troeger, C.; Ong, K. L.; Checchi, F.; Perel, P.; Joseph, S.; Gibbs, H. P.; Banerjee, A.; Eggo, R. M. Ctr Math Modelling Infect Dis, C. Global, Regional, and National Estimates of the Population at Increased Risk of Severe Covid-19 Due to Underlying Health Conditions in 2020: A Modelling Study. *Lancet Global Health* **2020**, *8*, e1003−e1017.
(31) Xia, P.; Peng, Y.; Fang, W.; Tian, M.; Shen, Y.; Ma, C.; Crump, D.; O'Brien, J. M.; Shi, W.; Zhang, X. Cross-Model Comparison of Transcriptomic Dose-Response of Short-Chain Chlorinated Paraffins. *Environ. Sci. Technol.* **2021**, *55*, 8149−8158.
(32) Knapen, D.; Stinckens, E.; Cavallin, J. E.; Ankley, G. T.; Holbech, H.; Villeneuve, D. L.; Vergauwen, L. Toward an Aop Network-Based Tiered Testing Strategy for the Assessment of Thyroid Hormone Disruption. *Environ. Sci. Technol.* **2020**, *54*, 8491−8499.
(33) Piñero, J.; Manuel Ramirez-Anguita, J.; Sauch-Pitarch, J.; Ronzano, F.; Centeno, E.; Sanz, F.; Furlong, L. I. The Disgenet Knowledge Platform for Disease Genomics: 2019 Update. *Nucleic Acids Res.* **2020**, *48*, D845−D855.
(34) Clifford, R. L.; Fishbane, N.; Patel, J.; Macisaac, J. L.; Mcewen, L. M.; Fisher, A. J.; Brandsma, C.-A.; Nair, P.; Kobor, M. S.; Hackett, T.-L.; Knox, A. J. Altered DNA Methylation Is Associated with Aberrant Gene Expression in Parenchymal but Not Airway Fibroblasts Isolated from Individuals with Copd. *Clin. Epigenet.* **2018**, *10*, 32.
(35) Zhang, Y.; Schulz, V. P.; Reed, B. D.; Wang, Z.; Pan, X.; Mariani, J.; Euskirchen, G.; Snyder, M. P.; Vaccarino, F. M.; Ivanova, N.; Weissman, S. M.; Szekely, A. M. Functional Genomic Screen of Human Stem Cell Differentiation Reveals Pathways Involved in Neurodevelopment and Neurodegeneration. *Proc. Natl. Acad. Sci. U.S.A.* **2013**, *110*, 12361−12366.
(36) Raudvere, U.; Kolberg, L.; Kuzmin, I.; Arak, T.; Adler, P.; Peterson, H.; Vilo, J. g:Profiler: a web server for functional enrichment analysis and conversions of gene lists (2019 update). *Nucleic Acids Res.* **2019**, *47*, W191−W198.
(37) Hodge, E.; Nelson, C. P.; Miller, S.; Billington, C. K.; Stewart, C. E.; Swan, C.; Malarstig, A.; Henry, A. P.; Gowland, C.; Melén, E.; Hall, I. P.; Sayers, I. Htr4 Gene Structure and Altered Expression in the Developing Lung. *Respir. Res.* **2013**, *14*, 77.
(38) Xu, S.; Zheng, H.; Ma, R.; Wu, D.; Pan, Y.; Yin, C.; Gao, M.; Wang, W.; Li, W.; Liu, S.; Chai, Z.; Li, R. Vacancies on 2d Transition Metal Dichalcogenides Elicit Ferroptotic Cell Death. *Nat. Commun.* **2020**, *11*, 3484.
(39) Cai, X.; Dong, J.; Liu, J.; Zheng, H.; Kaweeteerawat, C.; Wang, F.; Ji, Z.; Li, R. Multi-Hierarchical Profiling the Structure-Activity Relationships of Engineered Nanomaterials at Nano-Bio Interfaces. *Nat. Commun.* **2018**, *9*, 4416.
(40) Lujan, H.; Romer, E.; Salisbury, R.; Hussain, S.; Sayes, C. Determining the Biological Mechanisms of Action for Environmental

https://doi.org/10.1021/acs.est.1c07945
Environ. Sci. Technol. XXXX, XXX, XXX−XXX

Exposures: Applying Crispr/Cas9 to Toxicological Assessments. *Toxicol. Sci.* **2020**, *175*, 5−18.
(41) Arslan-Acaroz, D.; Bayşu-Sozbilir, N. Ameliorative Effect of Boric Acid against Formaldehyde-Induced Oxidative Stress in A549 Cell Lines. *Environ. Sci. Pollut. Res.* **2020**, *27*, 4067−4074.
(42) Andersen, M. E.; Clewell, H. J., Iii; Bermudez, E.; Dodd, D. E.; Willson, G. A.; Campbell, J. L.; Thomas, R. S. Formaldehyde: Integrating Dosimetry, Cytotoxicity, and Genomics to Understand Dose-Dependent Transitions for an Endogenous Compound. *Toxicol. Sci.* **2010**, *118*, 716−731.
(43) Hester, S. D.; Benavides, G. B.; Yoon, L.; Morgan, K. T.; Zou, F.; Barry, W.; Wolf, D. C. Formaldehyde-Induced Gene Expression in F344 Rat Nasal Respiratory Epithelium☆. *Toxicology* **2003**, *187*, 13−24.
(44) Hester, S. D.; Barry, W. T.; Zou, F.; Wolf, D. C. Transcriptomic Analysis of F344 Rat Nasal Epithelium Suggests That the Lack of Carcinogenic Response to Glutaraldehyde Is Due to Its Greater Toxicity Compared to Formaldehyde. *Toxicol. Pathol.* **2005**, *33*, 415−424.
(45) Beane Freeman, L. E.; Blair, A.; Lubin, J. H.; Stewart, P. A.; Hayes, R. B.; Hoover, R. N.; Hauptmann, M. Mortality from Lymphohematopoietic Malignancies among Workers in Formaldehyde Industries: The National Cancer Institute Cohort. *J. Natl. Cancer Inst.* **2009**, *101*, 751−761.
(46) Freeman, L. E. B.; Blair, A.; Lubin, J. H.; Stewart, P. A.; Hayes, R. B.; Hoover, R. N.; Hauptmann, M. Mortality from Solid Tumors among Workers in Formaldehyde Industries: An Update of the Nci Cohort. *Am. J. Ind. Med.* **2013**, *56*, 1015−1026.
(47) Chung, K. F.; Caramori, G.; Adcock, I. M.; Di Stefano, A. Cytokine Inhibition in the Treatment of Copd. *Int. J. Chronic Obstr. Pulm. Dis.* **2014**, *9*, 397−412.
(48) Houghton, A. M. Mechanistic Links between Copd and Lung Cancer. *Nat. Rev. Cancer* **2013**, *13*, 233−245.
(49) Rout-Pitt, N.; Farrow, N.; Parsons, D.; Donnelley, M. Epithelial Mesenchymal Transition (Emt): A Universal Process in Lung Diseases with Implications for Cystic Fibrosis Pathophysiology. *Respir. Res.* **2018**, *19*, 136.
(50) Liu, Q.; Yang, L.; Gong, C.; Tao, G.; Huang, H.; Liu, J.; Zhang, H.; Wu, D.; Xia, B.; Hu, G.; Wang, K.; Zhuang, Z. Effects of Long-Term Low-Dose Formaldehyde Exposure on Global Genomic Hypomethylation in 16hbe Cells. *Toxicol. Lett.* **2011**, *205*, 235−240.
(51) Jones, P. A. Functions of DNA Methylation: Islands, Start Sites, Gene Bodies and Beyond. *Nat. Rev. Genet.* **2012**, *13*, 484−492.
(52) Liang, G.; Weisenberger, D. J. DNA Methylation Aberrancies as a Guide for Surveillance and Treatment of Human Cancers. *Epigenetics* **2017**, *12*, 416−432.
(53) Du, Q.; Luu, P.-L.; Stirzaker, C.; Clark, S. J. Methyl-Cpg-Binding Domain Proteins: Readers of the Epigenome. *Epigenomics* **2015**, *7*, 1051−1073.
(54) Rager, J. E.; Smeester, L.; Jaspers, I.; Sexton, K. G.; Fry, R. C. Epigenetic Changes Induced by Air Toxics: Formaldehyde Exposure Alters Mirna Expression Profiles in Human Lung Cells. *Environ. Health Perspect.* **2011**, *119*, 494−500.
(55) Bai, M.; Zhu, X.-Z.; Zhang, Y.; Zhang, S.; Zhang, L.; Xue, L.; Zhong, M.; Zhang, X. Anhedonia Was Associated with the Dysregulation of Hippocampal Htr4 and Microrna Let-7a in Rats. *Physiol. Behav.* **2014**, *129*, 135−141.
(56) Kozomara, A.; Birgaoanu, M.; Griffiths-Jones, S. Mirbase: From Microrna Sequences to Function. *Nucleic Acids Res.* **2019**, *47*, D155−D162.
(57) Zheng, H.; Gu, Z.; Pan, Y.; Chen, J.; Xie, Q.; Xu, S.; Gao, M.; Cai, X.; Liu, S.; Wang, W.; Li, W.; Liu, X.; Yang, Z.; Zhou, R.; Li, R. Biotransformation of Rare Earth Oxide Nanoparticles Eliciting Microbiota Imbalance. *Part. Fibre Toxicol.* **2021**, *18*, 17.
(58) Ranjan, A.; Singh, A.; Walia, G. K.; Sachdeva, M. P.; Gupta, V. Genetic Underpinnings of Lung Function and Copd. *J. Genet.* **2019**, *98*, 76.
(59) Wilk, J. B.; Shrine, N. R. G.; Loehr, L. R.; Zhao, J. H.; Manichaikul, A.; Lopez, L. M.; Smith, A. V.; Heckbert, S. R.; Smolonska, J.; Tang, W.; Loth, D. W.; Curjuric, I.; Hui, J.; Cho, M. H.; Latourelle, J. C.; Henry, A. P.; Aldrich, M.; Bakke, P.; Beaty, T. H.; Bentley, A. R.; Borecki, I. B.; Brusselle, G. G.; Burkart, K. M.; Chen, T.-H.; Couper, D.; Crapo, J. D.; Davies, G.; Dupuis, J.; Franceschini, N.; Gulsvik, A.; Hancock, D. B.; Harris, T. B.; Hofman, A.; Imboden, M.; James, A. L.; Khaw, K.-T.; Lahousse, L.; Launer, L. J.; Litonjua, A.; Liu, Y.; Lohman, K. K.; Lomas, D. A.; Lumley, T.; Marciante, K. D.; Mcardle, W. L.; Meibohm, B.; Morrison, A. C.; Musk, A. W.; Myers, R. H.; North, K. E.; Postma, D. S.; Psaty, B. M.; Rich, S. S.; Rivadeneira, F.; Rochat, T.; Rotter, J. I.; Artigas, M. S.; Starr, J. M.; Uitterlinden, A. G.; Wareham, N. J.; Wijmenga, C.; Zanen, P.; Province, M. A.; Silverman, E. K.; Deary, I. J.; Palmer, L. J.; Cassano, P. A.; Gudnason, V.; Barr, R. G.; Loos, R. J. F.; Strachan, D. P.; London, S. J.; Boezen, H. M.; Probst-Hensch, N.; Gharib, S. A.; Hall, I. P.; O'Connor, G. T.; Tobin, M. D.; Stricker, B. H. Genome-Wide Association Studies Identify Chrna5/3 and Htr4 in the Development of Airflow Obstruction. *Am. J. Respir. Crit. Care Med.* **2012**, *186*, 622−632.
(60) Bayer, H.; Müller, T.; Myrtek, D.; Sorichter, S.; Ziegenhagen, M.; Norgauer, J.; Zissel, G.; Idzko, M. Serotoninergic Receptors on Human Airway Epithelial Cells. *Am. J. Respir. Cell Mol. Biol.* **2007**, *36*, 85−93.
(61) Kim, T.-H.; An, S.-H.; Cha, J.-Y.; Shin, E.-K.; Lee, J.-Y.; Yoon, S.-H.; Lee, Y.-M.; Uh, S.-T.; Park, S.-W.; Park, J.-S.; Kim, Y.-H.; Choi, J.-S.; Lee, S.-O.; Park, B.-L.; Shin, H.-D.; Park, C.-S. Association of 5-Hydroxytryptamine (Serotonin) Receptor 4 (5-Htr4) Gene Polymorphisms with Asthma. *Respirology* **2011**, *16*, 630−638.
(62) Han, B.; Eskin, E. Interpreting Meta-Analyses of Genome-Wide Association Studies. *PLoS Genet.* **2012**, *8*, No. e1002555.
(63) Berg, K.; Wright, J. L. The Pathology of Chronic Obstructive Pulmonary Disease Progress in the 20th and 21st Centuries. *Arch. Pathol. Lab Med.* **2016**, *140*, 1423−1428.
(64) Musri, M. M.; Coll-Bonfill, N.; Maron, B. A.; Peinado, V. I.; Wang, R.-S.; Altirriba, J.; Blanco, I.; Oldham, W. M.; Tura-Ceide, O.; García-Lucio, J.; De La Cruz-Thea, B.; Meister, G.; Loscalzo, J.; Barberà, J. A. Microrna Dysregulation in Pulmonary Arteries from Chronic Obstructive Pulmonary Disease Relationships with Vascular Remodeling. *Am. J. Respir. Cell Mol. Biol.* **2018**, *59*, 490−499.
(65) Zhang, J.; Yin, L.; Liang, G.; Liu, R.; Fan, K.; Pu, Y. Detection of Cyp2e1, a Genetic Biomarker of Susceptibility to Benzene Metabolism Toxicity in Immortal Human Lymphocytes Derived from the Han Chinese Population. *Biomed. Environ. Sci.* **2011**, *24*, 300−309.
(66) Kim, H.-M.; Kim, D.-S.; Chung, Y. Environmental Genomics Related to Environmental Health Biomarker. *Mol. Cell. Toxicol.* **2006**, *2*, 75−80.
(67) Zhang, L.; Steinmaus, C.; Eastmond, D. A.; Xin, X. K.; Smith, M. T. Formaldehyde Exposure and Leukemia: A New Meta-Analysis and Potential Mechanisms. *Mutat. Res. Rev. Mutat. Res.* **2009**, *681*, 150−168.
(68) Ritchie, H.; Roser, M. Smoking, 2013, https://ourworldindata.org/smoking (accessed 2022-04-18).

https://doi.org/10.1021/acs.est.1c07945
Environ. Sci. Technol. XXXX, XXX, XXX−XXX

Supplementary Materials

Toxicological Mechanism of Individual Susceptibility to Formaldehyde-Induced Respiratory Effects

Mingming Tian, Pu Xia, Lu Yan, Xiao Gou, John P. Giesy, Jiayin Dai, Hongxia Yu, Xiaowei Zhang

Corresponding author: Xiaowei Zhang

Number of pages: 70

Number of tables: 13

Number of figures: 15

Detail protocols for Methods

Sequencing of single clones. Ten (10) single clones were randomly selected from the genome-scale knockout A549 cells library using limited dilution. Cell mass reproduced from a single cell was collected, and their genomic DNA was extracted using QIAamp DNA Mini Kit (Qiagen). Genomic DNA in wild type A549 cells was also extracted as a control. A part of the genomic DNA was subjected to two polymerase chain reactions (Nested-PCR, see below) to amplify sgRNA inserts, the products of the second PCR were agarose gel-extracted, purified (Wizard SV Gel and PCR Clean-Up System; Promega), and sequenced on a HiSeq X-Ten (Illumina) to get sequence of the sgRNA in each clone. The PCR products from the amplification of DNA segments surrounding sgRNA-targeted sequences were purified (Promega Wizard SV gel and PCR clean-up system) and deoxyadenosine tail was added to the 3' end using Taq DNA polymerase (DBI Bioscience) according to manufacturer's recommendations. Then, products of PCR were linked to pMD 19-T Vectors (TaKaRa) to perform T vector sequencing. Five positive clones for each sgRNA were selected and sequenced using Sanger sequencing (Applied Biosystems SeqStudio, Thermo Scientific).

Generation of HTR4 knockout and overexpression cell lines. Oligonucleotide pairs (GeneScript) of sgRNA against a common sequence of the six transcript variants of HTR4 (Forward: 5'-caccGAAATCGATGCCGTTGTGAGC; Reverse: 5'-aaacGCTCA CAACGGCATCGATTTc) and non-targeting sgRNA (Forward: 5'-caccGGCTCGGTC CCGCGTCGTCG; Reverse: 5'-aaacCGACGACGCGGGACCGAGCC) were annealed

and cloned to link with pGK1.1 linear plasmid (Genloci) using T4 DNA ligase (Thermo Scientific). The recombinant vectors were transiently electro-transfected into A549 cells using an electro-porator (Celetrix). And 72 h post-transfection, the A549 cells were exposed to puromycin of 1.0 μg/mL for 48 h to remove the cells of negative transfection. The remaining cells were seeded into wells of ten of 96-well plates by limited dilution to select single cell clones. Western blotting (methods detailed below) and sequencing (methods were same as above single clone sequencing) were used to confirm knockout of HTR4 in A549 cells. To construct HTR4 overexpression A549 cells, the CDS of human HTR4 transcript variant a (HTR4-a, NM_001040169.2) was synthesized (GeneScript) and was cloned into a plenti-Puro plasmid (GeneScript) using T4 DNA ligase (Thermo Scientific). The recombinant plasmid was sequenced using Sanger sequencing (Applied Biosystems SeqStudio, Thermo Scientific). The recombinant plasmid or empty vector was transfected into HEK293T cells with two viral packaging plasmids pVSVg and psPAX2 (Addgene). The method for co-transfection of these plasmids was the same with that for GeCKO library plasmids. After 60 hours post-transfection, the supernatants were centrifuged at 24 000 rpm for 2 h at 4 °C and collected to produce concentrated lent virus. The transfection of A549 cells and screening using puromycin were same as procedures of GeCKO cell lines. Western blotting and real-time quantitative PCR were carried out to validate overexpression of HTR4 in A549 cells as described below.

Western blotting. For detection of HTR4, 60 μg of total protein for each sample was loaded into a SDS-PAGE gel. The primary antibodies (ab60359 for HTR4; ab9485 for

GAPDH, Abcam) were diluted in a ratio of 1:1000, the secondary antibody (IRDye 800 cw, Li-COR) was diluted in a ratio of 1:10000. An Odyssey Infrared Imaging System (Odyssey) was used to analyze the fluorescence signal. For analysis of the other proteins, the primary antibodies (ab76302 for p-p65, ab40772 for E-cadherin, ab32575 for α-SMA, ab216347 for Snail, Abcam) were used in a dilution ratio of 1:1000. 1.0 μg/μL of total protein was subjected to an auto protein analysis system (ProteinSimple, Wes) according to the protocol of the instrument. Lysate was withdrawn through a capillary, subjected to electrophoretic separation of proteins by size, and followed by HRP-based detection of target proteins using an HRP-conjugated secondary antibody (1:100, Thermo Scientific, 32260). Graphs of protein bands were produced by the workstation of instrument (Compass Software).

Immunofluorescence analysis 1×10^5 A549 cells were seeded into each well of 12 wells plates of which a coverslip (Thermo Scientific) was placed on the bottom, and four coverslips were for each treatment. After treatment with FA or vehicle for 24 hours, the A549 cells on coverslips were fixed with 4% paraformaldehyde for 15 min at room temperature and permeabilized with 0.3% Triton X-100 for 10 min on ice. The cells were blocked using 1% BSA in PBST for 30 min at room temperature. The coverslips were incubated with primary antibody for p-p65 (ab86299, Abcam, 1: 500) at 4℃ overnight. A secondary antibodies (ab150077, Abcam, 1: 500) was used and the incubation was at room temperature for 1 h in dark. The coverslips were mounted in ProLong Gold Antifade Reagent with DAPI (Invitrogen) and the fluorescence signaling was analyzed using a Zeiss laser scanning confocal microscope (Zeiss LSM 880 with

Airyscan). All the images were obtained continuously under the same condition of the microscope. Mean of integrated optical density per unit area (MIOD) for p-p65 in whole cells and nuclear were determined by using of Image-Pro Plus 6.0 software after transforming the images of areas of interest to grayscale images. Four coverslips were for each treatment and three random views were selected for each coverslip to perform the analysis. Mean value of MIOD of the three views for each coverslip was used in the followed calculation. The formulate for calculation of relative potency (ReP) of nuclear p-p65 was as followed:

$$\text{ReP of nuclear p-p65} = \frac{(\text{nuclear MIOD} - \text{whole cell MIOD})}{(\text{nuclear MIOD}_{\text{WT,Ctrl}} - \text{whole cell MIOD}_{\text{WT,Ctrl}})}$$

Exposure of animals to FA. Wild type ($HTR4^{+/+}$) and $HTR4^{+/-}$ C57BL/6 mice (KOCMP-23817-htr4) were purchased from Cyagen Biosciences. $HTR4^{-/-}$ mice were generated by $HTR4^{+/-}$×$HTR4^{+/-}$ breeders. All mice (male) were 8-9 weeks of age (weight: 23.1- 26.4 g) at the time of FA exposure. Experiments with animals were conducted in accordance with regulations of the Institutional Animal Care and Use Committee (IACUC) of Nanjing University. For sub-acute exposure, the concentration of FA in exposure chamber was 22.0 ppm (20.6-23.5 ppm). For sub-chronic exposure, it was a mimic of exposure to FA in occupational environment, the concentration of FA for high dose group was 4.0 ppm (3.1-4.7 ppm),[1] and it was 0.40 ppm (0.29-0.48 ppm) for low dose group.[2] For the sub-acute exposure, mutant mice ($HTR4^{+/-}$ or $HTR4^{-/-}$) were assigned to the following 2 groups (n = 6 per group): mice subjected to daily FA inhalation, and phosphate-buffered saline (PBS, Sigma) inhalation respectively.

Correspondingly, wild type (HTR4 $^{+/+}$) mice were also assigned to similar 2 groups. An ultrasonic nebulizer device (Yuehua) coupled to a standard glass chamber (0.7 m×0.3 m×0.3 m, Beijing YSKD Bio-technology) was used to generate a constant airstream from an aqueous solution of formalin diluted to 0.2 wt.% of FA (PBS was used as the diluent). Samples of air in exposure chambers were collected every 20 min, concentrations of FA, ambient temperature and humidity levels were measured by a PPM-400st analyzer (PPM Technology), and concentrations of FA were 20.6-23.5 ppm. The mice (six mice in one chamber) were exposed via inhalation of either FA or PBS for 14 consecutive days at 2h/day. For the sub-chronic exposure, HTR4 $^{-/-}$ mice were assigned to the following 3 exposures (n = 6 per group): two groups of mice were challenged by inhalation of one of two concentrations of FA, and the other group of mice was challenged by inhalation of PBS. Correspondingly, wild type (HTR4 $^{+/+}$) mice were also assigned to similar 3 groups. Aqueous solutions of formalin diluted to 0.04 wt.% and 0.004 wt.% of FA were used to generate airstream, and the concentrations of FA in chambers were 3.1-4.7 ppm and 0.29-0.48 ppm, respectively. The mice (six mice in one chamber) were administrated FA or PBS by inhalation for 5 weeks at 4h/day. During the exposure period, the ambient temperature and humidity in exposure chambers were maintained at 20-24 °C and 70%-85%, respectively. The air flow rate (10 L/min) was controlled by the nebulizer.

Lung function measurements. 24 hours after the last exposure, all mice were anesthetized with an intraperitoneal injection of 2.5% avertin (200 μL/10 g weight of mouse). A rodent ventilator (flexiVent, SCIREQ) was used to measure the resistance

of the respiratory system (Rrs) of each mouse. Each mouse was challenged with increasing dose of nebulized methacholine (MCh, Sigma) (0, 4, 12 and 40 mg/kg body weight) for 30 seconds. Maximal Rrs were measured within 3 min after challenge of each dose of MCh at intervals of 1 min.

Analyses of inflammatory cells and cytokines in bronchoalveolar lavage fluid (BALF). After measurements of lung function, BALF was collected from 0.6 mL PBS (Sigma) for the right lung of each mouse. The supernatant from centrifugation (2000 rpm, 6 min, 4 °C) of BALF was subject to enzyme-linked immunosorbent assay (ELISA) for determination of cytokines (IL6 and TGFβ1) according to the manufacturer's instruction (R&D, VAL604 for IL6, VAL611 for TGFβ1). Pellets of cells from BALF were collected and resuspended in PBS, and total cells were counted by using a TC20 Automated Cell Counter (Bio-Rad), differential inflammatory cells were counted after Wright-Giemsa staining (Diff-Quick stain kit, YEASEN).

Histological analysis. The left lungs of mice were removed and fixed in 10% formalin solution for 48 hours. They were then dehydrated and embedded in paraffin, and 5 μm sections were cut and stained with hematoxylin and eosin (H&E) or Masson's trichrome. The severity of airways fibrosis (Masson's trichrome staining) was semi-quantitatively scored according to the scale proposed by Ashcroft [3] and modified by Hübner.[4]

Immunohistochemical analysis Sections of lung were treated with 0.3% H2O2 (Sigma) for 20 min after deparaffinization, rehydration and antigen retrieval. Anti-NF-κB p65 (phosphor S536) (ab86299, Abcam) was used at dilution ratio of 1: 200 for detection of p-p65 protein. After overnight incubation at 4 °C, the sections were

incubated with secondary antibodies (anti-rabbit IgG, ab6112, 1: 500) for 1 hour at room temperature. DAB Quanto Kit (Thermo Scientific) was used to incubate the sections according to the manufacturer's instruction. The sections were then counterstained with haematoxylin. Images of the slides were obtained by using an auto-scanner (3DHistech, Pannoramic MIDI). Counts of positive cell nuclei (in brown) and total cell nuclei (in blue+ in brown) were analyzed by using Image-Pro Plus 6.0 software, the percentage of p-p65 positive nuclei was calculated through dividing over the number of total nuclei.

Measurement of proinflammatory cytokines and TGFβ1. Proinflammatory cytokines (IL6 and IL8) and TGFβ1 secreted from A549 cells into cellular supernatant were quantified using Valukine (R&D) ELISA Kits and Quantikine ELISA Kit (R&D), respectively. The cellular culture was centrifuged and treated according to manufacturer's protocols. Absorbance was measured at 450 nm using with a Synergy H4 Hybrid Multi-Mode Microplate reader (BioTek).

RNA oligoribonucleotides and transfection. miRNA (let-7a-5p, miR-103a-3p, miR-197-3p and miR-16-1-3p) mimics, inhibitors, and negative controls were provided by GenePharma (Shanghai, China; see Table S3). 2×10^5 A549 cells per well were seeded into 12-well plates. RNA oligoribonucleotides and lipofectamine 2000 (Thermo Scientific) were diluted using Opti-MEM Reduced Serum Medium (Thermo Scientific). The protocols for transfection were according to manufacturer's recommendation about lipofectamine 2000. When cells were grown to 80% confluence, the transfection was carried out using RNA oligoribonucleotides-lipid complex. Final concentrations of

RNA oligoribonucleotides were 25 nM, and 3 μL of lipofectamine 2000 was added into each well. Total RNA containing small RNA was extracted (RNeasy Plus Mini Kit, Qiagen) after 36 hours post transfection.

Retrieve genes associated with COPD susceptibility in DisGeNET database. DisGeNET is a database containing the collections of genes and variants associated with human diseases.[5] There were 12 disease items that were similar with COPD in DisGeNET database.[6, 7] For the genes in each disease item, two criteria including the gene-disease association score was greater than or equal to 0.09 (a tenth of the max score) and the number of PMID (PubMed ID) was more than 0, were used to remove the genes with low relevancy. Finally, a total of 409 genes were identified as the genes associated with genetic susceptibility of COPD.

Reanalysis of methylation dataset Methylation dataset of GSE111396 [8] in NCBI was reanalyzed in R using DESeq2 package.[9] Samples from non-smokers and ex-smokers were selected and were grouped by COPD stages. The gene annotation for each probe was according to Illumina Human Methylation 450 Bead Chip (GPL13534). The criteria (Log2 foldchange was less than -0.26 and *p* value was less than 0.01) were used to identify hypomethylated genes, and the probes with the minimum Log2 foldchanges were retained.

Data of COPD prevalence. The data for COPD prevalence in different regions around the world were obtained from the previous reports, in which the COPD criterion of the fixed ratio based on (forced expiratory volume in 1 second, FEV1)/(forced vital capacity, FVC) < 70% with post-bronchodilator spirometry was used.[10]

Genetic variants of HTR4. The HTR4 variants, which were associated with human lung function, were obtained from previously published studies. In addition, the expression quantitative trait loci (eQTLs) of HTR4 in GTEx database were obtained by using a cutoff of >0.38 for the absolute value of normalized effect size (NES).[11] A SNP (rs4905179) of SERPINA1 gene was a reference variant associated with increased risk of COPD.[12]

Allele frequency analysis. Allele frequencies of single nucleotide polymorphisms (SNPs) in different populations were achieved from Human 1000 Genomes Project through "MafDb.1Kgenomes.phase3.GRCh38" in R.[13]

198 **Supplementary texts for CRISPR screen**

199 Genome-scale CRISPR knockout (GeCKO) was a technology of genome editing by
200 using CRISPR-Cas9. There is a CRISPR-Cas9 plasmid pool, and each plasmid consists
201 of a sgRNA targeting one gene, Cas9 and puromycin resistance. The plasmid pool
202 contains 64751 sgRNAs targeting 18080 genes with an average of 3−4 sgRNAs per
203 gene. The sgRNAs work as barcodes that can be identified and quantified by deep
204 sequencing. The GeCKO plasmids were merged into the lentiviral vectors by lentivirus
205 package, and then lentiviral vectors were used to deliver sgRNA plasmids with Cas9
206 and puromycin marker into A549 cells. Stable transduction of GeCKO plasmids can be
207 achieved by lentivirus transfection. By optimizing the used lentivirus volume for
208 multiplicity of infection (MOI) of 0.3, one plasmid was transduced into one A549 cell
209 when transducing GeCKO plasmid pool into enough A549 cells. After removing the
210 A549 cells with negative transduction by treatment of puromycin, one CRISPR-Cas9
211 plasmid was transduced into each A549 cell, and then only one gene in each A549 cell
212 was knockout. Detailed protocols can be available in some previous studies.[14, 15]

213 CRISPR-Cas9 can mediate absolutely loss-of-function of a specific gene by
214 deleting one or several DNA sections in the coding sequence (CDS) of the gene. By
215 using GeCKO plasmids, genome-scale knockout can be achieved in human cells, and
216 only one gene is knockout in one cell. The GeCKO is a proven technology which has
217 been widely used in functional genomics. Some conventional technologies, such as
218 siRNA, only mediate inhibition of gene expression, rather than gene knockout. Detailed
219 statements can be available in some review papers.[16, 17]

Firstly, before lentivirus packaging, we qualified the GeCKO plasmids pool consisting of 64751 sgRNA plasmids. Greater than 98% of the sgRNAs were covered at an abundance of at least 10 reads (Figure S1), indicating a relatively complete representation of sgRNAs. Secondly, when the genome-scale knockout A549 cells were established, 10 single clones were randomly selected from the cells pool. By deep sequencing and single clone sequencing, we confirmed that only one CRISPR-Cas9 plasmid was transduced into one A549 cell, and the corresponding gene was disrupted (see Table S5). Thirdly, when CRISPR-Cas9 plasmid was transduced into A549 cell, the sgRNA sequence can be merged into the genome of A549 cell, the sgRNAs in A549 cells work as barcodes that can be identified and quantified by deep sequencing. Enough genome-scale knockout A549 cells (3×10^7 cells) were collected, the genomic DNA was extracted, and sgRNAs sequences were analyzed by deep sequencing. The number and abundance of sgRNAs were identified and quantified. To make sure a gene was knockout, a criteria was used: when the abundance of a sgRNA was more than 10 reads, the sgRNA was regarded as an effective sgRNA which may mediate gene knockout.[14, 15] In the genome-scale knockout A549 cells, 17678 genes were deleted, and the sgRNAs targeting the remaining 402 genes didn't meet the criteria (Figure S2).

In the CRISPR screen, if a sgRNA knocked out a gene required for cellular resistance to FA, the gene-knockout cells would be more sensitive to FA than wild-type cells. The sgRNAs for that gene would be underrepresented in surviving cells compared with their representations in untreated cells, and that gene was termed underrepresented gene. By contrast, if a sgRNA knocked out a gene required for cellular sensitivity to

242 FA, the gene-knockout cells would be more resistant to FA than wild-type cells. The
243 sgRNAs for that gene would be overrepresented in surviving cells, and that gene was
244 termed overrepresented gene.
245

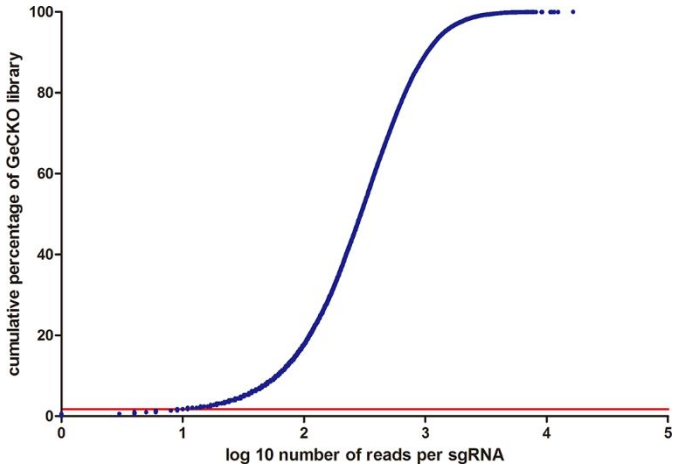

Figure S1 Cumulative distribution of sequencing reads for each sgRNA in the genome-scale CRISPR knockout (GeCKO) plasmid library. Each dot represented one sgRNA. Dots below the red line indicated that less than 1.7 % sgRNAs were covered by less than 10 reads.

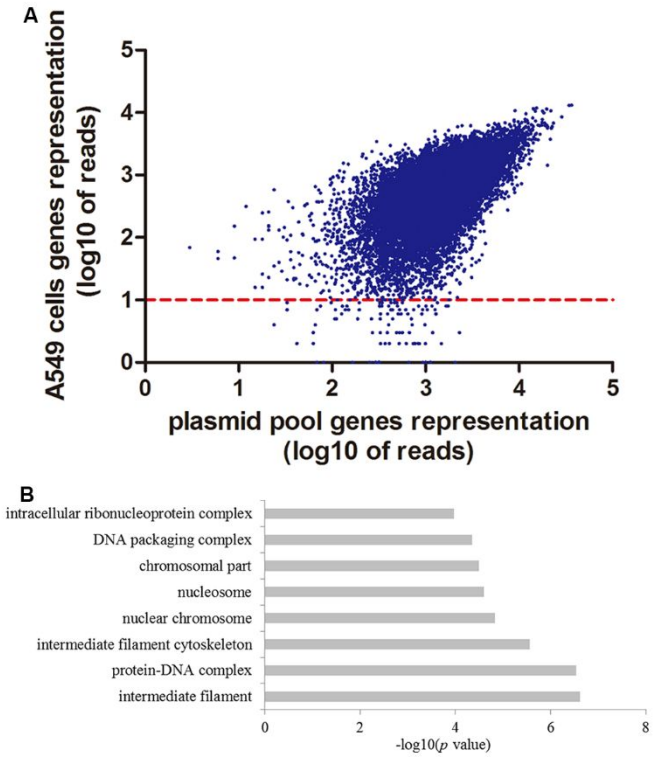

Figure S2 Quality analysis of genome-scale knockout A549 cell lines. **A** Comparison of gene representation between in the GeCKO plasmid pool and in the transduced A549 cells. Dots below the red lines indicated that less than 2.3% of genes were presented at less than 10 reads. **B** Gene Ontology (GO) term analysis of the 402 genes that were not knocked out in A459 cells after transfection, these genes enriched significantly eight Gene Ontology terms which are associated with basic life support for cell growth.

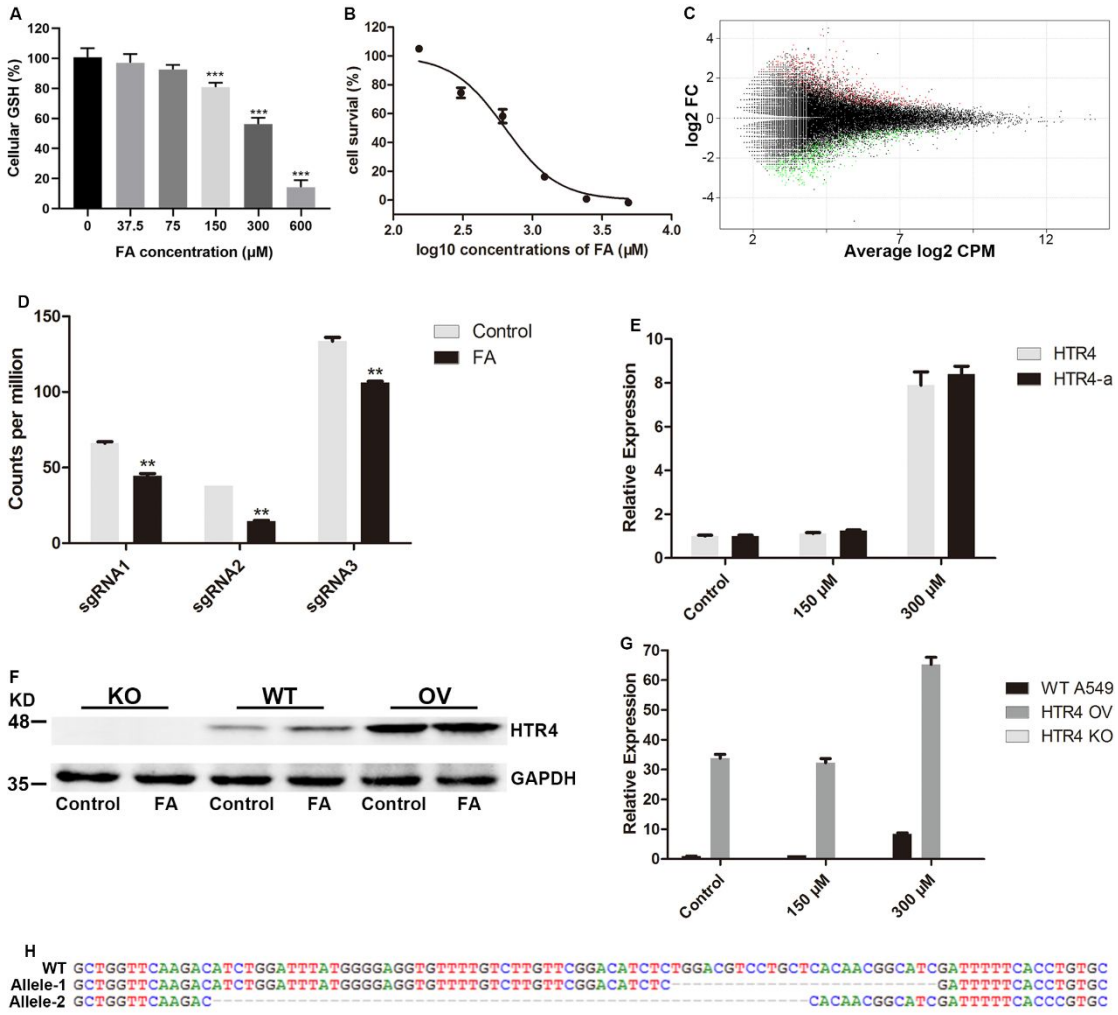

Figure S3 Evaluation of glutathione levels and viability of A549 cells, analysis of sgRNA representation after CRISPR screening and characterization of HTR4 expression in A549 cells. **A** Levels of cellular glutathione (GSH) in wild type A549 cells after exposure to formaldehyde (FA) for 24h, bar plot represented mean with SEM (n=4), ***p <0.001 compared with vehicle by one-way ANOVA test. **B** Cellular viability of wild type A549 cells after exposure to FA for 24h (n=4). **C** Analysis of sgRNA representation in treated (150 μM of FA) versus control cells; each dot represented one sgRNA. Red dots presented over-represented sgRNAs and green dots presented under-represented sgRNAs (FDR<0.05), (counts per million reads ,CPM; fold change, FC). **D** Abundance of individual sgRNA targeting HTR4 in surviving cells after exposure to FA or vehicle (control) in CRISPR screening, bar plot represented mean with SEM (n=2), **p <0.01 compared with control by two-way ANOVA test followed by Bonferroni post-tests. **E** mRNA expression of HTR4 and HTR4-a in wild type A549 cells exposed to negative control or FA (150 or 300 μM). The expression was relative to the expression of HTR4 mRNA in cells treated with negative control. GAPDH was the housekeeping gene. **F** Representative western blotting analysis of HTR4 protein in HTR4 knockout (KO), wild type (WT) and HTR4 overexpression (OV) A549 cells exposed to negative control or 300 μM of FA. **G** mRNA expression of HTR4-a in WT, HTR4 OV and KO A549 cells exposed to negative control or FA (150 or 300 μM), expression of HTR4-a was negative in HTR4 KO cells. The expression was relative to the expression of HTR4-a mRNA in WT cells

treated with negative control. GAPDH was the housekeeping gene. **H** Alignment of HTR4 sequence sections in WT A549 cells and mutant alleles in HTR4-null cells. For panel **E**, **F** and **G**, the FA exposure was for 24h, the bars represented means with SEMs (n=4).

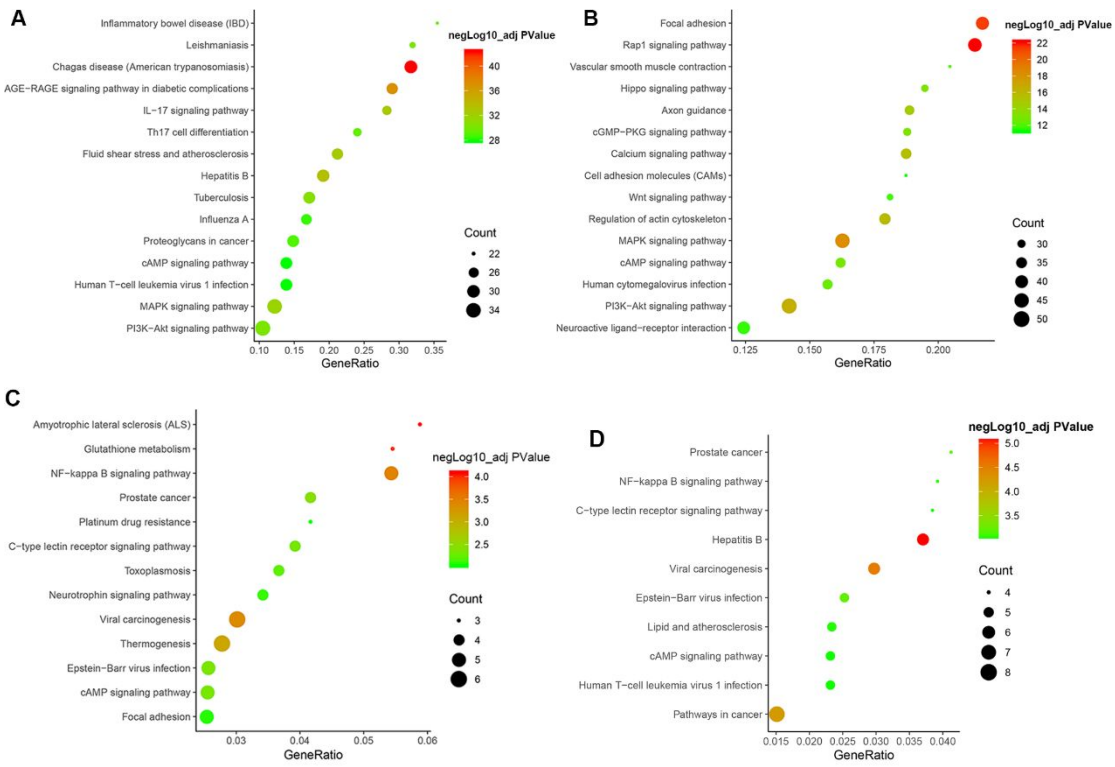

Figure S4 KEGG pathways analysis of 409 genes of COPD susceptibility (**A**) and 2085 hypomethylated genes in COPD lung (**B**), and top 15 pathways were presented. **C** 13 KEGG pathways significantly enriched (adjusted *p*-value <0.01) by 168 under-represented genes from CRISPR screen. **D** Top 10 KEGG pathways enriched by the genes in the molecular initiating event (MIE, covalent binding of protein) of the AOP in Figure **1C**. GeneRatio was the ratio of number of the covered genes in each pathway and number of total genes in the corresponding pathway.

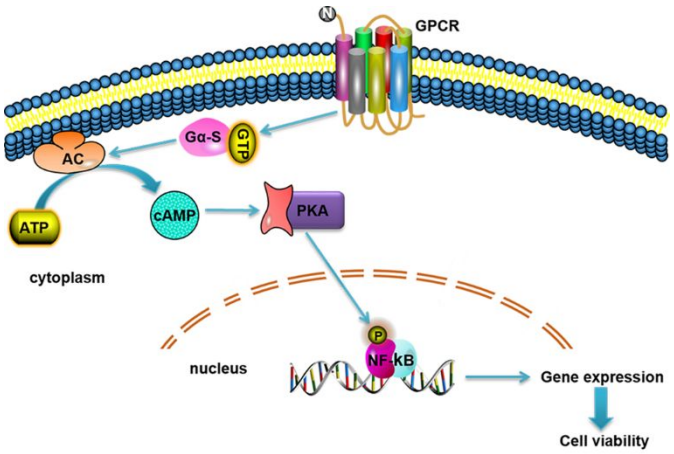

Figure S5 Upstream HTR4 was linked to NF-κB signaling in cAMP signaling pathway. HTR4 is an initiation gene in cAMP signaling pathway,[18, 19] and the coded protein is a G-protein coupled receptor (GPCR) located in cell membrane. At the same time, activation of NF-κB was regulated by cAMP/ protein kinase A (PKA) signaling.[20, 21] This biological pathway showed the linkages among HTR4, cAMP signaling pathway and NF-κB signaling pathway in Kyoto Encyclopedia of Genes and Genomes (KEGG) pathway database.

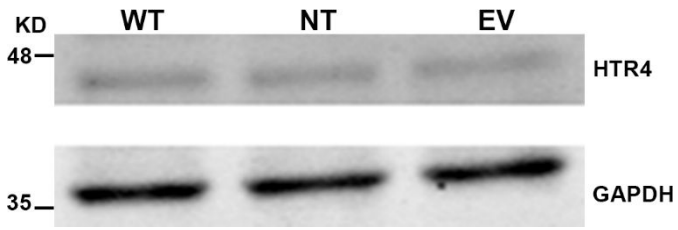

Figure S6 Representative western blotting analysis of HTR4 protein levels in wild type (WT) A549 cells and WT cells transfected with non-targeting (NT) sgRNA or empty vector (EV) plasmid.

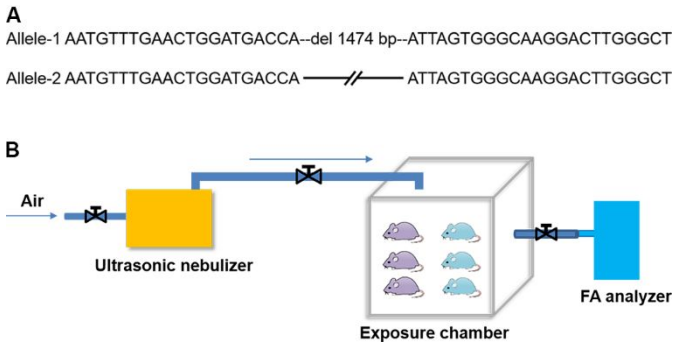

Figure S7 Overview of the *in vivo* inhalation exposure to FA. **A** Sequence sections of mutant (Allele-1) and wild type (Allele-2) alleles of HTR4 in HTR4$^{+/-}$ mice, **B** Schematic of inhalation exposure of mice to FA.

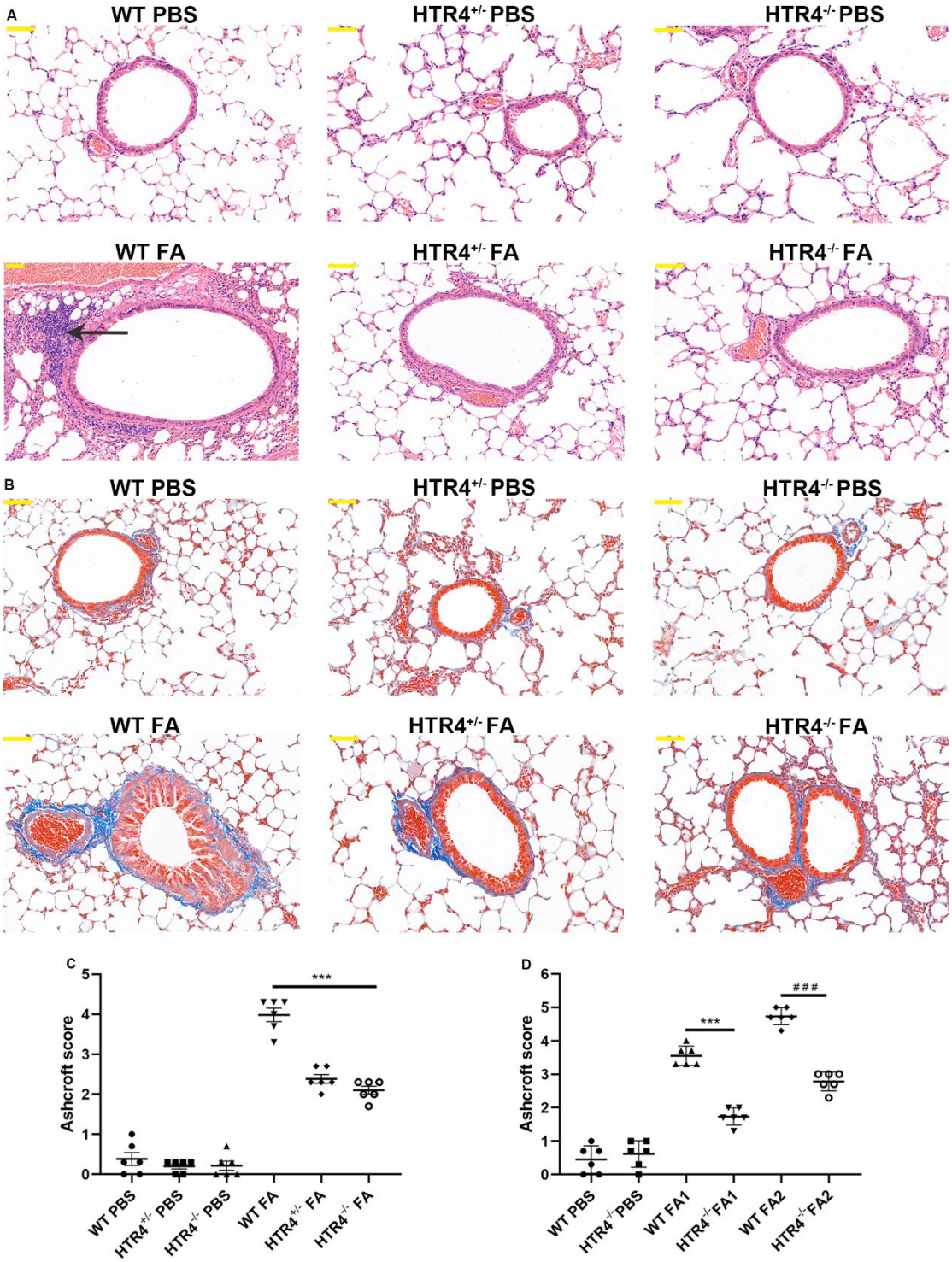

Figure S8 A and **B** Histology of lung airway sections of wild type (WT), HTR4$^{+/-}$ and HTR4$^{-/-}$ mice challenged by 14 days of FA or phosphate-buffered saline (PBS) inhalation. Panel **A** are hematoxylin and eosin (H&E) staining, and panel **B** are Masson trichrome staining. Black arrow points positions with inflammatory cells infiltration. Yellow scale bars represent 100 μm. All histological images were representative, and 6 images for each treatment were evaluated. **C** and **D** Ashcroft score for grade of airway fibrosis in the lung of mice after sub-acute (14 days, panel **C**) or sub-chronic (5 weeks, panel **D**) exposure to FA. In panel **D**, FA1 and FA2 represented low dose and high dose of FA (FA1, low dose: 0.29-0.48 ppm; FA2, high dose: 3.1-4.7 ppm), respectively. For

panel **C** and **D**, bars represented means with SEMs (n=6) and means with SD (n=6), respectively. ***p<0.001 and $^{###}p$<0.001 compared with WT mice by one-way ANOVA test.

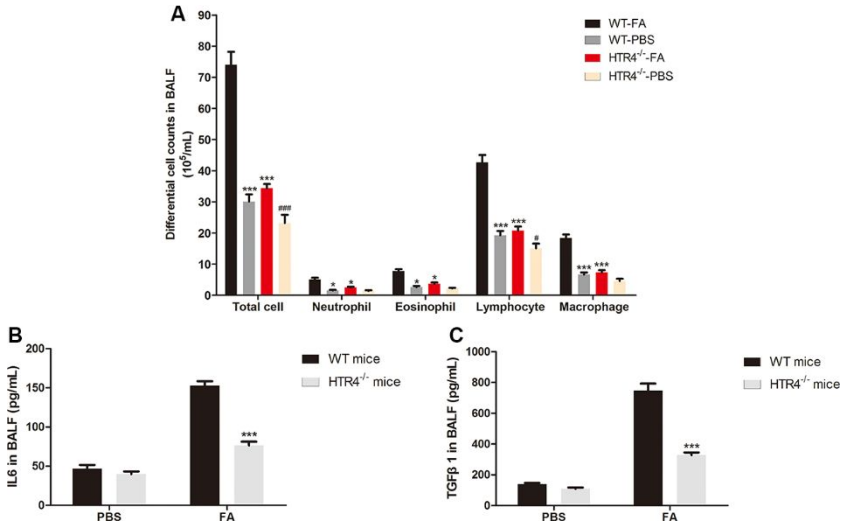

Figure S9 Counts of immune cells (**A**) and the concentrations of IL6 (**B**) and TGFβ1 (**C**) in bronchoalveolar lavage fluid (BALF) from WT or HTR4-null mice challenged by inhalation of FA or PBS for 2 weeks. For all panels, bar plot represented mean with SEM (n=6 mice), *p <0.05, ***p <0.001 compared with WT mice exposed to FA by two-way ANOVA test followed by Bonferroni post-tests, $^{\#}p$ <0.05, $^{\#\#\#}p$ <0.001 compared with HTR4 $^{-/-}$ mice exposed to FA by two-way ANOVA test followed by Bonferroni post-tests.

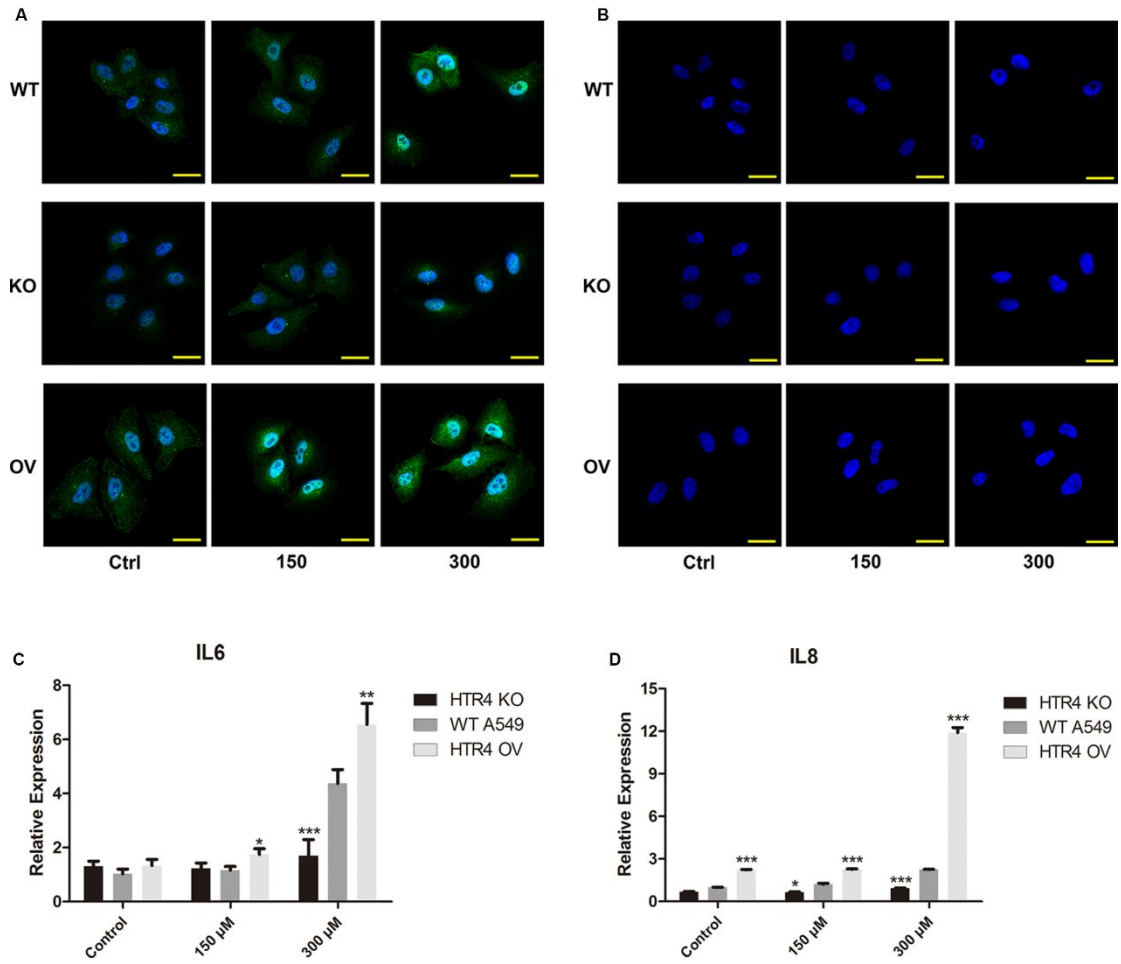

Figure S10 Expression of p-p65 (**A** merged and **B** DAPI) and proinflammatory cytokines (**C** IL6 and **D** IL8) were detected using immunofluorescence and RT-qPCR respectively, in HTR4 knockout (KO), wild type (WT) and HTR4 overexpression (OV) A549 cells exposed to 0 (Ctrl, Control), 150 and 300 μM of FA for 24h. For panel C and D, the expression was relative to mRNA expression of IL6 and IL8 in WT cells treated with negative control, respectively. GAPDH was the housekeeping gene. The yellow scale bars represent 20 μm. Bar plot represented mean with SEM (n=4), *p <0.05, **p <0.01 and ***p <0.001 compared with WT cells by two-way ANOVA test followed by Bonferroni post-tests.

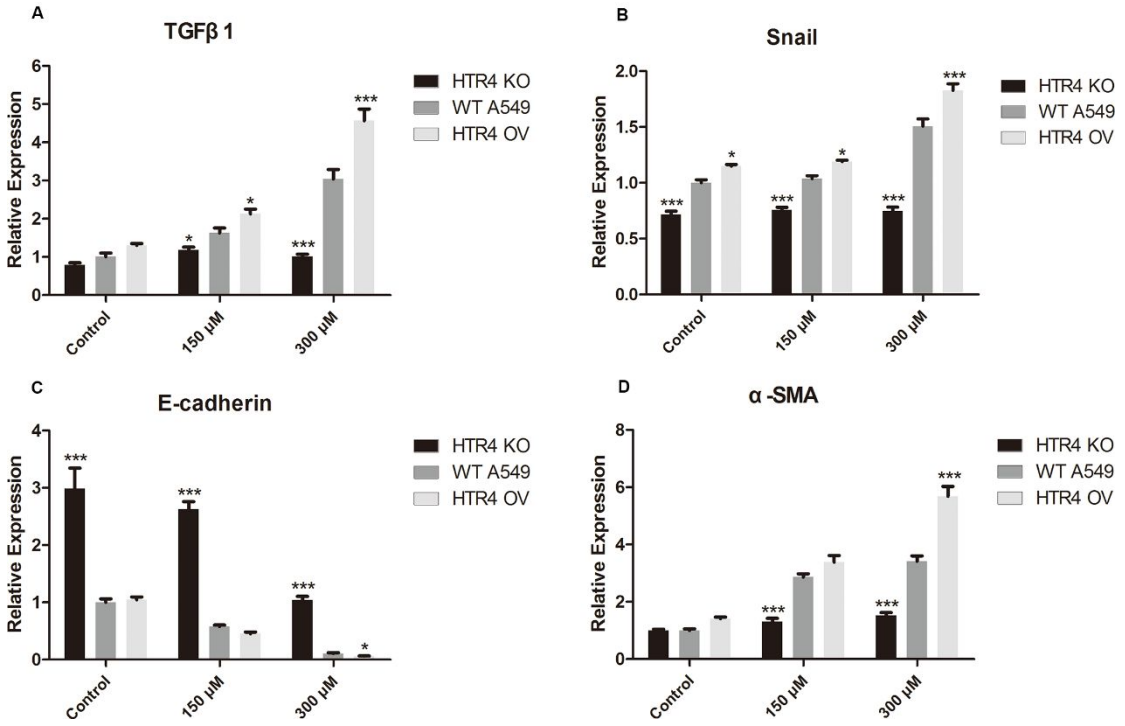

Figure S11 Relative expressions of fibrogenesis biomarkers detected using RT-qPCR in three A549 cell lines exposed to 0 (negative control), 150 and 300 μM of FA for 24h, respectively. **A** for TGFB1 (TGFβ1), **B** for SNAI1 (Snail), **C** for CDH1 (E-cadherin), **D** for ACTA2 (α-SMA). For each panel, the expression was relative to mRNA expression of the corresponding biomarker in WT cells treated with negative control. GAPDH was the housekeeping gene. Bar plot represented mean with SEM (n=4), **p* <0.05 and ****p* <0.001 compared with WT cells by two-way ANOVA test followed by Bonferroni post-tests.

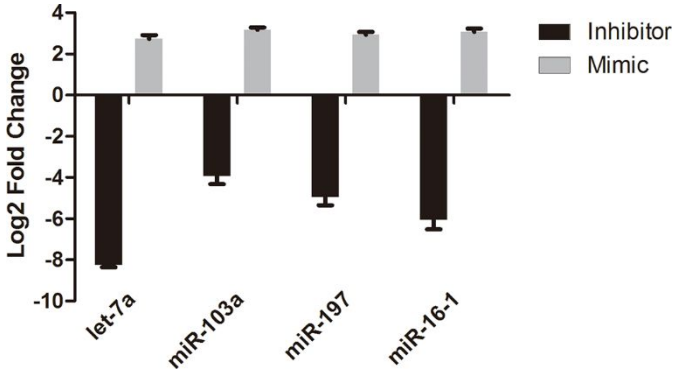

Figure S12 Differences in the abundance of four microRNAs in WT A549 cells transfected with 25 nM of inhibitor or mimic (see Table S3) for corresponding microRNA, respectively. The abundance of four microRNAs were detected by using TaqMan RT-qPCR, and U6 was the housekeeping gene. Bar plot represented mean with SEM (n=3).

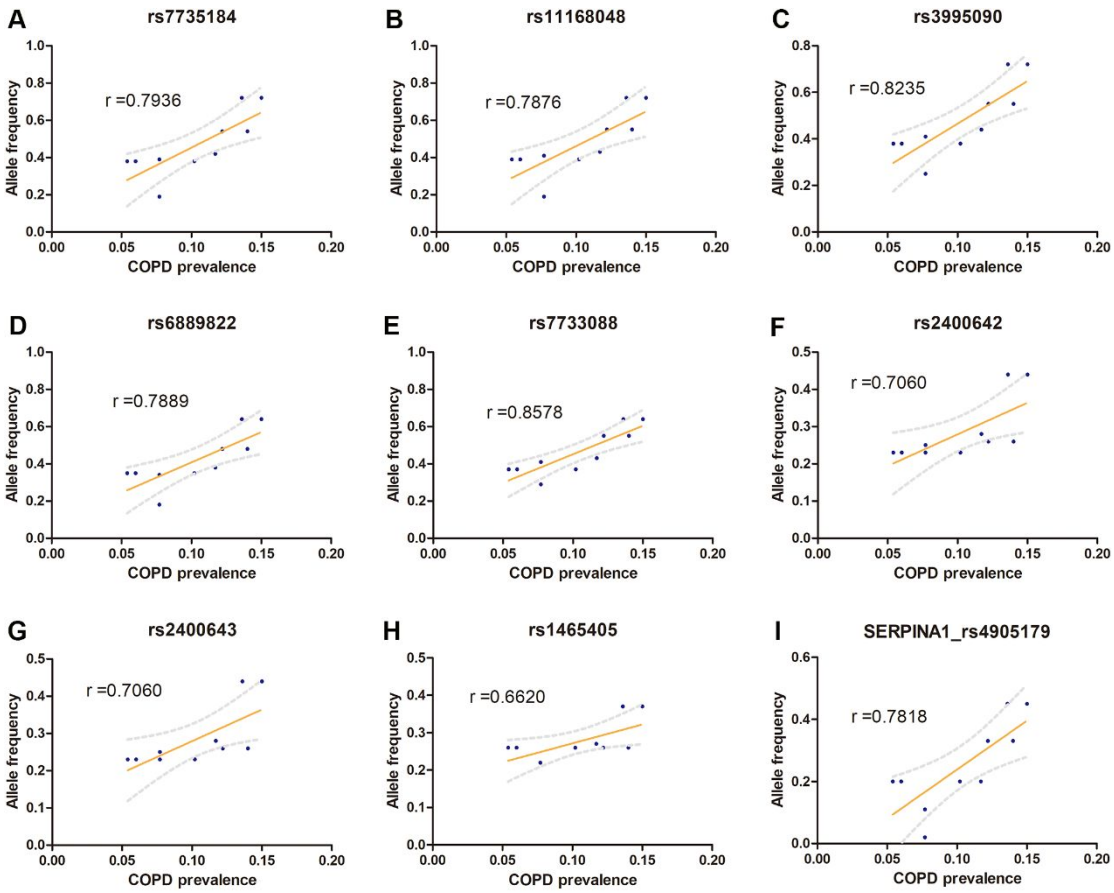

Figure S13 Correlation analysis of allele frequencies of nine variants (**A**-**H**, eight SNPs for HTR4; **I**, rs4905179 for SERPINA1) and COPD prevalence in different populations (East Asian: China, Japan; European: Spain, United Kingdom, Finland; African: Africa; South Asian: India; Ad Mixed American: USA, Latin America; Global: Global; see Table S13). The gray dotted lines indicate the 95% confidence intervals. The value of Pearson r is presented in each panel.

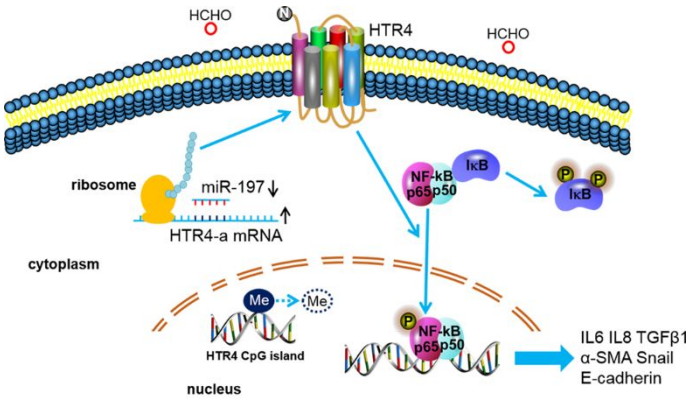

Figure S14 Schematic to show the HTR4-mediated molecule events responding to FA exposure. The dotted circle marked with "Me" indicated the demethylation of HTR4 CpG island.

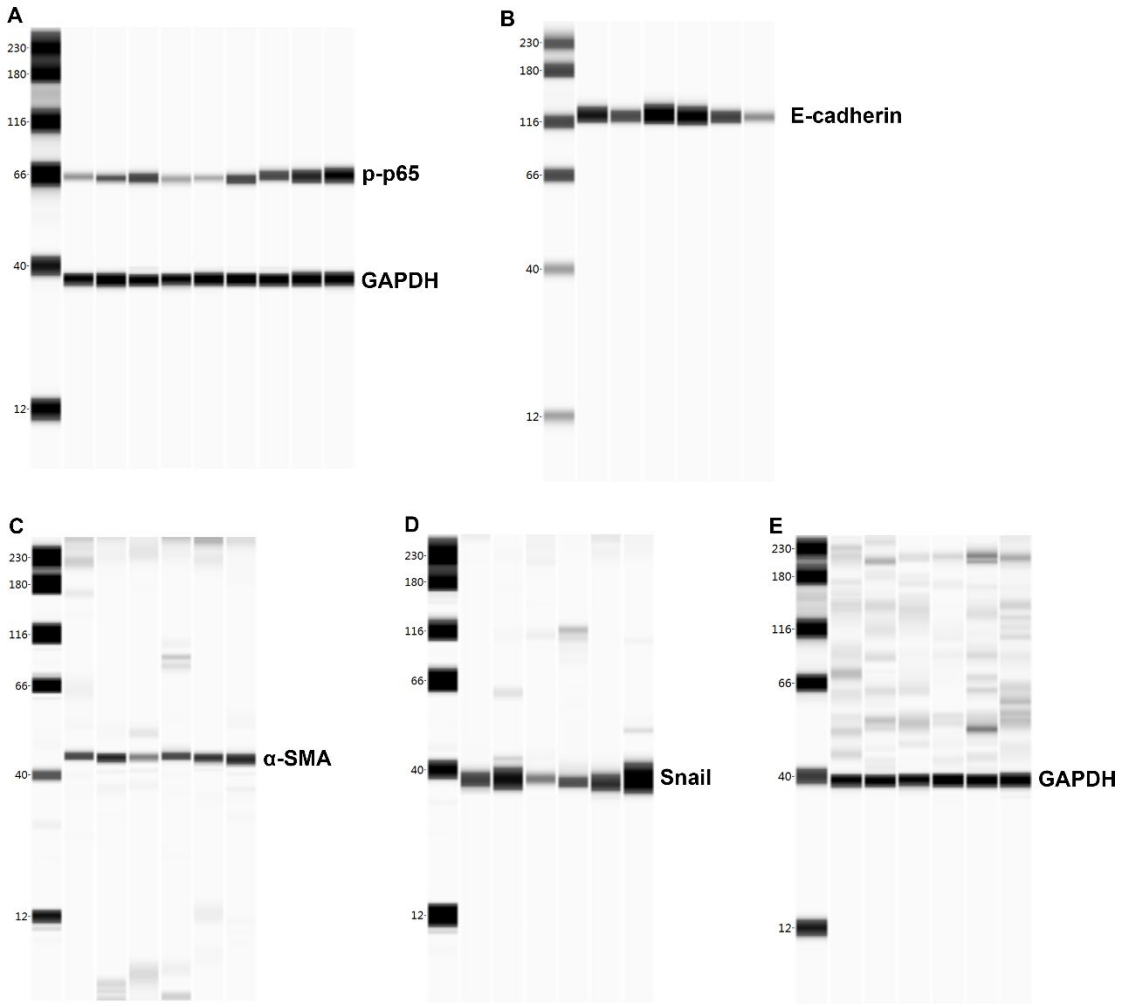

Figure S15 The original western blotting of Figure 4. Panel A is for Figure 4A, and the other panels are for Figure 4F.

Table S1 Primers sequences to amplify lentiCRISPR sgRNAs.

	Primer	Sequence (5'-3')
First PCR	F	AATGGACTATCATATGCTTACCGTAACTTGAAAGTATTTCG
	R	CTTTAGTTTGTATGTCTGTTGCTATTATGTCTACTATTCTTTCC
Second PCR	F-A	ACACAGTAGATTCTTGTGGAAAGGACGAAACACCG
	F-B	ACAGTCAATGATTCTTGTGGAAAGGACGAAACACCG
	F-C	ACTCTGATCGGATTCTTGTGGAAAGGACGAAACACCG
	F-D	ACTGACTAGCTGATTCTTGTGGAAAGGACGAAACACCG
	F-E	AGACTCTTGACTGATTCTTGTGGAAAGGACGAAACACCG
	F-F	AGTCACAGCAGTCGATTCTTGTGGAAAGGACGAAACACCG
	F-G	TCAGAGATAGCTAGGATTCTTGTGGAAAGGACGAAACACCG
	F-H	TGACTGATGACCGTAGGATTCTTGTGGAAAGGACGAAACACCG
	R	ATGGGCAGTCGGTGATCAAGTTGATAACGGACTAGCCTTAT

Note: The sequences in red represent barcodes of each sequencing library. The PCR conditions included initial heat-denaturing step at 98°C for 2 min, 20 cycles of 98°C for 10 s, 60°C for 20s and 72°C for 30s, and a final extension step at 72°C for 3 min on SureCycler 8800 (Agilent technologies).

Table S2 Primers for RT-qPCR using SYBR Green qPCR mix.

Gene Symbol		Sequence (5'-3')
IL6	Forward	AACCTGAACCTTCCAAAGATGG
	Reserve	TCTGGCTTGTTCCTCACTACT
CXCL8	Forward	CAGAGACAGCAGAGCACACAA
	Reserve	TTAGCACTCCTTGGCAAAAC
TGFB1	Forward	GACATCAACGGGTTCACTACCG
	Reserve	TAGTTGGTGTCCAGGGCTCG
SNAI1	Forward	GGTTCTTCTGCGCTACTGCT
	Reserve	TGCTGGAAGGTAAACTCTGGAT
CDH1	Forward	AGCTTGCGGAAGTCAGTTCA
	Reserve	GCAGAGCCAAGAGGAGACC
ACTA2	Forward	GACCCTGAAGTACCCGATAGAAC
	Reserve	GGGCAACACGAAGCTCATTG
GAPDH	Forward	CCAGGTGGTCTCCTCTGACTTC
	Reserve	TCATACCAGGAAATGAGCTTGACA

Table S3 The sequences of RNA oligonucleotides for the mimics and inhibitors of microRNAs.

MicroRNA	Mimics (5'-3')		Inhibitor (5'-3')
	Sense	Anti-sense	
Negative control	UUCUCCGAACGUGUCACGUTT	ACGUGACACGUUCGGAGAATT	CAGUACUUUUGUGUAGUACAA
let-7a-5p	UGAGGUAGUAGGUUGUAUAGUU	CUAUACAACCUACUACCUCAUU	AACUAUACAACCUACUACCUCA
miR-103a-3p	AGCAGCAUUGUACAGGGCUAUGA	AUAGCCCUGUACAAUGCUGCUUU	UCAUAGCCCUGUACAAUGCUGCU
miR-197-3p	UUCACCACCUUCUCCACCCAGC	UGGGUGGAGAAGGUGGUGAAUU	GCUGGGUGGAGAAGGUGGUGAA
miR-16-1-3p	CCAGUAUUAACUGUGCUGCUGA	AGCAGCACAGUUAAUACUGGUU	UCAGCAGCACAGUUAAUACUGG

Table S4 Primer sequences for bisulfite sequencing PCR to amplify the CpG island of HTR4.

	Sequence (5'-3')	Product length
Forward	GATGAGTAGYGTTTYGGTTAG	435 bp
Reverse	CTAACAAATTCRAACRACC	

Table S5 Targeted genes and sgRNA sequence in the 10 single clones. The primer pairs were used to amplify the DNA segments surrounding the corresponding sgRNA sequence.

Gene	sgRNA Sequence (5'-3')	Allele Modification	Forward Primer (5'-3')	Reverse Primer (5'-3')
SEMA6D	TGCCTACATACTGCTGCTGA	-/-	CTGAGCTGATTACAAACAAG	CTCTGCCTCTTTCTGAAAAT
EIF4E2	CCAAGAACTCACAGAGGCAA	-/-	GCCGTCCCACGAGCTCAC	GATGATACCACTGCATTCCAGCCTG
HCAR2	ACAAATTTGCACCGCCATTC	+/-	GACAGCAGCCATCATCTCTTGCC	AGGAGGAACATGGCTTCGTGC
HCAR2	ACAAATTTGCACCGCCATTC	+/-	GACAGCAGCCATCATCTCTTGCC	AGGAGGAACATGGCTTCGTGC
ALDH2	CTGACAAGAGGCGGCGGCCC	-/-	CCCTGAGACCCTAGCTCTGC	GGCAGATGTGCTTCCAGGTC
UGT1A9	AGTTCTCTGATGGCTTGCAC	-/-	GAAAGGATAAAAACACGCCC	GTCCAGATCCTCCAGGGTATTA
FBLN7	CCTCGGCGAAGCGTGTCTCC	-/-	TGGGTGGTGGCGGCG	CCTGGAAGGGCATCTGGGC
TLR10	AGTATTGTTATGACAGCAGA	-/-	AGGGTTTTGAGCTCATCTTC	AAATACCTGAGACCTGCCAG
ST3GAL3	GCTAGAGTGACTATACTTAC	-/-	GGTTAGAAGATGCCATGATA	AAGTCCCAGAAATGTTCAGT
CACNA1C	CGATGGCCGCCTGCCACGAC	-/-	ACCGCCTGCAATAGCTTGAA	GCACAGCTGACACAGCTCGT

Note: The symbol -/- represents both two alleles of the targeted gene were modified, and symbol +/- represents only one allele were modified.

Table S6 168 underrepresented genes (p<0.01) identified by CRISPR screening in A549 cells using formaldehyde.

Gene	NES	Gene rank	p-value	Gene	NES	Gene rank	p-value	Gene	NES	Gene rank	p-value
HTR4	0.004035	1	0.0001	LDHD	0.04267	57	0.0043	CADPS	0.05866	115	0.0075
GALNTL6	0.005073	2	0.0002	ZNF548	0.04321	58	0.0064	C9orf78	0.05921	118	0.0075
PTPRN	0.006129	3	0.0002	SPEF2	0.04344	59	0.0014	ZPBP	0.05928	119	0.0075
DCAF12L2	0.008763	4	0.0001	CRYGC	0.04432	60	0.0046	FAM155B	0.06027	120	0.0053
GSTM4	0.01047	5	0.0004	OTOF	0.0447	61	0.0068	AP5S1	0.06028	121	0.0077
TMEM186	0.01104	6	0.0002	PTPRR	0.04564	62	0.0087	PLEKHG1	0.06042	122	0.0054
IAH1	0.0124	7	0.0004	PSMD3	0.04581	63	0.0049	METTL14	0.06064	123	0.0054
DOC2A	0.01309	8	0.0003	TMED5	0.04595	64	0.0035	ZNF2	0.06088	125	0.0078
PQBP1	0.01455	9	0.0005	BRP44	0.04606	65	0.0049	EPS15L1	0.0612	126	0.0058
WFDC10B	0.01642	10	0.0007	DKK2	0.04657	66	0.0066	OPCML	0.06129	127	0.0078
GCLC	0.01688	11	0.0007	ADAM22	0.04686	67	0.0051	OR6N2	0.06193	128	0.006
KCTD8	0.01749	12	0.0011	ANGPTL1	0.04726	68	0.0063	ATP11C	0.06286	130	0.0063
CASP1	0.01756	13	0.0016	ZAK	0.04727	69	0.0052	CALB1	0.06381	132	0.0087
C5orf45	0.01762	14	0.0011	EOGT	0.04755	70	0.0039	ZFAND1	0.06388	133	0.0087
CCND3	0.01798	15	0.0016	KIFAP3	0.04763	71	0.0063	CCL18	0.06392	134	0.0067
WDR85	0.01871	16	0.0007	MAPKAPK2	0.04796	72	0.0039	TTC24	0.06399	135	0.0087
ARHGAP18	0.01974	17	0.0007	AGGF1	0.04796	73	0.0052	GPRIN2	0.06452	136	0.0044
RBM5	0.02024	18	0.0008	PTPRS	0.04844	74	0.004	GRIA3	0.06481	137	0.0089
TES	0.02078	19	0.0005	NCK2	0.04848	75	0.0072	CNFN	0.06488	140	0.009
BCL2	0.02193	20	0.0009	NINL	0.04864	76	0.0055	SOS2	0.06518	142	0.009
NUP88	0.02195	21	0.0009	TNIK	0.04961	77	0.0041	NFKBIA	0.0652	143	0.009
PSG6	0.02353	22	0.0014	ARSH	0.05015	78	0.0058	TARS2	0.06525	144	0.009
FGFR2	0.02358	23	0.0014	CATSPER1	0.05041	79	0.0043	KCNJ8	0.0657	146	0.0092
ADCY8	0.02472	24	0.0014	TRA2A	0.05061	80	0.0043	U2AF2	0.06579	147	0.007
RAB37	0.02536	25	0.0011	GSN	0.05071	81	0.0044	ZNF135	0.06628	148	0.0071
ZNF214	0.02587	26	0.0014	RNF175	0.05079	82	0.0044	PMAIP1	0.06643	149	0.0071
GPX1	0.026	27	0.0014	CYYR1	0.05082	83	0.0059	RPS27A	0.06697	152	0.0047
MEN1	0.02603	28	0.0014	PDE1C	0.05082	84	0.0094	CSMD1	0.06719	153	0.0098
TFPI2	0.02609	29	0.0014	GUCA1C	0.05091	85	0.008	MAGEC1	0.06731	154	0.0047
PTGDR	0.02728	30	0.0016	MMRN1	0.05137	86	0.0074	ZNF167	0.06819	156	0.0079
IKZF3	0.028	31	0.0029	PTPRN2	0.05141	87	0.0059	SMARCC2	0.06866	157	0.008
RUSC1	0.02803	32	0.0038	SYNJ1	0.05153	88	0.0075	FCGRT	0.06981	160	0.0085
RFX3	0.02918	33	0.0017	LAMC2	0.05164	89	0.0059	RHOD	0.07057	166	0.0087
TMEM25	0.02963	34	0.0039	TAB1	0.05207	91	0.0059	MOB1A	0.07102	167	0.0088
ARHGEF28	0.03212	35	0.0038	STK17B	0.05211	92	0.0084	ZNF428	0.07123	168	0.0088
NFATC4	0.03245	36	0.0023	NDUFA12	0.05242	93	0.0046	KIAA1462	0.0724	172	0.0089
GPR162	0.03264	37	0.0023	GPC6	0.05271	94	0.0059	IGFBP6	0.07248	173	0.0089
DCLRE1B	0.03267	38	0.0026	TRIB2	0.05276	95	0.0088	MYO18A	0.0725	175	0.0089
AGAP3	0.03323	39	0.0024	SURF4	0.05324	96	0.0059	TNPO1	0.07256	176	0.0089

UBN2	0.03325	40	0.0024	GABBR2	0.05329	97	0.0059	NXPH4	0.07281	178	0.0089
SLC25A20	0.03379	41	0.0009	ADAMTS13	0.0533	98	0.0046	CAV1	0.07379	183	0.0091
FAM129B	0.03485	42	0.003	NR1H3	0.05334	99	0.0081	C19orf69	0.07457	187	0.0093
KLK8	0.03486	43	0.0021	STRBP	0.05358	100	0.0046	ZNF740	0.07484	189	0.0094
KLF17	0.03625	44	0.0037	TMEM139	0.05445	101	0.0046	RPL36AL	0.07596	195	0.0056
METTL13	0.03632	45	0.0067	BTBD3	0.05485	102	0.0097	RPAIN	0.07648	197	0.0098
COX5A	0.03691	46	0.0023	FAM115C	0.05496	103	0.0064	TCEAL5	0.07847	208	0.0059
PC	0.03721	47	0.0024	ERLEC1	0.05553	105	0.0087	SERPINB12	0.07955	215	0.0061
MTFP1	0.03767	48	0.0025	NUP107	0.05592	106	0.0047	SPOCK1	0.08241	228	0.0064
ZZZ3	0.03893	49	0.0051	LRP1	0.05594	107	0.0047	RNF152	0.0851	251	0.0065
PRELID2	0.03894	50	0.0045	UBE3A	0.05665	108	0.009	CRTC1	0.08607	261	0.007
SLC23A1	0.03904	51	0.0027	DYM	0.05681	109	0.0071	MRPL10	0.08763	274	0.0074
NFU1	0.04016	52	0.0079	PARD6A	0.05704	110	0.0073	TMEM158	0.09324	301	0.008
SOX18	0.04018	53	0.0039	ZNF248	0.05705	111	0.0047	C5orf60	0.1011	342	0.0092
MUM1	0.04027	54	0.0027	RHOT2	0.05713	112	0.0073	IER5L	0.1026	362	0.0092
CARD14	0.04174	55	0.004	SPSB4	0.05716	113	0.009	PCDHB6	0.1034	368	0.0093
OR8J3	0.04207	56	0.0014	GEMIN4	0.05849	114	0.0048	TICAM2	0.1043	377	0.0096

Note: The underrepresented genes were the genes of which the sgRNAs abundances were significantly lower in surviving A459 cells exposed to formaldehyde compared to those exposed to vehicle using CRISPR screen. NES (Normalized Enrichment Scores) and *p* values were calculated in RNAi Gene Enrichment Ranking (RIGER) using the options of "Second Best Rank" and "Signal to Noise". Gene rank of the underrepresented genes was according to the increasing order of NES.

Table S7 409 genes associated with genetic susceptibility to COPD.

ANKH	SERPINA1	KL	AIMP1	TAZ	EGF	CTNNB1	NR4A1
FAM13A	ELN	TIMP2	DNER	KLF9	ABCA1	VCAN	HLA-DQB1
TGFB2	TNF	TIMP1	APOM	BSG	GPR183	PWAR1	SERPIND1
HHIP	EPHX1	EPCAM	S100A4	SLC2A10	HBEGF	CNR1	GZMB
MMP3	TGFB1	PRTN3	CD14	EHMT1	AGT	ZNF816	EFEMP2
RIN3	ITGB6	MMP10	PTPN6	SLC52A2	SLC26A3	TPP1	GTF2H1
CHRNA3	HMOX1	GCG	ACVR1B	C3AR1	SGMS2	DBA2	GSTT1
KLHL7	CYP2A6	MMP14	PSG2	TXN	ALDH2	TUSC2	GSTM2
DLG2	TGFBR1	NM	PSMC5	TLR2	FDPS	C20orf181	GRN
PID1	TGFB3	NOS2	MSC	NKX2-1	FES	GPX1	IGFBP3
EEFSEC	TGFBR2	MTOR	XPR1	SCGB1A1	SIGLEC9	GULP1	IGFBP5
GSTCD	SMAD3	PPARG	MAN1C1	VDR	IL37	MIR133B	IGFBP7
TET2	BICD1	ANGPT1	PTMAP4	XK	PALD1	XRCC6P5	LCN1
ADAM19	SNRPF	VCP	RHO	KLF10	AMFR	MPO	NPSR1
HTR4	PPT2	HGF	PTMA	TGFBR3	ABI3BP	MMP7	JUND
ADGRG6	IL6	SFTPC	PTPRO	TFEB	PCSK9	MEFV	JUNB
AGER	ELANE	H2AX	SLIT2	STAT6	XRCC6	MDM2	JUN
ARMC2	GABPA	TERT	SFXN1	SOD1	IL17RA	CD46	JAK2
DSP	NFE2L2	IL18	DDIT4	SOAT1	NUP62	SMAD7	ITGAM
CHRNA5	COPD	ITGAX	TLR9	TNFSF10	ZGLP1	MIR34C	IRF3
THSD4	PPT2-EGFL8	CX3CL1	PLTP	ADAM9	FOSB	MIR223	IL16
CCDC101	VEGFA	GSTP1	PLAGL2	IL18R1	FOS	MIR22	IL10
CFDP1	MMP1	S100A8	PIK3CA	SFTPB	FLNA	MIR15B	IL6ST
MTCL1	IFNG	CD274	SERPINI1	SFRP1	NLRP1	MIR155	IL4
PDZD2	IL1B	LOXL2	CD74	ASAP2	FGFR1	LTBP2	IKBKB
CDRT15P1	IL13	MOK	ABCB1	NR1I2	DDIT3	LRP5	FAS
NUP42	SERPINA13P	STAT3	KEAP1	SQSTM1	ACE	MYD88	CCN1
SLC11A1	IL17A	TIMP3	PECAM1	CCL5	PAPOLA	MYH10	DEXI
PTEN	SERPING1	CADM1	KIF20B	WNT3A	MRPS30	ATD	NFKBIA
MMP12	CFTR	TM7SF2	CLOCK	BLVRA	CEACAM7	DCTN4	ADRB1
ADCY2	EGFR	MMP28	NREP	MBTPS1	LILRB1	RMDN1	CHRM2
IREB2	CXCL8	FLCN	TDP1	CAV1	CEACAM3	PCNA	DRD2
ADIPOQ	KDR	FOSL1	SYBU	HDAC10	KHDRBS1	FOXP3	PDE4D
SETD	SIRT1	A2M	PRCP	CASP9	CXCL13	ASAP1	PDE4A
MMP2	PGF	CTSS	EIF2AK3	SMS	PERCC1	REG3A	CHRM1
MMP9	PLF	ADRB2	RMDN3	SMPD2	FBLN5	SERPINE1	EDN1
NCR3	TP53	CHI3L1	PRMT6	SLPI	CEACAM5	CD207	NPPA
MN1	FEV	CASP1	MTPAP	SKP2	MPHOSPH10	SMARCAL1	PDE4B
CDC123	CASP3	SESN2	ACP3	PINK1	CDK4	ORC4	MAPK1
ASTN2	FUT8	ATP6V0A2	CD34	BMP1	LRPPRC	OAZ1	PDE4C
HDAC4	HIF1A	ABCA3	PGPEP1	NR0B2	LINC-ROR	NOS3	BDNF

CCDC38	HDAC2	ENTPD1	TBPL1	CAT	DNM1L	NOS1	VIP
C10orf11	TLR4	FOXO3	PDGFA	CH25H	ABHD2	NFKB1	VIPR2
KCNE2	GSTM1	CRP	IL33	ISYNA1	FSTL1	NFE2	ADCY1
NPNT	FBN1	H3P10	C3	GLP1R	PDAP1	LOXL1	MAPK10
TNS1	EGR1	PARP1	TGFA	ALB	CYP26A1	LGALS9	
RARB	SERPINA3	FGF7	CLPTM1L	FBL	CYP2B6	IGF1	
TRIP11	LOX	NLRP3	TERF2	EPHX2	AMOTL1	CLEC4D	
GPR126	CDKN2A	F2R	LMAN2L	EPAS1	CX3CR1	APOA1	
ZKSCAN3	CCL2	RGN	TRBV20OR9-2	ZBTB7C	RMDN2	HTC2	
MFAP2	LTBP4	MAPK3	CDT1	MARK2	CTSE	APEX1	
SFTPD	SERPINE2	RNF5	MAP1LC3B	CELA1	COMMD1	HPX	

Note: There were 12 disease items which were similar with COPD in DisGeNET database, including: chronic obstructive airway disease (C0024117); lung diseases, obstructive (C0600260), pulmonary emphysema (C0034067); bronchiolitis obliterans (C0006272); bronchitis, chronic (C0008677); acute exacerbation of chronic obstructive airways disease (C0340044); severe chronic obstructive pulmonary disease (C0730607); moderate chronic obstructive pulmonary disease (C0730605); COPD, severe early-onset (C1969833); chronic airflow obstruction (C1527303); obstructive emphysema (C0241876); asthma-chronic obstructive pulmonary disease overlap syndrome (C4038730). For the genes in each disease item, two criteria including the gene-disease association score was greater than or equal to 0.09 (a tenth of the max score) and the number of PMID (PubMed ID) was more than 0, were used to remove the genes with low relevancy. Finally, a total of 409 genes (see this Table) were identified as the genes associated with genetic susceptibility of COPD.

Table S8 2085 genes of hypomethylation (*p* value <0.01) in the lung of COPD patients who were non-smokers or ex-smokers belonging to COPD stage 1 to 2.

Probe ID	Gene symbol	log2FoldChange	*P* value	Probe ID	Gene symbol	log2FoldChange	*P* value	Probe ID	Gene symbol	log2FoldChange	*P* value
cg00417147	AACS	-0.723401525	1.97E-07	cg15760474	FOXP4	-0.580349511	2.23E-05	cg18861917	PGM5P2	-0.461511159	0.00169956
cg22059413	AAK1	-0.272867781	0.001239363	cg00188748	FPGS	-0.273950363	0.007585859	cg10784341	PHACTR2	-0.443911187	0.000859866
cg14699839	AANAT	-0.293924809	0.008036338	cg07753967	FRG1B	-1.036144306	0.004873604	cg26159541	PHACTR3	-0.299330959	0.006442093
cg22093121	ABCA9	-0.311326232	0.001516774	cg07629776	FRMD4A	-0.791566148	0.006877613	cg00956142	PHACTR4	-0.339291233	0.001503209
cg13185308	ABCC8	-0.411540324	0.00430597	cg20754145	FRY	-0.2736134	0.007618901	cg26280911	PHF15	-0.472388277	0.005816329
cg25116882	ABCD2	-0.342961325	0.00734217	cg20613889	FSHR	-0.462252041	0.002568283	cg25614364	PHF17	-0.421162333	0.001786994
cg10436877	ABCF2	-0.304560442	0.000642273	cg26982104	FTO	-0.790843692	0.000835713	cg06763568	PHGDH	-0.322309957	0.004694135
cg09866366	ABCF3	-0.437091707	0.007605768	cg04660111	FUT2	-0.281455318	0.004389039	cg24667736	PHLDB2	-0.477250031	0.00995029
cg21602768	ABHD12	-0.26673734	0.001495788	cg21105227	FXYD7	-0.759878792	0.001286063	cg03042971	PHOSPHO1	-0.343368654	0.001308666
cg23112192	ABHD15	-0.43746957	0.001229444	cg11710000	FZD3	-0.671958201	0.00217848	cg09802835	PHOX2A	-1.06553123	1.79E-07
cg12850396	ABHD2	-0.279816033	0.008454016	cg06020238	FZD8	-0.330648919	0.004506939	cg14153069	PHYHD1	-0.413179357	0.0003079
cg10340038	ABI2	-0.391232447	0.000865951	cg24686911	G2E3	-0.300136726	0.007542157	cg05947740	PHYHIP	-0.420681618	0.002545475
cg00997917	ABLIM1	-0.553237023	0.000709691	cg13532463	GABBR2	-0.351965312	0.001883817	cg09463522	PIBF1	-0.368830714	0.001305584
cg08034867	ABR	-0.462466818	0.005485887	cg27134386	GABRA2	-0.569768983	0.003734407	cg01791104	PIGV	-0.309018454	0.007549773
cg08663298	ABTB2	-0.306531621	0.000949391	cg21242208	GABRB2	-0.628981909	0.001992061	cg00936626	PIGZ	-0.561647986	0.000335121
cg16822666	ACACA	-0.298137935	0.009336809	cg00580652	GABRD	-0.559776978	0.000551616	cg16989107	PIK3R3	-0.283273054	0.003222021
cg02859644	ACBD5	-0.313689865	0.005978465	cg14005211	GAD1	-0.569824296	0.005804792	cg05852040	PION	-0.588904939	0.00143042
cg02254574	ACCN1	-0.555873037	0.001728424	cg14780632	GAL3ST3	-0.308810057	0.00279928	cg00369151	PIP4K2A	-0.456052224	4.31E-06
cg10266490	ACOT11	-0.544043261	3.99E-05	cg15988345	GALE	-0.30916501	0.009812244	cg27142680	PIP4K2B	-0.353089377	0.009081717
cg03914735	ACPL2	-0.40100763	0.000515098	cg15127250	GALNT6	-0.517344297	0.000777959	cg01070272	PIP5K1C	-0.499958421	0.000326696
cg27121267	ACRV1	-0.434764789	0.008061275	cg15409133	GALNT9	-0.676685544	0.000309587	cg10082841	PIP5KL1	-0.455710004	0.008362282
cg05521982	ACSF3	-0.506407814	0.004085773	cg16204559	GALNTL4	-0.621005554	0.000217088	cg08235822	PITPNB	-0.312326181	0.002262171
cg19335412	ACTA2	-0.36374791	0.005047417	cg25230532	GALT	-0.261761858	0.003446356	cg02018291	PITPNC1	-0.457500235	0.000187232
cg23173910	ACTG2	-0.469884462	0.005302902	cg27317433	GAMT	-0.527734618	0.001970313	cg08464009	PITPNM2	-0.572440437	0.003526109
cg21516287	ACTR3C	-0.841138034	0.000368389	cg06339542	GAS7	-0.338810034	0.003115461	cg17949915	PITX2	-0.691218565	0.002094877
cg00525683	ADAM19	-0.800753522	0.000102155	cg22915582	GATA2	-0.810347726	8.00E-05	cg25353287	PKDCC	-0.75295796	0.002263242
cg17401106	ADAM33	-0.29485902	0.008278364	cg08015883	GATA5	-1.305862656	0.000170521	cg04897644	PKLR	-0.270177986	0.001127249
cg00436874	ADAMTS10	-0.552414237	1.18E-05	cg03385582	GATSL3	-0.509709868	0.002133783	cg17988830	PLA2G2A	-0.500106253	0.003481957
cg14557288	ADAMTS14	-0.316412812	0.000750942	cg11625933	GBE1	-0.509155309	0.002645104	cg23637396	PLAC9	-0.30651847	0.003828635
cg12007053	ADAMTS15	-0.505718792	0.008068717	cg19740353	GCLC	-0.314864215	0.003968151	cg15456925	PLAG1	-0.438242104	0.007458731
cg07199183	ADAMTS17	-0.818817152	0.001612587	cg14000361	GCM2	-0.510512446	0.004991047	cg25291978	PLAGL1	-0.451697336	1.78E-05
cg18720326	ADAMTS2	-0.725663048	0.002267273	cg22378252	GCNT2	-0.553394421	0.001615849	cg17168630	PLAUR	-0.409372241	0.006491654
cg01033938	ADAMTS8	-0.400126347	0.005716886	cg00773902	GDF1	-0.468488419	0.004982644	cg27488348	PLBD1	-0.470602221	0.004506131
cg14355939	ADAMTSL2	-0.332460477	0.009945093	cg13321164	GDF2	-0.378735232	0.002104086	cg03819243	PLCD1	-0.572885777	0.000197145

cg12974394	ADAMTSL4	-0.571476094	0.000122812	cg20380689	GDNF	-0.691088957	0.006148573	cg27638309	PLCE1	-0.435123778	0.007944685
cg04907257	ADCY2	-0.540742431	0.004658131	cg26427135	GEM	-0.351035411	0.007814881	cg18450931	PLCH1	-0.37956225	0.001516546
cg25976932	ADCY5	-0.339692591	0.002625312	cg21944455	GFAP	-0.443629306	0.002125323	cg25880834	PLCL1	-0.596014475	0.00362295
cg11661914	ADCY6	-0.631062493	5.30E-06	cg13930300	GFI1	-0.747083927	0.009932863	cg20145009	PLD4	-0.281780179	0.009244129
cg06223834	ADCY9	-0.664773231	0.007147861	cg14019186	GFM1	-0.303449864	0.008596453	cg11224624	PLEC1	-0.766092739	0.004830515
cg05149386	ADM	-0.9076482	0.00011896	cg07835809	GHITM	-0.281382971	0.007792304	cg14707162	PLEKHA7	-0.345117731	0.007533188
cg17580614	ADORA2B	-0.428068183	0.000661648	cg00901598	GHSR	-0.293313824	0.003576422	cg04051396	PLEKHG7	-0.32222995	0.000588499
cg08256939	ADORA3	-0.346368366	0.009682608	cg07127888	GINS4	-0.370819833	0.001105348	cg02815014	PLEKHM3	-0.464674276	0.003516156
cg18027174	ADPRH	-0.584257448	0.000261565	cg09107315	GIPC2	-0.398703995	0.006479608	cg05526269	PLXNA4	-0.471927599	0.005274403
cg20619751	ADPRHL1	-0.432417801	0.007071248	cg25749609	GJA3	-0.758673951	0.001094131	cg12030667	PLXNB1	-0.360626606	0.00121194
cg14614811	ADRA1B	-0.658227506	6.98E-06	cg03650119	GJC2	-0.500711984	0.003066378	cg08082355	PMEPA1	-0.479074034	2.30E-06
cg27200895	AFAP1	-0.546938241	0.003949602	cg00430080	GLB1L2	-0.455270247	0.006287602	cg11084266	PMF1	-0.37669288	0.001309086
cg13353679	AFF3	-0.584950469	0.009912178	cg13926553	GLDN	-0.34556314	0.001645486	cg23025654	PMS2L4	-0.321364136	0.000246004
cg16070743	AGA	-0.641363485	0.008280623	cg05550612	GLG1	-0.333953987	0.005307547	cg04952446	PNKD	-0.346669747	0.000432978
cg10096519	AGAP1	-0.34008622	0.000378243	cg04223863	GLI2	-0.545858287	0.002589261	cg16617301	PNMAL2	-0.385936276	0.009952546
cg18667086	AGAP2	-0.339076582	0.005869888	cg02415057	GLIPR1L2	-0.976019795	0.003579091	cg10416846	PNOC	-0.277181369	0.003913717
cg02973270	AGPAT1	-0.346687775	5.95E-05	cg01068808	GLT25D2	-0.58000301	0.006007187	cg25025866	PNPLA6	-0.260199246	0.00307096
cg09248054	AGRN	-0.265753317	0.003479133	cg03058444	GMDS	-0.443970478	0.001139633	cg20469507	POLD3	-0.524981212	0.001805402
cg00582941	AHCY	-0.31862847	0.007681799	cg14757107	GMPR	-0.563461652	0.00207677	cg11823159	POLR2D	-0.261957928	0.00077369
cg23447569	AHNAK	-0.6689561	0.001790375	cg13960192	GNA11	-0.428817081	0.009055972	cg10585293	POLR3B	-0.298603131	0.004744084
cg25648203	AHRR	-0.46343224	0.006403003	cg18998543	GNA12	-0.42080387	0.003735131	cg19678392	PON1	-0.731423633	0.000743512
cg23732845	AIM1L	-0.379025412	0.005828876	cg08644463	GNAI3	-0.288869493	0.005229346	cg08898155	PON3	-0.579141779	0.008580023
cg20802051	AK3L1	-0.278054383	0.008952575	cg10139742	GNAO1	-0.362076346	0.004967258	cg01236616	POP5	-0.410707909	0.006148959
cg06882298	AKAP1	-0.755477253	0.001034676	cg25407736	GNG12	-0.5205726	0.009281127	cg05628417	POPDC3	-0.571104742	0.003756763
cg13033898	AKAP12	-0.364958241	0.00577043	cg08001559	GNG2	-0.333982768	0.005646928	cg04922971	POSTN	-0.545158028	0.002038024
cg01954585	AKAP13	-0.480958865	0.003323288	cg25293251	GOLGA5	-0.630944349	0.000138302	cg22054191	POU2F2	-0.431480858	0.002048313
cg08097581	AKAP8L	-0.696351277	7.70E-05	cg22764289	GOLSYN	-0.463831359	0.003183018	cg19513834	POU3F3	-0.639351685	0.002320115
cg06648780	ALCAM	-0.302492257	0.001091282	cg20510272	GOLT1A	-0.384727491	0.005336799	cg23440004	POU4F1	-0.354200169	0.005616831
cg05906871	ALDH18A1	-0.412807241	0.003537494	cg10358780	GOLT1B	-0.362580653	0.00450121	cg24118856	PPAN-P2RY11	-0.456522959	0.004771365
cg00930873	ALDH1A2	-0.574064166	0.006872387	cg24234850	GOPC	-0.392493338	0.006433483	cg21859053	PPARG	-0.552003868	0.000364815
cg13615592	ALDH1A3	-0.750588601	0.000194913	cg15992420	GP5	-0.862115504	8.02E-06	cg19701879	PPARGC1A	-0.279339588	0.002789314
cg08481491	ALDH1L1	-0.705804958	6.99E-06	cg11134334	GPC6	-0.486419258	0.00065651	cg19763230	PPFIA3	-0.574176594	0.000426089
cg15726326	ALDH3A1	-0.574604796	0.00055321	cg21145686	GPD1L	-0.284832154	0.004917248	cg22485062	PPIL1	-0.270165141	0.002788173
cg26791665	ALDH4A1	-0.470515845	0.00872194	cg07904865	GPER	-0.546450369	0.003534461	cg06145800	PPL	-0.274972407	0.008842375
cg01986682	ALDOA	-0.338581932	0.005095598	cg03245641	GPHA2	-0.386274361	0.00033926	cg25802191	PPM1H	-0.381947579	0.001678741
cg09942743	ALK	-0.482460937	4.76E-05	cg16777028	GPHN	-0.260990989	0.002850181	cg04375036	PPP1CC	-0.495717107	0.000905365

cg02216481	ALOX15B	-0.263411625	0.001339507	cg23192824	GPR126	-0.285593494	0.002210647	cg08243728	PPP1R13L	-0.361028527	0.009833431
cg02269083	ALPK2	-0.588330767	0.006850133	cg12074966	GPR156	-0.49256621	0.00782279	cg09007470	PPP1R14A	-0.431034181	0.005677478
cg02409351	ALX1	-0.376470576	0.005637687	cg21105928	GPR176	-0.450288611	0.004020551	cg17574911	PPP1R16A	-0.282680683	0.009521692
cg22494858	ALX3	-0.34140584	0.006746015	cg20325921	GPR20	-0.497199025	0.000203347	cg15821319	PPP1R16B	-0.403028434	0.004651993
cg16360777	AMBN	-0.52304159	7.43E-05	cg14115756	GPR21	-0.371309853	0.001285371	cg20400248	PPP1R3B	-0.485218073	0.000227825
cg00299047	AMH	-0.498746844	0.002756574	cg13380502	GPR3	-0.271561642	0.005457112	cg04839761	PPP1R3C	-0.36062964	0.009693768
cg18348142	AMIGO2	-0.287713705	0.008053766	cg15488122	GPR4	-0.42322701	0.007526427	cg23021638	PPP2R3A	-0.482778481	3.84E-06
cg24921089	AMPD3	-0.351001708	0.004256362	cg19254163	GPR44	-0.423354574	0.003524451	cg01360067	PPP3CB	-0.453192147	0.0002515
cg18015301	AMPH	-0.596407244	0.00159679	cg25773386	GPR62	-0.496824842	0.001302042	cg16179607	PPP3R1	-0.321129931	0.000244974
cg19807716	ANGPTL1	-0.600137394	0.005123363	cg26745551	GPR63	-0.37266754	0.001569364	cg04404772	PPP5C	-0.493311317	0.003950273
cg07533533	ANK1	-0.673180991	0.006412002	cg09408571	GPR88	-0.777854645	0.000259298	cg20900524	PPT1	-0.530088512	0.002239836
cg10097464	ANKDD1A	-0.587122754	0.000512932	ch.1.2840814R	GPR89A	-0.284900745	0.006910104	cg05904869	PRDM13	-0.646052138	0.004808343
cg08098868	ANKFN1	-0.419446025	0.007627908	cg13573474	GPRC5A	-0.626187978	0.005676965	cg02919936	PRDM14	-0.495451455	0.003291411
cg02052762	ANKFY1	-0.301960061	0.003968589	cg25884399	GPSM1	-0.485828775	0.002444711	cg12900929	PRDM4	-0.313229846	0.000247875
cg16437021	ANKRD11	-0.800408423	0.000139695	cg12401918	GPSM3	-0.295109325	0.008404779	cg10453550	PRDM5	-0.390803126	0.002190543
cg25574724	ANKRD31	-0.415293703	0.00632058	cg23793500	GPT	-0.264489846	0.009755123	cg07056285	PRDM6	-0.618613323	0.004938637
cg15680620	ANKRD45	-0.344951321	0.001096937	cg02059637	GRB14	-0.363482167	0.00854434	cg02631906	PRDX1	-0.396560731	0.008828706
cg06289589	ANKRD5	-0.69609356	0.00265867	cg11504078	GREM2	-0.570721412	0.000320659	cg09546802	PRELID2	-0.463994899	0.00409029
cg06046430	ANKRD56	-0.869084764	0.002870772	cg20648229	GRHL1	-0.444959416	0.001891724	cg23591302	PRICKLE1	-0.575011501	0.000945169
cg26504263	ANKRD6	-0.713166842	8.21E-06	cg12121318	GRK4	-0.582758655	0.00407131	cg20895877	PRIMA1	-0.673732056	0.001488948
cg12019494	ANKS1B	-0.489726588	0.005409805	cg23881299	GRK5	-0.376974157	0.000932084	cg19412964	PRKAG2	-0.387802056	0.008067717
cg26340149	ANO1	-0.682247285	0.000312381	cg00636527	GRK6	-0.446816953	0.002167827	cg16190265	PRKAR1B	-0.603380446	0.000433626
cg00830420	ANO2	-0.646845808	0.00403296	cg00444360	GRM5	-0.340489742	0.003205645	cg03832839	PRKCG	-0.506031095	0.004543538
cg06339606	ANP32A	-0.503276618	0.008528438	cg13073773	GSC	-1.147299936	0.002408035	cg19512969	PRKCH	-0.732653663	0.003056227
cg23161492	ANPEP	-0.375260919	0.003185845	cg27554156	GSG1	-0.465083518	0.006900075	cg18188739	PRKCZ	-0.392181939	0.006787208
cg08611402	ANTXR2	-0.307158681	0.001267105	cg13569051	GSN	-0.36359945	1.38E-05	cg21247948	PRKD3	-0.443008218	0.004523433
cg25512683	AOC3	-0.642885179	0.000387577	cg19888869	GSX2	-0.570478813	0.006551235	ch.5.762713R	PRLR	-0.290083856	0.007966628
cg10413944	AP1S3	-0.402363129	0.008373222	cg11389618	GTDC1	-0.536536634	0.001337081	cg23283320	PRMT2	-0.462251038	0.000820568
cg02252907	AP3D1	-0.265948163	0.003080653	cg05426006	GTF2F2	-0.424404378	0.002441149	cg09655952	PROK2	-0.526749144	0.005017882
cg05020685	APBB2	-0.795256168	0.000321819	cg12209693	GTF2IRD1	-1.213069101	0.002586371	cg26260038	PROM1	-0.515434806	0.008254498
cg21888989	APH1B	-0.29662958	0.00055382	cg23206520	GULP1	-0.410037476	0.000756805	ch.8.885117R	PROSC	-0.337471327	0.000215885
cg10104451	ARC	-0.410584162	0.002976935	cg11492040	H19	-0.498046278	0.000421194	cg02200207	PRR15	-0.435404624	0.003057993
cg16079898	ARHGAP10	-0.403761247	0.008107503	cg16255816	HAP1	-0.585882288	0.003523434	cg20914572	PRRT1	-0.466310398	0.009643305
cg12058385	ARHGAP15	-0.440260836	0.004496721	cg03542891	HAPLN1	-0.62402489	0.003676334	cg26048630	PRRX1	-0.57142292	0.005242798
cg13438236	ARHGAP18	-0.282171274	0.000873882	cg20737909	HCCA2	-0.49935136	0.003185613	cg14288424	PRRX2	-0.544945108	4.61E-05
cg06106428	ARHGAP20	-0.836361609	8.80E-08	cg06710082	HCG9	-0.636494357	0.008789347	cg08687825	PRSS35	-0.69414767	0.009734511

cg09023869	ARHGAP22	-0.276029101	0.002325342	cg17326769	HCK	-0.414274619	0.000126332	cg14580287	PRTFDC1	-0.404990353	0.001752152
cg22866565	ARHGAP24	-0.403039852	0.001713709	cg07564287	HCN1	-0.402328712	0.009989739	cg19104422	PRTG	-0.56563914	0.000450063
cg26682510	ARHGAP5	-0.2639999	0.008426729	cg06773216	HCP5	-0.520971981	0.000277809	cg00479101	PSEN2	-0.703772782	1.10E-05
cg08544606	ARHGEF10	-0.328176538	1.93E-05	cg26469895	HDAC4	-0.41984711	0.006603895	cg13886725	PSIP1	-0.308346324	0.002659761
cg25979543	ARHGEF10L	-0.89282082	0.001522271	cg10133908	HECTD2	-0.617724964	0.001265999	cg03958208	PSMD13	-0.308209158	0.004125407
cg01960096	ARHGEF11	-0.36972446	0.004721872	cg20649663	HECW2	-0.524265685	8.54E-05	cg00375608	PSMG3	-0.640712838	0.002894686
cg11644424	ARID1B	-0.41903736	0.001260698	cg18013782	HELZ	-0.271931168	0.008441955	cg26888012	PSORS1C1	-0.555839511	0.000791959
cg07691306	ARID3A	-0.665352241	2.18E-05	cg14390018	HERC2	-0.325721025	0.005886268	cg10749792	PSPH	-0.315451382	0.004118228
cg00663739	ARID4B	-0.321850832	0.009618715	cg24785532	HEY1	-0.622795102	0.000457313	cg26878949	PTCH1	-0.858678516	0.000960906
cg16260241	ARID5A	-0.340085032	9.44E-05	cg23407970	HEY2	-0.4504407	0.003814848	cg20487710	PTF1A	-0.637654423	0.009471124
cg00504569	ARID5B	-0.272759963	0.008189166	cg24938727	HHATL	-0.470028212	0.001920529	cg06738602	PTGER2	-0.262335001	0.0032248
cg04619120	ASPH	-0.271242052	0.001693283	cg10203922	HHIP	-0.705690866	3.07E-05	cg09685982	PTGFR	-0.459677901	0.002604481
cg16077226	ASRGL1	-0.488001633	4.34E-05	cg11724147	HIBADH	-0.329675955	0.002292087	cg23093116	PTGFRN	-0.346455104	2.29E-06
cg23780110	ASXL2	-0.372766401	0.00107955	cg16672562	HIF3A	-0.449647206	0.001053035	cg08533745	PTHLH	-0.422978276	0.008268317
cg09963640	ASXL3	-0.708319496	0.001251062	cg01293485	HIGD1A	-0.326326186	0.008349427	cg22053720	PTK7	-0.475812928	0.003360055
cg09126308	ATAD5	-0.260250718	0.002220714	cg24536933	HIP1R	-0.375397801	1.29E-05	cg13037201	PTPN21	-0.479486377	0.008856954
cg27519958	ATF6	-0.47008543	0.005677022	cg08529825	HIPK1	-0.536953824	0.007802656	cg21268658	PTPRF	-0.383187202	0.009550201
cg15546353	ATG16L1	-0.296722698	0.008236817	cg03221914	HIST1H2AJ	-0.426634317	0.000899824	cg03826247	PTPRG	-0.556900955	0.00082585
cg23900681	ATG2B	-0.810543896	0.000354715	cg18589478	HIST1H2BD	-0.331239756	0.00152434	cg12601353	PTPRO	-0.46696218	0.004845027
cg26467809	ATG7	-0.430980475	0.003666864	cg02481934	HIST1H3G	-0.511080889	0.001818764	cg19003733	PTRF	-0.282431452	0.002447195
cg02417360	ATP11A	-0.41555744	6.60E-05	cg27120683	HIST1H4A	-0.469955175	0.006114733	cg03438416	PURG	-0.321973132	0.001763312
cg07177379	ATP1A2	-0.372316473	0.001853281	cg16096631	HIVEP3	-0.588511011	0.001471673	cg10366053	PXDN	-0.535515739	0.001352835
cg24774891	ATP2A3	-0.296273374	0.008019211	cg05030953	HLA-C	-0.324929564	0.002767606	ch.8.1157478F	PXDNL	-0.283043225	0.005839725
cg13691247	ATP5G2	-1.255462752	0.008659408	cg18052547	HLA-DRB1	-0.589975105	0.004586395	cg07419011	PXN	-0.391893084	0.003941154
cg12384004	ATP8A2	-0.299837257	0.003273631	cg18816397	HLA-DRB5	-0.615273185	0.000219277	cg09738429	PYROXD1	-0.288283047	0.003138639
cg19599368	ATP8B4	-0.343910484	0.003618542	cg09296453	HLA-F	-0.392336562	0.00517274	cg26796190	PYY	-0.361516681	0.003481558
cg11731414	ATXN1	-0.375298366	0.001708914	cg03432955	HLA-G	-0.483937421	0.008780271	cg24273028	QDPR	-0.276364623	0.007749015
cg08715146	ATXN10	-0.581024713	6.23E-08	cg16444198	HLTF	-0.373659325	0.004345303	cg24727399	QRFPR	-0.588687272	0.002678157
cg23051598	ATXN2L	-0.279356153	0.001571818	cg05481991	HMGA2	-1.081598482	5.10E-06	cg25779645	R3HDML	-0.310157101	0.001060833
cg06077738	ATXN7	-0.541077495	0.000721064	ch.22.528917R	HMGXB4	-0.293344057	0.002455681	cg27303986	RAB11A	-0.279053758	0.0085119
cg16797751	ATXN7L1	-0.513554216	0.003902914	cg04670666	HMX3	-0.503290106	0.007684565	cg13791644	RAB11FIP2	-0.297819522	0.009314336
cg02344735	B3GAT2	-0.32865598	0.009299964	cg15246719	HNF1B	-0.377340107	0.006412909	cg00806214	RAB11FIP3	-0.442036778	0.002217127
cg06574960	B3GNT7	-0.468226149	0.005531522	cg23398700	HOMER1	-0.807773324	0.002576189	cg03253303	RAB11FIP4	-0.584883042	0.009310179
cg03989711	B3GNTL1	-0.28583716	0.009940936	cg14509403	HORMAD2	-0.494227102	0.002016254	cg16311186	RAB19	-0.50069638	0.00010321
cg01723148	B4GALNT1	-0.499248037	0.005176741	cg07450037	HOXA1	-0.453653164	0.001955213	cg00664609	RAB26	-0.480973147	0.004447816
cg01090609	B4GALT6	-0.587229791	0.001659736	cg15623480	HOXA11AS	-0.710943655	1.01E-05	cg12453687	RAB30	-0.321739547	0.000424049

cg11318251	BAALC	-0.549672882	0.001441125	cg00644317	HOXA13	-0.517810518	0.005294653	cg04421271	RAB38	-0.602894105	0.005116848
cg25670076	BACH2	-0.570573961	0.00565908	cg00445443	HOXA2	-1.009209451	0.004993172	cg24118052	RAB42	-0.409158604	0.009329957
cg10294853	BAHCC1	-0.711311782	0.003968312	cg24360871	HOXA3	-0.927525668	0.009089471	cg00164716	RAB5B	-0.306967989	1.26E-05
cg05750029	BAMBI	-0.38071242	0.003936783	cg21367811	HOXA4	-0.694024095	0.000499498	cg06235224	RABL4	-0.271813222	0.003993313
cg25959149	BANF2	-0.565325377	0.000765987	cg20517050	HOXA5	-0.47004244	0.001487665	cg19578161	RAD51L1	-0.607883958	0.00053339
cg14855874	BANK1	-0.846049433	1.60E-05	cg23590202	HOXA6	-0.631080017	0.008839474	cg08285589	RAG1	-0.392464186	0.005232519
cg08893585	BARX2	-0.498689273	0.00101439	cg12600174	HOXA9	-0.688310276	0.003649758	cg26976412	RAI1	-1.138192935	0.00113092
ch.2.3268406F	BAZ2B	-0.27594084	0.007686038	cg01882880	HOXB2	-0.29503393	0.003710795	cg26352006	RAI14	-0.690779646	0.002639317
cg25996835	BBS4	-0.867800202	8.61E-05	cg25116388	HOXB8	-0.492098145	0.00025787	cg02605461	RALY	-0.469079546	0.001603565
cg00933859	BBS9	-0.627391164	0.001046113	cg13615998	HOXC10	-0.526659179	0.001703562	cg03647559	RAMP1	-0.433017263	0.009048139
cg00908828	BCAR1	-0.547431611	3.04E-06	cg23063338	HOXC12	-0.408113289	0.009412332	cg17184245	RAP1GAP	-0.260381454	0.007203799
cg13178910	BCAS3	-0.282181046	0.003073748	cg06714180	HOXC4	-0.581697766	0.009853083	cg20563854	RAPGEF3	-0.628334839	2.47E-05
cg24770856	BCCIP	-0.301318249	0.001815521	cg16356837	HOXC9	-0.443227856	0.003639373	cg19153228	RAPGEF4	-0.47291019	2.78E-06
cg08328483	BCKDK	-0.267243479	0.0031921	cg23105697	HOXD10	-0.392816682	0.006064385	cg03982787	RARA	-0.589104656	0.000189404
cg08627352	BCL11A	-0.766932237	3.10E-05	cg11754318	HOXD12	-0.393667203	0.001584352	cg17436656	RARG	-0.574439894	0.004712211
cg07025989	BCL11B	-0.58123752	0.00532431	cg04739647	HOXD9	-0.946681485	7.07E-07	cg14473016	RASD2	-0.628341593	0.005248914
cg21602520	BCL2	-0.406671295	0.000373086	cg16593917	HPDL	-0.322618947	0.004673629	cg25506726	RASGRF1	-0.477241864	5.06E-05
cg26781524	BCMO1	-0.363824335	0.002068365	cg16674860	HPS1	-0.41700788	0.00245657	cg16165651	RASGRP3	-0.635864441	0.000287076
cg07260820	BCR	-0.268843552	0.006008725	cg00612625	HPSE2	-0.350573253	0.001993309	cg15383276	RASL10A	-0.277697436	0.007337969
cg18424965	BDKRB2	-0.474991836	0.006053839	cg23300529	HR	-0.367655113	0.009113794	cg03786743	RASL11B	-0.363554669	0.00073317
cg17413943	BDNF	-0.546845401	5.96E-05	cg13256912	HRH1	-0.477642905	0.000186906	cg19992375	RASSF3	-0.46636569	0.000187071
cg21193577	BEGAIN	-0.408348109	0.00548169	cg14496450	HRNBP3	-0.383497826	0.009322123	cg20311544	RBM15	-0.469250918	0.008738373
cg05669853	BEND3	-0.377074654	0.007402	cg24093763	HS3ST1	-0.589966784	0.002367399	cg12580156	RBM20	-0.511348155	0.001702089
cg01626459	BEND6	-0.524977686	0.008155791	cg24918767	HSD17B11	-0.401837036	0.001296352	cg02311932	RBM24	-0.758171379	1.95E-06
cg24686497	BEND7	-0.777676191	0.000501759	cg07996880	HSD17B14	-0.702686304	0.000572855	cg18062140	RBM38	-0.568973039	0.00013185
cg16122072	BHLHA9	-0.440993598	0.00683714	cg04845649	HSF4	-0.379275789	0.004267601	cg26530701	RBMS2	-0.779098188	0.001734334
cg01377006	BHLHE22	-0.677214828	0.001580156	cg01246617	HSPB3	-0.769270512	0.004723761	cg11493241	RBMXL1	-0.314427807	0.00123654
cg08353444	BICC1	-0.484021704	5.42E-05	cg01948201	HSPC159	-0.420101565	0.005412921	cg12298268	RBP1	-0.92061408	0.004736892
cg07360805	BLCAP	-0.397724023	0.000273234	cg18788940	HTATIP2	-0.272387514	0.003555763	cg20602843	RBP4	-0.622366323	0.00014313
cg21156320	BLOC1S1	-0.601761123	0.000712489	cg22442841	HTR1E	-0.397899523	0.008268568	cg12167489	RBPMS	-0.633879571	4.47E-05
cg12929983	BMF	-0.546813635	0.006786052	cg19500607	HTR4	-0.301275	0.0083679	cg13474370	RBPMS2	-0.408999151	0.005708919
cg11308639	BMP10	-0.275183611	0.000728575	cg11247289	HTR6	-0.273525004	0.001394113	cg11801959	RCBTB1	-0.292651024	0.000507097
cg17619993	BMP6	-0.32301852	0.006889672	cg12583095	HTR7	-0.460390963	0.005535855	cg16171860	RCC2	-0.288630024	0.001983596
cg15400671	BMPER	-0.371027901	0.003433697	cg00701951	HTRA1	-0.8348322	0.003907912	cg13170728	RCCD1	-0.332489949	0.009718949
cg25426203	BMPR1A	-0.45008034	0.000487402	cg10651168	ICAM1	-0.463315135	0.005747004	cg01782826	RCSD1	-0.282891425	0.000446332
cg07312854	BMPR2	-0.262155982	0.001948551	cg13981319	ICAM3	-0.413954903	0.002982142	cg17243643	RDH5	-0.69040988	0.009007403

cg01227028	BMS1	-0.297888411	0.005141951	cg13437870	ICK	-0.297867116	0.004894984	cg01574481	REC8	-0.431745669	0.004536305
cg00578530	BPNT1	-0.28619307	0.005617239	cg23191772	IDH3B	-0.31816371	0.001793138	cg24129115	REM2	-0.406311932	0.000941763
cg21311996	BRD2	-0.284092532	0.000833358	cg00760014	IFFO2	-0.704485057	0.00014311	cg22236375	REV1	-0.323397985	0.000202522
cg26771969	BRD4	-0.458619316	2.42E-05	cg23893332	IFI27	-0.370170271	0.002017523	cg27430977	REXO1	-0.553978308	0.000611203
cg04269188	BRF1	-0.356870642	0.004393899	cg16395953	IFIT1	-0.273098789	0.001978812	cg08143133	RFPL2	-0.387298377	0.003781375
cg19713911	BRSK2	-0.800092271	0.000320758	cg07013955	IFT140	-0.292781925	0.003248645	cg07200280	RFTN1	-0.491996536	0.002376171
cg25399162	BRUNOL4	-0.441807888	0.003313949	cg08806558	IGF1	-0.461375951	0.002089253	cg27476456	RFX1	-0.37131955	0.002522159
cg03233876	BSG	-0.383096061	0.004629663	cg08729686	IGF1R	-0.605870863	0.000643556	cg03789294	RGL2	-0.270108778	0.009364768
cg11711057	BTBD11	-0.35358179	0.008028231	cg09029085	IGF2BP1	-0.2966503	0.002457234	cg08119553	RGMA	-0.31352821	0.005836535
cg05281603	BTG4	-0.403139953	0.009116673	cg23991636	IGF2BP3	-0.696052241	8.15E-05	cg00634665	RGS20	-0.499707492	0.005587748
ch.2.2322307F	BUB1	-0.303058587	0.001207645	cg22108980	IGFBP1	-0.567243065	0.000361614	cg00250454	RGS9	-0.280583053	0.00040987
cg20918218	BUB1B	-0.677641945	0.003647702	cg16447589	IGFBP3	-0.528090543	0.006553956	cg08672410	RHBDF2	-0.485862942	7.75E-06
cg17186163	C10orf10	-0.390196668	0.001081886	cg22467567	IGFBP5	-0.445655542	6.20E-05	cg17935233	RHBG	-0.38707303	0.003520289
cg18903093	C10orf107	-0.47631864	0.009592286	cg19861288	IGFBP7	-0.803323735	0.000861208	cg24531520	RHEB	-0.466456088	0.000430004
cg06286521	C10orf11	-0.377062858	0.001917073	cg26279025	IL11	-0.395159661	0.006204208	cg17125688	RHOB	-0.428861176	0.000271644
cg25824127	C10orf118	-0.310262991	7.71E-05	cg00993824	IL12RB2	-0.648940659	0.008643409	cg08887961	RHOBTB1	-0.728143572	0.005656233
cg03846926	C10orf140	-0.793427296	0.005736131	cg15095327	IL17RE	-0.357745365	4.51E-05	cg26251101	RHOQ	-0.798108196	0.000437893
cg06789550	C10orf4	-0.644351012	0.00849517	cg05934682	IL4I1	-0.803198508	0.000144354	cg24531915	RHOU	-0.742467012	0.009531333
cg03958038	C10orf41	-0.634193679	0.006054696	cg05472934	IL6	-0.324342518	0.001532559	cg09320717	RIC8A	-0.341718239	0.008074323
cg16353350	C10orf55	-0.265879645	0.005473357	cg19031085	IL9	-0.362786025	0.003093695	cg00219210	RICH2	-0.616816228	0.0006992
cg11824509	C10orf57	-0.344676634	0.005882316	cg04724540	ILDR2	-0.437632404	0.000121587	cg04863573	RIMS3	-0.262200951	0.005895741
cg24098603	C10orf79	-0.520913292	0.005818277	cg00351047	ILVBL	-0.401479821	0.005481107	cg18578263	RINL	-0.284671624	1.94E-05
cg25150929	C10orf82	-0.384773451	0.005000221	cg22757447	IMPACT	-0.565182959	0.002079404	cg12091376	RIPK4	-0.762824839	0.000467011
cg06680201	C11orf51	-0.347131442	0.004472812	cg20179942	INCENP	-0.438580441	0.000210644	cg23390920	RMST	-0.266194807	0.005509229
cg00219330	C11orf57	-0.26354333	0.003858906	cg04084236	INPP4B	-0.819974412	0.000303644	cg10162691	RND2	-0.348011673	0.00562781
cg16463558	C11orf70	-0.540337287	0.002073609	cg09415366	INPP5A	-0.303123347	0.005950373	cg07144730	RND3	-0.29362366	0.007411009
cg15102749	C11orf80	-0.499030155	2.99E-06	cg01223673	INSC	-0.411213656	0.006219226	cg15136797	RNF103	-0.323128948	0.000915674
cg05216730	C11orf88	-0.515432911	0.000477654	cg21635588	IPCEF1	-0.417367783	0.001444382	cg02298193	RNF145	-0.332961685	0.000218015
cg22627427	C11orf9	-0.437225988	0.001251441	cg09817283	IQCE	-0.452892081	0.000114065	cg08660876	RNF175	-0.480120131	0.003708851
cg09907758	C11orf95	-0.54734948	0.001603751	cg05321109	IQCH	-0.546021236	9.41E-06	cg23626546	RNF182	-0.663187524	0.008569759
cg10664305	C13orf30	-0.324965949	0.000151513	cg02387679	IQGAP2	-0.505523199	0.009324604	cg11977605	RNF212	-0.700587171	0.000190828
cg18174881	C14orf106	-0.362508669	0.007334182	cg20395892	IRAK3	-0.445594041	0.000561973	cg18180569	RNF220	-0.448518102	0.006261384
cg06603649	C14orf143	-0.685945332	0.000626327	cg25192855	IRF6	-0.656593126	0.003451586	cg06569121	RNF5P1	-0.310303498	0.001792313
cg04127998	C14orf179	-0.522031056	3.07E-05	cg25924746	IRS2	-0.435122584	0.000831817	cg10978355	RNU5E	-0.56778439	0.005345971
cg24128590	C14orf43	-0.401407821	0.002464538	cg10805956	ISG20L2	-0.561040312	0.003694569	cg16989059	ROBO1	-0.639503142	0.009412556
cg16506185	C14orf48	-0.442196235	0.001117541	cg14834938	ISL1	-0.307305898	0.001948185	cg13266327	ROCK2	-0.308282654	0.003185591

cg23358740	C14orf72	-0.265262675	0.009665024	cg01843020	ISL2	-0.327153201	0.003126212	cg17371621	RORA	-0.58833946	0.002464339
cg14916983	C15orf23	-0.49409021	0.003292081	cg25515269	ITGA4	-0.323674939	0.003497697	cg01789150	RPA2	-0.53577141	0.001420284
cg04819351	C15orf41	-0.3131419	0.000131702	cg19925054	ITGA6	-0.287744402	0.007211937	cg08770870	RPH3AL	-0.510458347	0.005602149
cg09685682	C16orf7	-0.652667864	9.51E-05	cg04665374	ITGA7	-0.803106075	0.000174658	cg08798701	RPL32P3	-0.261130531	0.007985744
cg25228625	C17orf44	-0.442436839	0.004285154	cg03192874	ITGAV	-0.270039493	0.000158102	cg20526303	RPL35A	-0.286969209	0.00235909
cg23508887	C18orf1	-0.958739038	0.0002449	cg01033299	ITGB7	-0.263420345	0.008796818	cg18507032	RPLP0P2	-0.567687729	0.006426377
cg06440065	C19orf12	-0.309004163	0.006664118	cg18389827	ITPK1	-0.507810808	0.001494096	cg10716823	RPLP1	-0.668136204	0.001266692
cg12068124	C19orf26	-0.365219522	0.008737732	cg20272979	ITPKA	-0.478104976	3.92E-05	cg00271210	RPS6KA2	-0.484625753	0.001944118
cg26872588	C1orf198	-0.591072918	0.000980482	cg23387597	ITPRIP	-0.492413043	0.002752174	cg26191576	RPS6KL1	-0.339139064	0.002298474
cg03603260	C1orf56	-0.429620003	0.002090247	cg16452651	ITSN1	-0.64997616	0.002428437	cg09491897	RPTOR	-0.275288814	0.004367378
cg22610676	C1orf61	-0.315336627	0.004043331	cg20691080	JAKMIP1	-0.447871379	0.004725558	cg19516340	RRM2	-0.500546375	0.002832537
cg09176275	C1orf87	-0.385681691	0.008634169	cg10466421	JAM2	-0.556769924	0.002894153	cg17176676	RTDR1	-0.56912618	0.002472859
cg16348470	C1orf94	-0.707769212	0.002454331	cg14186846	JARID2	-0.497020654	0.005225993	ch.15.433532F	RTF1	-0.279588607	0.002234368
cg23598718	C1QL1	-0.576528794	0.006880458	cg09929567	JDP2	-0.630976676	0.000214678	cg16758662	RTN1	-0.734925545	0.00255592
cg23882796	C1QTNF1	-0.490901325	0.00983247	cg05037622	JPH2	-0.666777783	1.09E-05	cg05550893	RTN4RL1	-0.354695893	0.006885707
cg05826607	C20orf108	-0.31521053	0.003937317	cg23040064	JPH3	-0.274651782	0.00585552	cg21824162	RUNDC1	-0.497786061	0.002486666
cg14162940	C20orf160	-0.587589085	0.005888963	cg01751802	KANK2	-0.373618596	0.006148743	cg02115818	RUNDC3A	-0.38280728	0.007157591
cg03331263	C20orf166	-0.853508904	4.69E-05	cg21195235	KATNAL2	-0.502781942	0.009801527	cg01664727	RUNX1	-0.467567737	4.17E-07
cg00759619	C20orf199	-0.327630402	0.006606229	cg09587640	KAZALD1	-0.300155407	0.001600058	cg05468028	RWDD2B	-0.991470073	5.35E-06
cg13884903	C20orf56	-0.38660398	0.005260708	cg00838874	KCNA1	-0.491526849	0.004838642	cg18294646	RXFP3	-0.505276746	0.000468991
cg20517099	C21orf125	-0.494355706	0.00049165	cg00375025	KCNAB1	-0.338016377	0.005376762	cg13677043	RXRA	-0.293817758	8.79E-05
cg25726756	C21orf56	-0.678935719	7.51E-05	cg21318380	KCNG1	-0.270414066	0.006600676	cg09508496	RYR1	-0.759651589	0.006929041
cg06787912	C21orf82	-0.32177295	0.004847684	cg05364164	KCNH2	-0.727839117	5.37E-05	cg19907725	S100A2	-0.608628709	1.64E-05
cg16334524	C21orf84	-0.601458306	7.11E-05	cg19502709	KCNIP1	-0.950922308	0.000101513	cg01754041	SAA3P	-0.552371997	0.000939914
cg00325866	C2CD4A	-0.520224561	0.001482085	cg03557857	KCNIP2	-0.575553286	0.001049368	cg15600398	SACM1L	-0.309923858	0.008544024
cg01184271	C2CD4B	-0.421020494	0.000944362	cg17412560	KCNIP3	-0.532900053	0.002605303	cg00805193	SAMD10	-0.338393507	0.002302543
cg12760041	C2orf67	-0.382830063	0.009782841	cg03122532	KCNJ15	-0.312400488	0.005449792	cg05040429	SAMD12	-0.389638758	0.008006208
cg08130668	C2orf73	-0.29939143	0.005100371	cg06942027	KCNJ2	-0.615282449	0.005092206	cg13305246	SAMD13	-0.358769386	0.001756277
cg10168635	C2orf88	-0.357851701	0.006983807	cg22732603	KCNMA1	-0.425223354	8.67E-06	cg19758859	SASH1	-0.750710396	0.007252265
cg05974788	C3orf19	-0.282629498	0.00172466	cg22646937	KCNMB1	-0.453090011	0.003891239	cg03139053	SATB2	-0.465455951	0.009721249
cg17617228	C3orf21	-0.360187785	0.000539771	cg22904711	KCNN4	-0.283240707	0.004554838	cg19955956	SBDSP	-0.416663124	0.000758393
cg21589858	C3orf26	-0.35278579	0.008329335	cg07979757	KCNQ1	-0.414611602	0.002981181	cg14604369	SC4MOL	-0.385479498	0.004627081
cg24029436	C3orf38	-0.35710722	0.008274855	cg11272547	KCNQ1OT1	-0.545645503	0.008285302	cg14917706	SCARA5	-0.598059713	0.003869683
cg12105691	C3orf50	-0.261166505	0.000883113	cg13372488	KCNT2	-0.301517739	0.003775414	cg00188627	SCHIP1	-0.375507825	0.004505677
cg01012330	C3orf59	-0.73965449	0.00043628	cg09982773	KCP	-0.373676339	0.009514531	cg11749828	SCN1B	-0.770971098	0.001090756
cg22988507	C4orf10	-0.264867457	0.005845322	cg23877008	KCTD10	-0.297074681	0.007686834	cg04774040	SCN8A	-0.331605984	0.008979262

cg08286012	C4orf22	-0.522834083	0.003594402	cg02973307	KCTD15	-0.270992813	0.001968089	cg07087293	SCNN1B	-0.823257996	0.002072007
cg27286840	C4orf33	-0.527286516	0.000200608	cg07505433	KDM4B	-0.294078366	0.007063846	cg07444408	SCOC	-0.382502785	0.003309516
cg12402800	C5orf35	-0.35380428	0.009229984	cg26719995	KHK	-0.377071969	0.005491279	cg00659559	SCRN1	-0.331707518	0.004807724
cg21999939	C5orf38	-0.745909897	0.000242933	cg05746407	KIAA0182	-0.281564477	0.008095653	cg19237879	SCUBE2	-0.563644867	0.003453113
cg19610869	C5orf52	-0.465715282	0.007081384	cg04555107	KIAA0247	-0.586355884	0.000388884	cg25451765	SDK1	-0.266468966	0.00093704
cg24878755	C6orf115	-0.524900014	0.005906408	cg06465196	KIAA0922	-0.26304758	0.005464996	cg22786903	SDR39U1	-0.263855833	0.001626468
cg24627621	C6orf132	-0.461951243	0.003835001	cg02835848	KIAA1026	-0.335568736	0.008968283	cg13868393	SEC14L1	-0.553669446	0.002506282
cg05829479	C6orf141	-0.782652753	0.000133868	cg17239876	KIAA1274	-1.066477743	0.009330746	cg02557269	SEC61G	-0.282395502	0.000147659
cg21283926	C6orf150	-0.374146653	0.000866718	cg27430662	KIAA1324	-0.371005208	0.005455433	cg22177364	SELT	-0.284534105	0.004980552
cg21097036	C6orf174	-0.811763188	0.001141511	cg01834151	KIAA1370	-0.260476686	0.005404323	cg05742308	SEMA3A	-0.665147854	0.003883425
cg19997946	C6orf176	-0.521591358	0.005007423	cg19331777	KIAA1462	-0.487952273	0.001582977	cg25597623	SEMA3B	-0.307224727	0.005761344
cg01431340	C6orf186	-0.436300367	0.008267261	cg06753901	KIAA1486	-0.53516309	0.005962264	cg08011008	SEMA3C	-0.417399635	0.007593723
cg03290281	C6orf195	-0.707760875	0.000567913	cg18124413	KIAA1632	-0.603237508	0.001713515	cg21187258	SEMA3E	-0.362775423	0.002475822
cg19274606	C6orf223	-0.375501104	0.003517869	cg26426395	KIDINS220	-0.417061834	0.003956072	cg16529883	SEMA3F	-0.548596165	0.000344144
cg17561891	C7orf23	-0.284627922	0.002056657	cg07058086	KIF13B	-0.591524675	0.00071261	cg09241381	SEMA5B	-0.357493703	0.002654672
cg08707078	C7orf46	-0.307094247	0.008216783	cg15821605	KIF16B	-0.468177012	0.001344734	cg02633924	SEPT9	-0.843115476	0.009530636
cg20496693	C7orf50	-0.929489778	0.009261456	cg05390356	KIF1B	-0.415726126	0.00670805	cg17465920	SERINC3	-0.569616191	0.005671915
cg17423419	C7orf52	-0.332959595	0.005145343	cg17126435	KIF26B	-0.472456288	0.006197049	cg20793341	SERPINE2	-0.346717654	0.008965564
cg06792186	C7orf54	-0.274808017	0.0030595	cg06118384	KIF5C	-0.702953431	0.001176243	cg17039262	SETD4	-0.315557659	0.001979621
cg25202791	C7orf58	-0.312014644	0.001535543	cg21480743	KILLIN	-0.65357506	0.000668939	cg15544402	SF3B14	-0.346439331	0.000110997
cg22735749	C8orf34	-0.638124404	1.76E-05	cg12689529	KIRREL3	-0.441124946	0.008907943	cg23274030	SFXN4	-0.499764143	0.001802295
cg12990392	C8orf40	-0.298377195	0.003454357	cg25281029	KITLG	-0.479805772	0.003051513	cg23498273	SGCE	-0.65807855	0.002962956
cg23109344	C8orf42	-0.730429066	0.000380303	cg23282559	KL	-0.474589302	0.009786743	cg06573459	SGEF	-0.525772394	0.005378347
cg07222863	C8orf56	-0.574522055	0.005807751	cg26031613	KLC1	-1.167963777	0.00588234	cg04951797	SGOL1	-0.342474506	0.006599232
cg27132335	C8orf84	-0.558233684	0.008375968	cg03883348	KLC3	-0.587060882	5.04E-05	cg05409597	SGOL2	-0.419628663	0.004368176
cg27099274	C9orf125	-0.457588567	0.001952901	cg03939688	KLF4	-0.264462174	0.009131051	cg01984322	SGSM1	-0.482460121	0.008385345
cg21120249	C9orf139	-0.475297027	0.000210425	cg23522817	KLHDC10	-0.602508973	0.004678204	cg00018181	SH2B2	-0.580874634	5.14E-05
cg13637871	C9orf16	-0.568075758	0.000248396	cg05830220	KLHDC4	-0.384130804	0.001796684	cg08975445	SH2D4B	-0.591704556	0.001233079
cg13427827	C9orf71	-0.465175607	0.00043582	cg19884658	KLHL21	-0.763792653	0.002842875	cg01319323	SH3GLB2	-0.358231998	0.004943342
cg25063515	CA10	-0.360006957	0.001220541	cg15803765	KLHL24	-0.302657457	0.002039315	cg05168015	SH3PXD2B	-0.656665887	0.00546684
cg10394757	CA7	-0.463714491	0.000241173	cg18405786	KLHL26	-0.521916419	0.006993428	cg03326608	SH3RF2	-0.277652768	0.002528586
cg19257550	CA9	-0.460025618	0.005627511	cg14826211	KLHL29	-0.530619009	0.001481035	cg00010078	SH3RF3	-0.377709609	0.001107434
cg03697708	CACNA1A	-0.314681006	0.00116747	cg05740254	KLKB1	-0.358067583	0.002424713	cg04370174	SH3TC1	-0.293866951	0.003674205
cg14637685	CACNA1C	-0.287990957	0.00571297	cg17360680	KRT1	-0.373094686	0.009732151	cg21789620	SHC4	-0.286271301	0.001868086
cg19075717	CACNA1G	-0.32292752	0.004338923	cg15056128	KRT222	-0.330120581	0.001810083	cg18581445	SHD	-0.62885455	0.00191375
cg01351992	CACNA1H	-0.687850453	2.91E-05	cg14645027	KRT7	-0.383610916	0.000685552	cg27088306	SHISA3	-0.544629436	0.003867723

cg04764839	CACNB2	-0.705222999	0.00281818	cg03691818	KRT77	-0.760232592	0.002158671	cg26763362	SHMT1	-0.362074306	1.32E-05
cg11025974	CACNB4	-0.697306028	0.000658532	cg19092735	KRT80	-0.450646632	0.0029229	cg24317285	SHOX2	-0.489142342	0.000141015
cg26787020	CACYBP	-0.385772456	0.006550529	cg26034919	KRTCAP3	-0.288622566	0.000569611	cg04777971	SHQ1	-0.36100431	0.0003608
cg18160302	CADM1	-0.287365225	0.002388371	cg16518167	KSR1	-0.503116131	0.004516119	cg06900164	SHROOM1	-0.437367504	0.004951902
cg07238401	CALCA	-0.421820927	0.009068129	cg10910512	LAMA4	-0.546180476	0.005080924	cg18628449	SHROOM3	-0.396632761	0.001360986
cg17449465	CALCR	-0.373314109	0.007132258	cg08234664	LAMB2	-0.29012362	0.001195951	cg06907405	SIAH1	-0.357858652	0.004303735
cg11425149	CALD1	-0.584995496	0.000421442	cg08905629	LAMC2	-0.352941412	0.001088977	cg27504195	SIDT1	-0.694292578	0.009040073
cg23889047	CAMTA1	-0.500661423	0.000269916	cg11552287	LANCL2	-0.469850901	0.000866408	cg04927931	SIM1	-0.82878772	0.000408074
cg23036213	CAP2	-0.538313567	0.000854679	cg26838532	LARP1B	-0.379037302	0.007755075	cg23896164	SIM2	-0.344367278	0.005727124
cg25363789	CAPN1	-0.595508139	0.006969471	cg24413781	LASS4	-0.598304524	0.004987361	cg10179569	SIPA1L1	-0.455864239	6.14E-06
cg13416249	CAPN10	-0.309337391	0.001621602	ch.12.1019410F	LASS5	-0.284477021	0.000432896	cg18780167	SIRPA	-0.394582189	0.004097392
cg21167643	CAPN2	-0.278338824	0.008822968	cg15882591	LATS2	-0.457904263	0.00024975	cg06954855	SLAMF8	-0.571744922	1.61E-05
cg06713671	CAPS	-0.438217957	0.00222251	cg02825765	LBR	-0.392114197	0.009908223	cg08571821	SLC12A4	-0.332624774	0.000611569
cg16694480	CAPZB	-0.596849471	0.008121547	cg04255230	LBX2	-0.691967314	0.002582249	cg00420510	SLC12A7	-0.263172275	0.004290465
cg08862742	CARS	-0.297413367	0.006457644	cg00656860	LBXCOR1	-0.829922719	9.41E-06	cg10643271	SLC15A4	-0.627232765	0.002220614
cg19108881	CASR	-0.651233991	0.00330353	cg08748308	LCP2	-0.461867055	0.008588082	cg07011163	SLC16A11	-0.3828972	0.006908025
cg05654925	CASZ1	-0.52263917	0.000982831	cg19861824	LDB2	-0.28791896	0.000953061	cg03616221	SLC16A12	-0.376423832	0.009406037
cg05579598	CBFA2T3	-0.666363543	0.002595826	cg19286437	LDB3	-0.709265833	0.000812713	cg07763231	SLC16A3	-0.373217597	0.009690479
cg03561455	CBLN2	-0.508743307	0.009866403	cg02232751	LDHA	-0.335787089	0.00930181	cg20956278	SLC16A8	-0.688495855	0.000688334
cg01856529	CBX5	-0.617590194	0.003451592	cg17296588	LDLRAD3	-0.346072198	0.008420095	cg21961771	SLC17A8	-0.634189481	0.005098053
cg12695707	CCDC105	-0.290947346	0.006871715	cg01141438	LEPREL1	-0.399463034	9.53E-05	cg08411235	SLC1A2	-0.605698195	0.002473608
cg06240200	CCDC12	-0.55050822	0.003216416	cg07793207	LGI1	-0.899470858	0.001273897	cg16610086	SLC1A3	-0.877604844	0.000538074
cg09879794	CCDC136	-0.564897323	0.001056227	cg03763118	LGR4	-0.381784557	0.001374177	cg08737116	SLC22A15	-0.383097091	0.000704347
cg14688579	CCDC140	-0.497952058	0.007969023	cg21558545	LGR5	-0.520810327	0.00248537	cg14527280	SLC22A23	-0.405397579	0.004928279
cg06749819	CCDC149	-0.507399637	0.000139462	cg17830682	LGR6	-0.445893977	0.004960907	cg05231888	SLC22A4	-0.630141603	0.00124862
cg05980785	CCDC150	-0.460940336	0.001487689	cg20566475	LHPP	-0.736386016	6.06E-05	cg21948465	SLC22A5	-0.273994561	0.006454368
cg04856896	CCDC28B	-0.311998351	0.008854242	cg03306024	LHX2	-0.413830261	0.00520659	cg22807402	SLC25A19	-0.37395412	0.00603261
cg26038589	CCDC55	-0.326291817	0.00386761	cg26225694	LHX4	-0.989398018	1.81E-05	cg07643355	SLC25A26	-0.347374542	0.000502447
cg05385248	CCDC6	-0.278510959	0.002173643	cg08883223	LHX9	-0.528667082	0.003561589	cg26607031	SLC25A33	-0.26295277	0.007617948
cg12315713	CCDC67	-0.379912794	0.007562305	cg14531530	LIMCH1	-0.736016772	0.001237602	cg26615176	SLC25A45	-0.412678224	0.000599328
cg03292040	CCDC74A	-0.384789066	0.001917804	cg10512202	LIMD1	-0.406179718	0.002188065	cg14494721	SLC26A10	-0.304567575	0.000669633
cg22360649	CCDC85B	-0.61156252	0.000251861	cg22961457	LIME1	-0.452632311	0.007424999	cg00261900	SLC29A1	-0.583081106	0.001847849
cg14051236	CCDC85C	-0.664797446	0.002376825	cg03226958	LIN28	-0.37083075	0.003177164	cg02354828	SLC29A3	-0.268835637	0.009001536
cg05040501	CCDC88C	-0.913954453	1.00E-06	cg19130180	LIN7A	-0.333973937	0.001224559	cg20294984	SLC2A1	-0.413136552	1.30E-08
cg26512045	CCHCR1	-0.510744314	0.000437416	cg15677957	LIPG	-0.550459163	0.004086147	cg20313963	SLC2A3	-0.261061276	0.001433272
cg13732201	CCK	-0.334529195	0.009556755	cg08268266	LITAF	-0.291806845	0.000480413	cg14565651	SLC2A5	-0.49522631	0.006371246

cg05440824	CCL2	-0.520277857	0.000162942	cg21396211	LIX1L	-0.282111449	3.77E-05	cg24594459	SLC30A3	-0.445429691	0.005573769
cg24626079	CCND2	-1.003276079	0.001942635	cg06560887	LMO2	-0.339874349	0.003869839	cg17073023	SLC35F2	-0.301829374	0.005853105
cg10505740	CCNF	-0.539506235	0.005951871	cg10143811	LMO3	-0.399800282	0.008822886	cg05133578	SLC38A1	-0.532312024	0.000278974
cg01768981	CCNO	-0.643732485	0.001796769	cg09871637	LMO4	-0.400631723	0.001099308	cg25988214	SLC38A10	-0.405674149	0.000219444
cg11730023	CCNY	-0.490181134	0.000970278	cg15511928	LMOD1	-0.276127075	0.002531163	cg05339727	SLC38A11	-0.605772781	0.001583857
cg23112950	CCS	-0.874614515	3.84E-05	cg20771240	LOC100128239	-0.940688903	0.002787954	cg08382534	SLC38A8	-0.505160167	0.007191937
cg23004174	CD109	-0.590318168	2.03E-05	cg27586487	LOC100128292	-0.4935959	0.005204505	cg06812574	SLC39A12	-0.422057165	0.006626083
cg10671907	CD164	-0.264716537	0.004295542	cg07474312	LOC100129387	-0.268433402	0.004812753	cg13402055	SLC3A2	-0.287129477	0.001720248
cg07681748	CD200	-0.482283342	0.00149327	cg08531140	LOC100130987	-0.468569397	0.004503706	cg19075346	SLC40A1	-0.270205443	0.003651664
cg02130027	CD2AP	-0.957000672	0.000523631	cg02606403	LOC100132215	-0.477938084	0.000324932	cg08509840	SLC41A3	-0.297589109	0.007514207
cg12331932	CD300A	-0.515693055	0.005108983	cg20494635	LOC100133545	-0.674077384	0.003414735	cg00505133	SLC44A3	-0.354198937	0.00317953
cg08347373	CD302	-0.307677132	0.005747787	cg12995090	LOC100192426	-0.506711742	0.00790322	cg04567302	SLC44A4	-0.308459943	0.003975007
cg07458509	CD320	-0.563276102	0.001154717	cg12409149	LOC100270710	-0.340598507	0.003712866	cg24743310	SLC47A2	-0.343963895	0.001502472
cg02189760	CD37	-0.634555459	0.005808193	cg10972625	LOC100286793	-0.718772708	3.49E-07	cg26131670	SLC4A4	-0.319668462	0.004219583
cg04290171	CD46	-0.314701645	0.000483167	cg19664945	LOC100302652	-0.588564881	0.009982316	cg19686001	SLC6A15	-0.666640047	0.002310864
cg26129545	CD74	-0.427380201	0.007488673	cg22121570	LOC145845	-0.354495769	0.006992012	cg04874129	SLC6A2	-0.67177188	0.000260611
cg19583076	CD79A	-0.373973885	0.004618667	cg08940787	LOC146880	-0.558948585	0.00596369	cg08530317	SLC6A5	-0.452413877	0.007678108
cg17605814	CD82	-0.664217026	0.000760341	cg27263506	LOC148145	-0.270091802	0.006612615	cg04487857	SLC7A11	-0.443744014	0.00275009
cg00519069	CD97	-0.703585303	0.001461747	cg15176829	LOC149134	-0.472720658	0.004195468	cg26569315	SLC7A5	-0.426605403	0.003742264
cg27210565	CDC10L	-0.34749163	0.001306095	cg08355260	LOC151534	-0.691286516	0.000329941	cg19599045	SLC7A7	-0.344960317	1.83E-05
cg05469695	CDC42EP3	-0.553637068	0.000459105	cg00528902	LOC157627	-0.385878459	0.001464517	cg19473656	SLC7A8	-1.177427484	0.000908816
cg05005217	CDCA2	-0.624143377	0.003624388	cg04577441	LOC256880	-0.263190368	0.008516468	cg02870829	SLC8A1	-0.402520961	0.000342366
cg24776469	CDCA7	-0.601412743	0.001071121	cg14955259	LOC283050	-0.264354627	0.008751759	cg20267521	SLC8A3	-0.43076993	0.006352051
cg01251360	CDH1	-0.5488051	0.004999286	cg04138492	LOC283731	-0.391096486	0.003310455	cg14574489	SLC9A9	-1.006989438	0.000250435
cg12830671	CDH23	-0.556831357	0.000450901	cg08767637	LOC283867	-0.511738826	0.000164838	cg02633036	SLCO3A1	-0.730793198	0.000157323
cg05397033	CDH4	-0.522566391	0.002217266	cg22849543	LOC284749	-0.3183231	0.001773154	cg22005565	SLFNL1	-0.279092114	0.000192926
cg10502957	CDK2AP1	-0.452974169	0.004107693	cg15826810	LOC285419	-0.415303466	9.23E-06	cg05265607	SLIT1	-0.503700202	0.006604042
cg16198692	CDO1	-0.625697007	0.002996204	cg20435387	LOC285740	-0.357383086	0.002129553	cg03260566	SLIT2	-0.36278753	0.003562333
cg26677584	CDX2	-0.5304468	0.005073103	cg11520439	LOC286367	-0.361210872	0.008548647	cg06020130	SLITRK3	-0.613703141	0.009132516
cg00884093	CELSR1	-0.782934246	0.002141751	cg16683160	LOC339524	-0.672653603	0.004001789	cg02971575	SMAD1	-0.396858065	0.002853768
cg06884314	CENPE	-0.456897561	0.000981455	cg26245256	LOC388428	-0.507481939	0.002221468	cg05100634	SMAD2	-0.343334028	0.005480381
cg14631576	CENPP	-0.437391206	0.002862328	cg15472739	LOC388692	-0.654571609	1.71E-05	cg23172828	SMAD6	-0.26575817	0.005014756
cg11639001	CEP164	-0.433871781	0.004573436	cg01054755	LOC389333	-1.1183925	0.004976414	cg05311180	SMARCAL1	-0.500656467	0.007942341
cg06766034	CERK	-0.26636459	3.98E-05	cg06270545	LOC390595	-0.472489818	0.004433152	cg20808693	SMARCD3	-0.324631346	0.000784837
cg11911679	CERKL	-0.754487787	1.54E-06	cg13036381	LOC401097	-0.52890739	0.000282543	cg14353079	SMC5	-0.290313658	0.006220101
cg10627839	CFHR4	-0.667851768	0.001161233	cg08188993	LOC401463	-0.53013218	0.00659568	cg00790307	SMCR5	-0.285522486	0.001426738

cg17616554	CFTR	-0.408600347	0.00058094	cg11967431	LOC440461	-0.545161448	0.004913951	cg21180572	SMU1	-0.543572599	0.006667775
cg06255037	CHADL	-0.306482223	0.008955822	cg00504896	LOC642846	-0.489840704	0.009513711	cg16357768	SMURF2	-0.291629178	0.008455353
cg14719959	CHD7	-0.420804313	0.001188581	cg22055687	LOC645323	-0.43728754	0.003573896	cg11355215	SNAP25	-0.344341068	0.008177678
cg21472642	CHN2	-0.667796715	8.08E-05	cg03649288	LOC646405	-0.739345921	0.000535458	cg01426303	SNAP47	-0.290468286	0.001077306
cg24631222	CHRNA5	-0.396126167	0.009443985	cg06890747	LOC646999	-0.418951635	0.000542189	cg17725477	SNAPC5	-0.322309949	0.008505053
cg14275842	CHRNE	-1.521218258	7.98E-08	cg07604732	LOC728276	-0.588620265	0.007057223	cg05241924	SNCA	-0.639624178	0.002460209
cg07696842	CHST11	-0.726869782	0.000220437	cg13937272	LOC728875	-0.297895847	0.005757373	cg03740025	SND1	-0.27364798	0.00082989
cg17228698	CHST12	-0.417469288	8.10E-05	cg04118741	LOH12CR1	-0.404869067	0.001038857	cg20969675	SNORD104	-0.28099533	0.000213335
cg04268405	CHST3	-0.411396978	1.78E-06	cg00144550	LONRF2	-0.431388681	0.001054551	cg25932239	SNRNP35	-0.319904115	0.003501352
cg02298612	CHST6	-0.397006371	0.008040559	cg19257102	LOXL1	-0.343559004	0.006434304	cg15167547	SNRNP48	-0.405561309	0.005435252
cg14923652	CIDEA	-0.478331887	0.000901299	cg04521765	LOXL4	-0.287078966	0.00770501	cg14258243	SNRPD1	-0.269965589	0.004387683
cg27393372	CIR1	-0.322757869	0.003026162	cg10521852	LPAR2	-0.264600169	0.002479077	cg18453884	SNRPF	-0.48794811	0.005547193
cg07095330	CISD3	-0.391663374	0.003221497	cg01751134	LPCAT2	-1.272319357	0.000218865	cg26495357	SNTG2	-0.560858494	0.000564869
cg05786809	CKB	-0.572599721	0.00081415	cg14565903	LPHN1	-0.306735985	0.001461554	cg19808643	SNX2	-0.508749401	0.003018245
cg12545882	CLASP1	-0.64051955	0.00017596	cg00869941	LPP	-0.309394996	0.003177818	cg05203809	SNX29	-0.531012531	0.000458532
cg12741994	CLDN11	-0.797159339	0.000486675	cg13683361	LPPR1	-0.421857049	0.001041766	cg17199658	SNX31	-0.46885342	0.004052759
cg10205852	CLDN12	-0.322466251	0.000792217	cg27072996	LPPR3	-0.968621138	0.000120481	cg01123186	SOCS7	-0.29060248	0.00164014
cg00282244	CLDN15	-0.353589819	4.02E-05	cg23676439	LRAT	-0.264975117	0.007257796	cg10307548	SOD3	-0.305398842	2.97E-06
cg02882785	CLDN22	-0.43011223	0.002618159	cg26075356	LRCH1	-0.534289666	0.007933331	cg18318006	SORBS1	-0.61960192	0.000162714
cg17865114	CLDN6	-0.424612113	0.001086702	cg03393017	LRCH3	-0.310242116	0.005043848	cg14516100	SORBS2	-0.738197115	0.003067732
cg05373723	CLGN	-0.787115637	2.80E-07	cg13146674	LRP5	-0.739570137	0.000357623	cg01275038	SORCS2	-0.724358987	0.002124499
cg20638683	CLIC5	-0.637513472	0.008512912	cg23597288	LRP5L	-0.421018387	0.006289357	cg13588483	SOX5	-0.519890218	0.000111825
cg19200589	CLIC6	-1.621488758	1.23E-05	cg06772295	LRRC16B	-0.413864956	0.006899376	cg16448102	SP8	-0.606411762	0.002429088
cg03115444	CLIP1	-0.464153035	0.005369786	cg24224501	LRRC17	-0.436130612	0.007454682	cg10536349	SPAG9	-0.499264096	1.56E-06
cg19501108	CLIP2	-0.333943782	0.006656258	cg20941258	LRRC2	-0.482598487	0.00361765	cg04461197	SPATA16	-0.407898287	0.006063611
cg22952787	CLN5	-0.445034623	0.001774277	cg13696351	LRRC26	-0.348370889	0.0006375	cg03940064	SPATA18	-0.72531076	0.003204838
cg06085476	CLOCK	-0.30626345	0.002555776	cg00748958	LRRC37B	-0.354400303	0.000489637	cg12903001	SPATS2L	-0.373122233	0.007380857
cg00559234	CLSTN1	-0.531074669	0.009582272	cg15328271	LRRC52	-0.403213904	0.005596871	cg25619638	SPEG	-0.397123586	0.002875075
cg13630493	CLTA	-0.582889231	0.000596781	cg24629215	LRRC58	-0.262969772	0.007937707	cg02821871	SPHK2	-0.585995176	0.003373681
cg12790874	CLYBL	-1.260245058	7.65E-05	cg11026333	LRRC61	-0.850731292	0.000297139	cg13124801	SPNS2	-0.430411058	0.005867922
cg01494399	CMIP	-0.359927943	0.000111832	cg06641366	LRRC8C	-0.36048765	0.004797608	cg26435178	SPOCK2	-0.645918708	0.003896703
cg09849405	CMTM1	-0.50041089	0.001447373	cg15934958	LRRFIP2	-0.494232469	0.000547702	cg13796272	SPON2	-0.642441573	0.000132755
cg10273135	CMYA5	-0.760058596	0.000847402	cg25701164	LRRK1	-0.486658967	2.74E-05	cg20261167	SPP1	-0.301673933	0.002951027
cg12186816	CNBD1	-0.428650769	0.000665144	cg22817352	LRRN2	-0.846533914	0.000682847	cg09833785	SPRY2	-0.270908568	0.000260834
cg16175941	CNKSR3	-0.312666726	0.000325622	cg26897904	LSP1	-0.684612015	9.52E-05	cg01980735	SPSB1	-0.361532158	0.000361267
ch.1.2348804F	CNN3	-0.326998543	0.000121384	cg07621749	LTK	-0.38371402	0.004718382	cg07850967	SPTBN1	-0.856653856	0.002823706

cg21216118	CNRIP1	-0.527558724	0.001517298	cg17374727	LUZP6	-0.299183508	0.005371918	cg02795700	SPTBN4	-0.328700472	0.003477165
cg20141118	CNTLN	-0.48941562	0.003147719	cg09286468	LY6G6E	-0.656459388	0.000320445	cg20205704	SRR	-0.348572868	0.002462084
cg11830800	CNTN1	-0.465202064	0.005482476	cg06573604	LY75	-0.491216185	0.007653792	cg00700239	SRRM4	-0.509439384	0.00203868
cg08105471	CNTN3	-0.300067235	0.002799383	cg15665400	LYPD1	-0.578110527	0.00870967	cg12989217	SSPN	-0.441150371	0.002147288
cg26716902	CNTNAP1	-1.103619185	0.000174256	cg27367721	LYRM1	-0.584064565	0.00550923	cg14929208	SSR3	-0.784374016	0.000326588
cg07571451	COBL	-0.288940213	0.009544052	cg02357637	LYSMD4	-0.277773882	0.003488666	cg18182358	ST3GAL6	-0.358875462	0.003815915
cg14628708	COG5	-0.378237189	0.000142641	cg26906273	MACF1	-0.900886071	4.76E-05	cg03220455	ST6GALNAC2	-0.344824994	0.004893626
cg23586322	COL14A1	-0.741478345	0.003310048	cg09908110	MACROD1	-0.726373057	0.006973438	cg10111629	ST7L	-0.294639101	0.000139292
cg16626809	COL18A1	-0.680148446	0.005345361	cg15089567	MAD1L1	-0.476958377	0.001144694	cg08222913	STAB1	-0.504353048	0.000460452
cg18816996	COL23A1	-0.617203379	0.001429606	cg25338423	MAGI1	-0.786964335	0.000294467	cg27275022	STAMBP	-0.395067281	0.000393972
cg14572845	COL27A1	-0.531697376	0.003287926	cg24543015	MAGI2	-0.857586757	0.008842187	cg19058865	STAP2	-0.590828218	0.003239191
cg23502162	COL3A1	-0.275284896	0.006699118	cg22311458	MALAT1	-0.274360911	0.002267723	cg00464095	STAR	-0.323783272	0.009705601
cg21478902	COL4A1	-0.495584619	0.009775417	cg26323077	MAML2	-0.583188132	2.68E-05	cg15008287	STARD10	-0.467426307	0.003828408
cg21212314	COL4A3BP	-0.278331012	0.001522304	cg03418002	MAML3	-0.481177864	0.001552933	cg24129390	STARD13	-0.753404927	3.85E-06
cg07875385	COL5A2	-0.272572631	0.004601794	cg21912162	MAP1B	-0.396805133	0.001998967	cg11925263	STARD4	-0.507022004	0.001307037
cg16523839	COL5A3	-0.433700674	0.005913728	cg18326562	MAP2K6	-0.427179977	0.000317054	cg05573378	STARD9	-0.50650852	0.000407748
cg27507687	COL7A1	-0.799273768	0.007915161	cg00348763	MAP3K10	-0.47187315	0.001812082	cg06270615	STAT3	-0.391838652	0.009967846
cg05283542	COL8A1	-0.319836497	0.004330818	cg15976910	MAP3K11	-0.261392065	0.006648227	cg23791611	STAT4	-0.581182466	0.005579701
cg21686379	COL9A3	-0.434374835	0.007883782	cg05354479	MAP3K9	-0.614484428	0.000952362	cg03001305	STAT5A	-0.478676186	0.000398025
cg07137336	COLEC12	-0.677052909	0.000680047	cg22468751	MAP7	-0.485708566	0.000192234	cg01104306	STIM1	-0.527029111	0.004821304
cg18037808	CORO1C	-0.358764982	0.001679329	cg03715980	MAPK8IP3	-0.272234234	0.004544927	cg23764900	STK33	-0.585834865	0.006629782
cg23179181	CORO6	-0.424668621	0.002034103	cg22800273	MAPKAPK3	-0.458216681	0.001339903	cg22763753	STK38L	-0.348261592	0.000372573
cg09363068	COX19	-0.451415125	0.005100532	cg19297845	MAPKBP1	-0.300256184	0.005640593	cg26872305	STK39	-0.607991326	0.004670699
cg03249995	COX4NB	-0.433785511	0.008143538	cg16805068	MAPRE1	-0.565889035	0.000881865	cg11709544	STMN1	-0.379172313	0.001862702
cg09148494	COX6B2	-0.300000345	0.000978541	cg16520312	MAPT	-0.540258918	3.45E-05	cg07289618	STON1-GTF2A1L	-0.461939516	6.21E-05
cg06809298	COX7A2	-0.64357321	0.005512515	cg17828445	MARCH9	-0.371420061	1.47E-07	cg02610600	STX1A	-0.345688682	0.001294761
cg09428251	CPA6	-0.430665061	0.004279924	cg02107842	MAST4	-0.864199785	0.000227523	cg21208029	STYX	-0.388445414	0.008866117
cg16903913	CPAMD8	-0.279032719	0.001876387	cg03059048	MAT2B	-0.614513886	0.002114114	cg21447550	SUSD4	-0.505610551	0.008183382
cg07809027	CPEB2	-0.492056837	0.005642772	cg09093931	MATN2	-0.45413718	0.007892965	cg04678141	SVIL	-0.71413574	2.91E-05
cg05674659	CPNE2	-0.267819059	0.008386318	cg24109116	MBLAC1	-0.634322493	0.001278471	cg05059304	SYCP2L	-0.312977239	0.009369572
cg08813944	CPSF4L	-0.296029755	0.000198394	cg24922596	MC2R	-0.590904007	0.00438502	cg12634957	SYNC	-0.621411167	0.000371354
cg16275960	CPSF6	-0.29269695	0.006401925	cg21096399	MCAM	-0.44727529	0.001097729	cg02364518	SYNE1	-0.297753515	0.000173582
cg12948920	CPZ	-0.393746173	0.007572787	cg26489251	MCART2	-0.328177133	0.001433629	cg06472065	SYNGAP1	-0.552418881	4.01E-05
cg14826226	CRABP1	-0.318216326	0.00636134	cg01827908	MCAT	-0.308886374	0.000150935	cg07919145	SYNGR1	-0.364197679	0.006741937
cg04102199	CRADD	-0.31802714	0.001419174	cg21081729	MCC	-0.670564136	0.004957642	cg05881135	SYNM	-0.637384873	0.004836078
cg03478719	CRB2	-0.287450496	0.000886848	cg05669497	MCF2L	-0.45015577	0.005802186	cg05714559	SYNPO	-0.69244719	0.000355239

cg05222850	CREB3L2	-0.623686529	0.00513276	cg25737410	MCF2L2	-0.724871253	0.008701181	cg24637261	SYNPO2L	-0.54447208	0.004233065
cg26441486	CRELD2	-0.317675525	0.001563579	cg12037450	MCOLN3	-0.343424498	0.003283079	cg01974027	SYT6	-0.601221741	0.004364981
cg03405789	CRH	-0.661540324	9.21E-05	cg14572252	MECOM	-0.921148661	3.19E-06	cg01963906	SYTL1	-0.338510481	0.000584147
ch.17.59059R	CRK	-0.269719265	0.007668975	cg06312132	MED12L	-0.405747446	0.001201603	cg23553576	SYTL2	-0.438967444	0.00623373
cg07356483	CRTAC1	-0.301376669	0.000218496	cg18681998	MED28	-0.277993704	0.00086244	cg23331156	TACC2	-0.454557366	0.003224574
cg24085885	CRTC1	-0.408790676	0.00160785	cg23495116	MED30	-0.534931056	0.001587627	cg15584401	TACR1	-0.814622121	1.99E-05
cg03073714	CRY1	-0.283895776	0.001803981	cg16225168	MEF2C	-0.663936399	0.002841921	cg26984805	TACR2	-0.80997189	0.000330949
cg15780540	CRYBA2	-0.525537959	0.002649705	cg08051604	MEG3	-0.584434144	0.006093476	cg20353780	TAOK3	-0.290595562	0.002347997
cg23273694	CRYGN	-1.303706021	0.000357688	cg17163527	MEGF6	-0.479545035	0.002943541	cg03780271	TAPBP	-0.346661133	0.009752781
cg11345143	CRYL1	-0.293903949	0.000218519	cg12055515	MEIS1	-0.661065043	0.001901111	cg14217589	TBC1D1	-0.347089536	0.002510865
cg00687714	CRYM	-0.822279686	0.00024379	cg17850518	MEIS2	-0.272220708	0.0052365	cg26843872	TBC1D10B	-0.475679592	0.000333417
cg25447894	CSDC2	-1.033698285	0.00076196	cg12686920	MEOX1	-0.347106203	0.003132445	cg04730047	TBC1D23	-0.466907951	0.000580459
cg21449646	CSGALNACT1	-0.315189984	0.004951791	cg05979619	MERTK	-0.71647218	0.006490849	cg16383910	TBC1D2B	-0.590772347	0.001514622
cg23282837	CSMD3	-0.312296384	0.00740962	cg09059945	MEST	-0.273053211	0.006043252	cg00370962	TBC1D5	-0.459507319	0.000828071
cg03540589	CSRNP1	-0.410998031	0.000599961	cg24035107	METT10D	-0.44349594	0.00056736	cg22631616	TBC1D9	-0.492335353	0.004154987
cg21139587	CSRP1	-0.699792338	0.000555231	cg01973394	MEX3B	-0.265104785	0.003952438	cg07883762	TBL1XR1	-0.263934304	0.00119606
cg01454519	CST5	-0.362237305	0.005754604	cg05055766	MFAP2	-0.595597398	6.49E-05	cg10997718	TBR1	-0.567882472	0.004400881
cg18976418	CTAGE5	-0.447445373	0.004052485	cg06997997	MFAP4	-0.580244122	0.000196957	cg03142634	TBRG4	-0.279967097	0.00553275
cg11784626	CTBP2	-0.509770207	0.000145212	cg10272675	MFGE8	-0.288951807	0.007274613	cg06158650	TBX15	-0.426246943	0.000616208
cg12605080	CTDSPL	-0.300810438	5.65E-05	cg11784887	MFHAS1	-0.482874673	0.000245417	cg20209009	TBX21	-0.436421793	0.001971809
cg19364688	CTF1	-0.29947901	0.007343957	cg09711970	MFN1	-0.383257759	0.000386903	cg01209635	TBXA2R	-0.713560066	0.000191093
cg13572145	CTNNA2	-0.398547463	0.004975244	cg16924045	MFSD6	-0.306267323	0.008378311	cg04467618	TCF21	-0.629374248	0.007672714
cg08617354	CTNNA3	-0.577815198	0.00538471	cg06799422	MGA	-0.75757042	0.002892853	cg10607059	TCF7L2	-0.331951092	0.003391985
cg20380649	CTNND2	-0.696712668	0.001794996	cg09277376	MGC12982	-0.41286694	0.004452696	cg07901138	TDRD5	-0.47949323	0.002067841
cg14436231	CTNS	-0.534005832	0.001689769	cg26393541	MGC45800	-0.89177383	0.000768059	cg22339486	TDRKH	-0.519776267	0.003861937
cg21880328	CTTNBP2	-0.485059082	0.001647315	cg23712522	MGC70857	-0.390283164	2.86E-05	cg00553886	TEAD1	-0.280809707	0.004517606
cg22980697	CUBN	-0.515543715	0.005384109	cg23465978	MGMT	-0.596664437	0.00770988	cg03459791	TEKT3	-0.822214075	1.68E-05
cg27608981	CUX1	-0.354707437	0.005074587	cg18233746	MGST1	-0.45105721	0.006835294	cg08699794	TELO2	-0.3732143	0.002374101
cg20427865	CX3CL1	-0.307417917	0.001202962	cg01770296	MIA3	-0.449908942	0.004760173	cg24505307	TENC1	-0.269605032	0.001594409
cg03167275	CXADR	-0.597760618	0.001128447	cg02527527	MICALL1	-0.392726701	0.004715275	cg07499477	TEP1	-0.709537931	0.004311471
cg04559909	CXCL5	-0.332568543	0.002024933	cg04383383	MIER2	-0.30664878	0.000666642	cg04370442	TEPP	-0.716357751	3.09E-05
cg20455854	CXXC5	-0.776603524	0.00958169	cg11142013	MIPEP	-0.261418106	0.002928422	cg17862558	TET2	-0.448168407	0.003263636
cg08925398	CYB5R1	-0.400464731	0.000107791	cg10489614	MIR137	-0.453924197	0.008887639	cg12659952	TFAP2A	-0.406997822	0.000714819
cg03826976	CYB5R2	-0.397904667	0.007777875	cg15759721	MIR21	-0.41180306	0.00779543	cg22335261	TG	-0.370830282	0.00256555
cg01194538	CYB5R3	-0.46923264	0.002501816	cg02471760	MIR210	-0.414963549	8.86E-06	cg08615333	TGFB3	-0.603445803	0.002294447
cg02603251	CYFIP2	-0.300531508	0.009895122	cg00705280	MIR375	-0.604227137	0.007950915	cg21116284	TGFBR3	-0.363941888	0.003264878

cg08620474	CYP1B1	-0.397070925	0.009335716	cg15077343	MIR548G	-0.278919173	0.001254266	cg10185099	THBD	-0.552686682	0.003264392
cg01416891	CYP26C1	-0.58573384	0.007806376	cg06022664	MIR548H4	-0.56575956	0.009753903	cg21732383	THBS2	-0.516280701	0.00400875
cg16751203	CYP27C1	-0.357657976	0.00136697	cg11636702	MIR572	-0.620217986	0.001519222	cg01194371	THBS4	-0.472180028	0.002317504
cg23218957	DACT1	-0.474247705	0.00176942	cg05650680	MIR596	-0.661913613	0.000217854	cg00323305	THRB	-1.681042415	6.20E-05
cg02362292	DAGLA	-0.270435227	0.00483882	cg06162516	MIRLET7I	-0.30314058	0.007913198	cg24453600	THSD4	-0.340665612	0.008193742
cg16854606	DAND5	-0.312428003	0.00785461	cg02360862	MIXL1	-0.336478294	0.000299114	cg27611263	THUMPD2	-0.626134682	0.000303314
cg23196123	DCAF4	-0.30085969	0.005804828	cg03010972	MKLN1	-0.385966514	0.004780749	cg19936885	THUMPD3	-0.287315476	0.008457257
cg25602457	DCC	-0.559050224	6.75E-06	cg26647303	MKNK2	-0.347076622	0.000532938	ch.10.2563868F	TIAL1	-0.327176496	0.001827254
cg21729798	DCDC2	-0.699733778	0.009836859	cg06108510	MLH1	-0.292179774	0.002591865	cg06535156	TIAM2	-0.329479953	0.002762617
cg13390800	DCHS1	-0.499350656	0.00230341	cg25746138	MLL4	-0.519035812	0.00367966	cg12517577	TIE1	-0.388886051	0.001618929
cg22940789	DCLK1	-0.576378373	0.007080637	cg20798249	MLNR	-0.412758298	0.003959804	cg13849419	TJP2	-0.536511601	0.00594425
cg13547559	DDAH1	-0.368346298	0.009795717	cg22955973	MME	-0.374252667	0.004284223	cg20740903	TK1	-0.306299315	0.006267539
cg13695585	DDR1	-0.496318178	0.000865426	cg20722590	MMP15	-0.585593128	0.001009957	cg19786988	TLN2	-0.323591001	0.005463362
cg24393699	DENND1B	-0.387267763	0.002461502	cg26757793	MMP20	-0.355366768	0.000556407	cg15448366	TLR5	-0.448090765	7.38E-05
cg09946870	DENND3	-0.398129598	8.03E-05	cg15270813	MMP24	-0.782849543	0.00037886	cg07471203	TM7SF2	-0.328197851	0.009956636
cg19286687	DES	-0.473892473	0.000767318	cg01062519	MMP28	-0.590727296	0.005595138	cg22352450	TMCO3	-0.349443085	0.001231572
cg17790129	DFNA5	-0.36768331	0.002857108	cg05936091	MNAT1	-0.46729539	0.005053271	cg00698908	TMEM132C	-0.435127355	0.003397927
cg13904267	DFNB31	-0.392429917	0.004940266	cg23472708	MNX1	-0.514096026	5.89E-05	cg05240166	TMEM159	-0.69085797	2.32E-06
cg03645851	DGCR2	-0.49126156	0.002809049	cg09023136	MOSC1	-0.268668334	0.005955018	cg25422880	TMEM163	-0.523870189	0.00115356
cg19443311	DGCR5	-0.536584757	0.009630264	cg03417473	MOV10	-0.382958615	0.000282811	cg14617041	TMEM171	-0.454995722	0.000161393
cg15354065	DGKA	-0.337704036	0.009857799	cg13682140	MPP2	-0.332138429	0.00021989	cg10708761	TMEM178	-0.666212207	0.004406579
cg02749735	DGKG	-0.822573777	0.002569668	cg01786466	MPP4	-0.771373493	4.63E-05	cg09113665	TMEM188	-0.283149493	0.000408863
cg19307180	DGKH	-0.278979521	0.003563622	cg10566121	MPPED2	-0.447412446	0.000320251	cg15377585	TMEM196	-0.501227372	0.001380298
cg18700199	DHPS	-0.270389605	0.000759693	cg04822018	MRM1	-0.625574171	0.006619367	cg11558474	TMEM2	-0.3456037	0.000223889
cg14929207	DHRS13	-0.628836219	0.002395226	cg16521040	MRPL34	-0.400446777	0.009602666	cg04815396	TMEM217	-0.346629611	0.001527312
cg04300065	DIO3OS	-0.394065892	0.003424927	cg02174359	MRPS18A	-0.762201104	0.001373845	cg26618874	TMEM231	-0.429576203	0.002623182
cg08530879	DIP2B	-0.352665486	0.007869021	cg14619640	MRPS18B	-0.269604959	0.001299572	cg06429214	TMEM232	-0.559990815	0.008650673
cg17463564	DIP2C	-0.359762159	0.006418995	cg09741222	MRPS27	-0.266224481	0.005191811	cg15694715	TMEM25	-0.484445509	0.002675611
cg18034637	DIXDC1	-0.492967153	0.001238322	cg21776010	MRPS33	-0.552951332	0.003284433	cg05499367	TMEM26	-0.395253347	0.008654863
cg13786171	DKFZp566F0947	-0.438561168	0.003257168	cg10599571	MRPS6	-0.351292311	0.000319069	cg10081469	TMEM30B	-0.359560515	0.006916934
cg27411220	DKK1	-0.607559025	0.003992804	cg08298091	MRVI1	-0.436300023	0.00089552	cg17063143	TMEM44	-0.335801211	0.001172752
cg01962428	DKK2	-0.743384169	0.00540012	cg01048107	MSC	-0.482338781	0.001038176	cg11399100	TMEM59L	-0.599854042	0.000832128
cg21620540	DKK3	-0.583757064	0.002689646	cg06709766	MSH3	-0.292838311	0.007898052	cg16847695	TMEM90B	-0.581023459	0.004584392
cg08768218	DLC1	-0.472878174	0.009603229	cg06234863	MSI2	-0.336697252	0.000722844	cg05272790	TMPRSS13	-0.424327382	0.006721468
cg00807586	DLEC1	-0.792785794	0.002571719	cg18393046	MSX2P1	-0.459077775	0.005356597	cg02765731	TMTC2	-0.485192154	0.00708416
cg17241776	DLEU7	-0.498229944	0.009383328	cg08404299	MT1F	-0.499197631	0.007579502	cg25934495	TNFAIP3	-0.42620274	0.000372228

cg20522104	DLG2	-0.371261495	5.22E-05	cg22198623	MT1G	-0.326132997	0.004046299	cg15408889	TNFAIP8	-0.311790013	0.005842351
cg16564940	DLG4	-0.644768459	0.005212576	cg10014293	MT1H	-0.453825817	0.002126834	cg00063471	TNFAIP8L3	-1.163150709	0.000216298
cg23963984	DLG5	-0.342706281	0.00918432	cg17545418	MT1IP	-0.550072148	9.01E-05	cg00502254	TNFRSF8	-0.285265239	0.001469488
cg12024311	DLL1	-0.282098321	0.006928332	cg09372728	MT3	-0.592147364	0.001848508	cg21008828	TNK2	-0.761912094	0.00207814
cg26212303	DLL4	-0.441206271	0.005348706	cg14480449	MTA1	-0.406238922	0.001224376	cg10419849	TNKS	-0.436765966	0.00170501
cg00822840	DLX1	-0.390003122	0.005442746	cg14412134	MTHFD1	-0.464343196	0.000697491	cg09582482	TNNI1	-0.399793641	3.56E-06
cg26002103	DLX2	-0.476577698	0.003786663	cg00619628	MTHFD1L	-0.323030253	0.00994519	cg13980719	TNP1	-0.513547667	0.00104602
cg01832036	DLX4	-0.900100424	0.007491888	cg22629853	MTPAP	-0.656859247	0.002495117	cg21577836	TNR	-0.674791092	0.0062202
cg02839802	DMC1	-0.361715862	0.000516008	cg22348298	MTUS1	-0.393436041	0.000547127	cg06320380	TNS1	-0.530369822	7.06E-05
cg06745944	DNAH10	-0.744874759	5.94E-05	cg19717326	MYADM	-0.363159284	0.007243647	cg20258698	TNS3	-0.387776415	0.004689653
cg21642988	DNAJA4	-0.576965574	0.000588272	cg23067881	MYBPC1	-0.412455761	0.009504625	cg08516507	TNXB	-0.577011189	0.007836881
cg26668151	DNAJB6	-0.488954045	0.003352072	cg03611598	MYCBPAP	-0.460146215	0.006573015	cg00849854	TOM1L2	-0.637699451	0.000172238
cg11059451	DNAJC21	-0.345050944	0.004710963	cg05426160	MYH11	-0.437248941	0.001266481	cg27028168	TOX	-0.557470723	0.00640089
cg21518937	DNAJC22	-0.536896582	0.001107485	cg15275017	MYLK	-0.29719315	7.75E-05	cg18693412	TOX2	-0.356982849	0.008196205
cg16587909	DNM1P35	-0.305282245	0.002817779	cg17129576	MYO18A	-0.43611658	0.006948195	cg03745002	TOX3	-0.487634659	7.18E-05
cg17207266	DNMT3A	-0.442354392	0.000387595	cg21225667	MYO1E	-0.411983317	0.007169579	cg12198913	TP53I11	-0.418889736	0.0075235
cg27076046	DNMT3L	-0.512271785	0.000258929	cg09948419	MYO1G	-0.517773946	0.001247268	cg17986341	TP73	-0.395868039	0.000752348
cg15676916	DOCK1	-0.387667501	0.001350412	cg15438314	MYO9B	-0.398482626	0.006258024	cg10805721	TPBG	-1.046149148	3.58E-05
cg04730794	DOCK2	-0.51709293	0.000259383	cg10257905	MYOCD	-0.546797441	0.005856446	cg24483493	TPM1	-0.623023077	0.003620349
cg21880720	DOT1L	-0.319797299	2.57E-05	cg24147498	MYOF	-0.470232343	0.009441358	cg21658153	TPM4	-0.422686943	0.001566841
cg26384993	DPF3	-0.541559145	0.000259829	cg19876649	MYOM1	-0.356428131	0.009577021	cg21772826	TPRG1	-0.316390045	0.009162212
cg04333485	DRD3	-0.477039785	0.001279265	cg07598199	MYOZ2	-0.720468739	0.000552748	cg09665336	TRAF4	-0.739959722	0.000338027
cg00129811	DSE	-0.457026296	0.005138579	cg24520885	MYST4	-0.272775786	0.007216552	cg05807991	TRAM1L1	-0.768542689	0.006970953
cg17378966	DUSP1	-0.621666546	0.002467319	cg07839208	N4BP1	-0.375127259	0.006021039	cg14279151	TRAM2	-0.480077641	0.000546613
cg11019437	DUSP10	-0.268356049	0.008322223	cg01373189	N4BP2L1	-0.382694976	0.008030076	cg00187535	TRAPPC5	-0.392061209	0.002172146
cg00319774	DUSP26	-0.618915167	0.000422819	cg00280758	NAA15	-0.904317479	0.000335932	cg03918756	TRAPPC9	-0.398457127	0.006248212
cg12314510	DYNLL2	-0.280056283	0.00296707	cg05401522	NAA16	-0.289890966	0.003042548	cg00199091	TRERF1	-0.403602234	0.006208077
cg03150515	EBF2	-0.342928799	0.00617101	cg04784618	NAALADL2	-0.716755573	0.000460832	cg06992846	TRIB1	-0.305330981	0.002587275
cg16589299	EBF3	-0.691203001	0.005466822	cg19074533	NANP	-0.284565557	0.007938318	cg23213230	TRIM13	-0.509159559	0.001538632
cg13329852	EBPL	-0.33215102	0.002844024	cg14282634	NAV1	-0.357992626	0.000524007	cg01074325	TRIM15	-0.454190923	0.004129394
cg09219688	ECHDC3	-0.337768574	0.007026863	cg01896424	NAV2	-0.483788711	0.000831209	cg24848599	TRIM17	-0.538851887	0.000331163
cg18787802	ECT2L	-0.388306375	0.007772029	cg07681935	NBLA00301	-0.712377357	0.000723157	cg04974775	TRIM36	-0.371249798	0.000692369
cg05515143	EDAR	-0.539454325	0.008420733	cg04110421	NBR2	-0.354219842	0.005906917	cg16027343	TRIM7	-0.312040034	0.007586618
cg00178850	EDARADD	-0.681156303	1.99E-05	cg22815766	NCAPD3	-0.305461227	0.001478888	cg01754713	TRIM72	-1.032662256	6.17E-08
cg12460433	EDIL3	-0.396763242	0.002342425	cg06172138	NCBP2	-0.348561279	0.00440033	cg18106312	TRIM9	-0.411995483	0.002639293
cg05377949	EEFSEC	-0.452150436	0.001905687	cg22402261	NCDN	-0.37757033	0.003947779	cg03360992	TRIOBP	-0.43661762	0.000752379

cg05221455	EFCAB4A	-0.347698913	0.003257704	cg09472600	NCF2	-0.339586393	2.50E-05	cg10208610	TRNP1	-0.358814986	0.00724496
cg16257681	EFNA3	-0.340158417	0.009734978	cg09423651	NCK1	-0.357056411	0.001885771	cg26679289	TRPC3	-0.489781664	0.003003011
cg16905506	EFNA4	-0.463152849	0.001261326	cg25804065	NCK2	-0.581352501	0.003644588	cg09465288	TRPM1	-0.314758709	0.001330081
cg16254962	EGFLAM	-0.533803186	0.008256859	cg01290856	NCKAP5	-0.841322916	2.63E-06	cg04104776	TRPV3	-0.395577692	0.005634852
cg05182679	EGR2	-0.268226652	0.004436341	cg01036806	NCLN	-0.410584548	0.000650185	cg02535735	TSC22D1	-0.667297131	0.000384489
cg23253448	EGR3	-0.419635257	0.000993612	cg09644157	NCOR2	-1.037375938	0.000470924	cg12513140	TSC22D2	-0.284863682	0.002412071
cg17290213	EHBP1L1	-0.509336995	0.00086417	cg06804705	NCRNA00114	-0.402669756	7.52E-08	cg06665453	TSEN54	-0.470776608	0.001087271
cg18560551	EHF	-0.723313698	4.41E-06	cg17611512	NCRNA00175	-0.325592034	0.006652177	cg26221293	TSGA13	-0.425841832	0.009389578
cg01595717	EHMT1	-0.358454525	0.001079847	cg06454226	NDC80	-0.464129801	0.000260108	cg02867216	TSHZ1	-0.766840373	0.000160868
cg06109664	EIF4E	-0.303998434	0.006049916	cg03715305	NDUFA11	-0.275372117	0.003167235	cg15557878	TSLP	-0.428408385	0.008171608
cg27484876	EIF6	-0.333399527	0.006995353	cg13433012	NDUFA4L2	-0.552410042	0.002972196	cg14778691	TSNARE1	-0.744327667	5.75E-05
cg23708211	ELAC1	-0.270469306	0.008056921	cg04865026	NDUFB3	-0.262793065	0.009227512	cg08638929	TSPAN1	-0.456774566	0.001822891
cg13932029	ELAVL2	-0.536584891	0.003037584	cg14914822	NEDD4L	-1.489895888	0.000196918	cg25327296	TSPAN18	-0.514168541	0.000843153
cg27643890	ELFN1	-0.270455288	0.003316454	cg22415969	NEK10	-0.673862285	0.006545488	cg13239252	TSPAN19	-0.432910074	0.006551717
cg19023977	ELL2	-0.610853931	0.001858784	cg10164885	NELL2	-0.365875736	0.004036556	cg23999170	TSPAN2	-0.463660018	0.003016472
cg07716847	ELMO3	-0.455160569	0.006835054	cg27021181	NET1	-0.57296831	0.00793849	cg14990644	TSSK1B	-0.335941269	0.001376296
cg22879408	ELMOD1	-0.51394827	0.009640115	cg02755525	NETO2	-0.681820383	0.0031445	cg22956431	TTC23L	-0.589969241	0.009962707
cg01799681	ELOVL2	-0.531111265	0.007317238	cg02836529	NEUROD1	-0.703034642	0.000475565	cg04437845	TTC7A	-0.321064922	0.004693931
cg14319235	ELTD1	-0.368824022	0.002070458	cg06865992	NEUROD2	-0.470204463	0.001789611	cg02048220	TTC7B	-0.664366398	0.002153969
cg12532667	EMCN	-0.27144913	0.000424656	cg08587845	NEUROG1	-0.282866818	0.008919865	cg14929883	TTC9	-0.448653007	0.000231402
cg15170715	EMILIN1	-0.515477608	0.001120119	cg07044422	NFAM1	-0.437694806	0.004425134	cg08315399	TTLL5	-0.529175972	0.005776181
cg21919819	EML1	-0.543108053	0.007517719	cg16848717	NFATC1	-0.364367202	0.004136047	cg08640923	TUBA4B	-0.520413841	0.004409384
cg16013966	EML3	-0.277193216	0.000522229	cg00401091	NFATC2	-0.809861427	1.83E-05	cg07599225	TUFT1	-0.44469045	0.00043405
cg16654801	EMX2	-0.439411671	0.004422407	cg06411578	NFE2	-0.522308784	7.60E-05	cg24505395	TUT1	-0.679354849	0.00399966
cg12242086	EN2	-0.390149928	0.000436925	cg17178175	NFE2L2	-0.452480358	0.005966589	cg02400740	TWIST1	-0.674006414	0.009747991
cg06998282	ENPP2	-0.343515774	0.004264282	cg14684457	NFE2L3	-0.542173249	0.002558741	cg19205847	TWIST2	-0.407353773	0.008852796
cg16822855	ENTPD3	-0.324148419	0.006820636	cg19097500	NFIA	-0.440050322	0.007891655	cg11077019	TXNDC12	-0.272538451	0.00334234
cg02446871	EPB41	-0.954009964	4.09E-05	cg01518631	NFIB	-0.276956712	0.001342744	cg24147582	TYRO3	-0.397069843	0.000802439
cg22423984	EPB41L1	-0.605943338	0.000287003	cg03583050	NFIC	-0.370523172	0.005705128	ch.7.1427355R	TYW1	-0.267555427	0.00959188
cg03002479	EPHA1	-0.340349894	0.003844122	cg25417223	NFIX	-0.482506054	0.000834026	cg14865907	UBA52	-0.363772323	0.001785557
cg22263131	EPHA7	-0.567153202	0.002901423	cg10336144	NFYC	-0.666151224	0.000152653	cg09561830	UBAC2	-0.330520982	0.001858379
cg15903282	EPHB1	-0.41164965	0.000397862	cg17339234	NIPAL1	-0.65993373	0.002356196	cg14174221	UBASH3A	-0.338444696	0.000474433
cg16184495	EPHX3	-0.492052914	0.009598826	cg22213386	NIPAL4	-1.001757939	0.00012546	cg15258696	UBE2G1	-0.588829798	0.006501437
cg04542977	EPS15	-1.052216326	0.000267105	cg21251018	NKAPL	-0.417247581	0.003675961	cg17957183	UBE2N	-0.349930718	0.004472025
cg26108843	ERG	-0.305351879	0.001696297	cg14469389	NKD2	-0.619141633	0.00784012	cg20324858	UBE2Q1	-0.6464422	0.00314
cg21918595	ERI3	-0.295944334	0.009112715	cg14506196	NKX2-3	-0.476261089	0.009425321	cg16359521	UBR4	-0.462497889	0.006230649

cg19477600	ESAM	-0.433804894	0.002913398	cg09579281	NOD1	-0.353687561	0.005951901	cg03719555	UBXN6	-0.547631319	0.006128096
cg08886823	ESRP2	-0.526883537	0.000624417	cg14174336	NOL3	-0.397148676	0.000338313	cg14223995	UCP1	-0.783694234	0.00056512
cg26975499	ESRRB	-0.626545281	0.004598399	cg15529727	NOP10	-0.589253013	0.002908566	cg06546722	UGP2	-0.361702893	0.000619942
cg03765041	ESYT2	-0.614087554	0.000167156	cg06522206	NOS1	-0.405474714	0.001987041	cg11389868	UGT3A1	-0.530297864	0.003093014
cg15256387	ETV1	-0.549658525	0.007120088	cg07568313	NOTCH2	-0.395461047	0.002002772	cg16807101	UHRF1BP1L	-0.396932324	0.000200366
cg11868356	ETV4	-0.424548879	0.006371376	cg24535130	NOTUM	-0.500563379	0.000900822	cg14715778	UNC13D	-0.409553001	0.009323535
cg12403778	ETV6	-0.617394171	0.000116196	cg24750308	NOX4	-0.381483499	0.001198764	cg26987690	UNC84A	-0.328394647	0.002212999
cg04724735	EVI5L	-0.411525946	0.006260989	cg09628601	NPAS1	-0.413422763	0.002097808	cg07765161	UNCX	-0.5499033	0.002383409
cg08787251	EVX1	-0.437461332	0.008485024	cg22957135	NPAS3	-0.838245824	0.000762471	cg16695548	URGCP	-0.326416217	0.006761626
cg05783185	EXT1	-0.299322366	0.000130322	cg25630123	NPAT	-0.315649334	0.000714194	cg13252580	USP12	-0.473874311	0.00823148
cg12189255	EXT2	-0.321802925	0.002293226	cg12611723	NPDC1	-0.409016682	0.002438977	cg19246197	USP2	-0.409439429	0.000110129
cg25075347	EYA4	-0.586086555	4.06E-05	cg04008252	NPFFR2	-1.032397778	0.003310087	cg16245868	USP24	-0.385884959	0.003786551
cg09069900	F10	-0.323876696	0.006893665	cg26864174	NPHS1	-0.476827121	0.000118498	cg11952340	USP3	-0.403785463	0.000839689
cg04528371	F2R	-0.65599724	0.001134074	cg13931925	NPHS2	-0.44725918	0.003964556	cg07213414	USP31	-0.38624817	0.005321066
cg07110043	FABP3	-1.162889333	0.000127286	cg00155526	NPR3	-0.568927077	0.000835568	cg08496387	USP47	-0.611445031	4.07E-05
cg17080893	FABP5	-0.504487944	0.004206588	cg15420318	NPTN	-0.260628332	0.008597647	cg27381822	UST	-0.584177266	0.000579836
cg21844038	FAM100A	-0.539025132	0.000240899	cg25598376	NR2C2	-0.392746436	0.0043098	cg21278764	UTP11L	-0.534466826	0.002433142
cg05669100	FAM103A1	-0.278210837	0.0032151	cg13720362	NR2E1	-0.430386436	0.002394762	cg08274538	VAMP2	-0.27387295	0.007648275
cg21893354	FAM105A	-0.315219072	0.009795526	cg16556111	NR2F1	-0.348858073	0.000710351	cg10321146	VAV1	-0.265814307	0.000564863
cg00298324	FAM110A	-0.34339795	0.005777932	cg15379412	NR2F2	-0.277325037	0.00571875	cg01959838	VAV3	-0.485772168	0.006064624
cg21495022	FAM117B	-0.3166805	0.002185493	cg06952416	NR3C1	-0.357631051	0.009048569	cg08891382	VCAN	-0.6654157	0.006753595
cg06315390	FAM118A	-0.574356924	0.002715533	cg17759535	NR5A2	-0.568421678	0.003291746	cg21603823	VEGFC	-0.355788613	0.000314494
cg00313750	FAM123A	-0.562995245	0.000234817	cg01540911	NRF1	-0.513299997	0.002736428	cg11970806	VEZF1	-0.346046671	0.002216368
cg14409104	FAM125B	-0.421393138	0.003532285	cg06397379	NRG1	-0.574538647	0.008364373	cg18062721	VGLL4	-0.718504277	0.003889089
cg01587630	FAM126A	-0.288689268	0.001741485	cg24897141	NRG2	-0.604791107	0.008720345	ch.3.1113149F	VPRBP	-0.292214502	0.00117306
cg16549073	FAM129B	-0.286952942	0.001183186	cg12757570	NRGN	-0.365706242	0.001202152	cg16853770	VPS37B	-0.348092896	0.003639468
cg08075452	FAM131A	-0.488078377	0.009266279	cg11784631	NRM	-0.442023743	0.008189352	cg24114936	VPS37D	-0.298941516	0.008799617
cg22904133	FAM134A	-0.273338045	0.007009071	cg25307691	NRN1	-0.701104215	0.000956135	cg12627844	VPS54	-0.358034424	0.009111059
cg26373716	FAM150A	-0.545975624	0.001370356	cg10118547	NRP2	-0.390203636	0.001899525	cg21929875	VSIG2	-0.347752841	0.006336708
cg00068622	FAM151B	-0.367999904	0.00030865	cg12129012	NRXN2	-0.526831839	0.000252081	cg15939466	VTI1A	-0.296828773	0.001189493
cg07223990	FAM155A	-0.606684697	0.006306498	cg17493885	NSD1	-0.63961449	0.004119013	cg12532653	VTRNA1-1	-0.433757317	0.008139374
cg25233709	FAM160B1	-0.682471308	4.69E-05	cg04396288	NSMCE1	-0.339686265	0.002527348	cg09668627	VWA1	-0.361887042	0.007112297
cg22602019	FAM167B	-0.403844919	0.00666783	cg00162862	NTAN1	-0.34795586	0.001701257	cg24275730	VWA3B	-0.522407373	0.001276749
cg05871601	FAM168A	-0.304233818	0.002741212	cg12433395	NUAK1	-0.428446504	0.000168864	cg02195657	VWA5B1	-0.281703669	0.005242053
cg27361865	FAM175A	-0.504549476	5.86E-06	cg04749197	NUMA1	-0.445588823	0.002600835	cg26533595	VWC2	-0.389739326	0.008506686
cg10391522	FAM178B	-0.473467763	0.004788201	cg26005146	NUP205	-0.360254651	0.000592984	cg09253679	WASF3	-0.535310577	0.000804578

cg13999086	FAM180B	-0.444185644	3.33E-05	cg10586756	NUP93	-0.343413499	0.000538719	cg05356778	WBSCR17	-0.66003197	0.001335946
cg24146090	FAM189A2	-0.568395493	0.000105606	ch.11.150762R	NUP98	-0.370042191	0.001223499	cg16163847	WDFY2	-0.673110072	0.002376726
cg26952618	FAM18A	-1.336840299	0.004114957	cg15132165	NXN	-0.784782495	8.97E-06	cg24141863	WDR17	-0.547556567	0.00632376
cg10251936	FAM192A	-0.302311567	0.005334247	cg01994275	NXPH1	-0.322959152	0.004764852	cg14343178	WDR38	-0.453056395	0.000118531
cg21422424	FAM194A	-0.29911532	0.00762032	cg02081701	NXPH2	-0.475473622	0.001011635	cg14870223	WDR48	-0.34777612	0.000352651
cg23767318	FAM19A2	-0.679553533	9.55E-05	cg11505661	NXPH4	-0.488332676	0.002370971	cg24007312	WDR82	-0.418602203	0.000733638
cg23746359	FAM19A3	-0.421888718	0.000502842	cg19983775	OAT	-0.346015031	0.001661927	cg02219997	WFDC1	-0.68520343	0.000231562
cg22871175	FAM19A4	-0.42037609	0.003801343	cg23545105	OCIAD2	-0.512625271	1.05E-05	cg13655803	WFIKKN2	-0.791915712	0.000372706
cg22227586	FAM35A	-0.329674246	0.002199965	cg13983686	ODZ2	-0.702668242	0.000907301	cg18690368	WIPF3	-0.269464546	0.001725451
cg02854554	FAM46C	-0.339106214	0.005615339	cg06527816	ODZ3	-0.496371736	0.001066656	cg14186963	WNT2B	-0.772911916	0.00148213
cg16907934	FAM50B	-0.300215923	0.002122664	cg00908927	ODZ4	-0.449031338	0.000494342	cg17179568	WNT7B	-0.348949353	0.007277995
cg16123101	FAM5B	-0.394680579	0.007976738	cg13796845	OGDHL	-0.643623436	0.001995477	cg03456968	WNT9B	-0.470129647	0.005189036
cg09906145	FAM65A	-0.297299188	0.008960256	cg13914893	OLFM1	-0.373607044	0.009943811	cg20464884	WRNIP1	-0.265922266	0.00224158
cg12497187	FAM81A	-0.410105017	0.000777708	cg21775176	OLFML1	-0.288162097	0.009555403	cg25782229	WT1	-0.686083835	0.00786058
cg02324806	FAM86D	-0.282023741	0.004541312	cg14103872	OLFML2A	-0.365980951	4.14E-06	cg01187496	WWC1	-0.675266864	1.27E-05
cg13791971	FANCC	-0.346625542	0.000298807	cg07122893	OLFML2B	-0.424322367	0.009531105	cg04344190	WWOX	-0.272459412	0.005290955
cg20653375	FARP1	-0.351297522	0.000249289	cg22020227	OLFML3	-0.32093573	0.007221385	cg26832686	WWP2	-0.268867401	0.000174938
cg17301987	FARS2	-0.600698231	2.28E-05	cg25661973	OLIG2	-0.584501932	0.005007409	cg04215287	WWTR1	-0.825190134	0.000769604
cg01337940	FAT1	-0.284363728	0.005938651	cg03602029	OLIG3	-0.586090606	0.001063272	cg09524907	XKR4	-0.26342295	0.005406529
cg24298860	FAT3	-0.405103955	0.003376975	cg22711676	ONECUT1	-0.427223202	0.006286376	cg02969380	XKR5	-0.364136384	0.004822423
cg06933752	FAU	-0.386160509	0.002354977	cg00196827	ONECUT2	-0.505972932	0.003032253	cg09665325	XRN2	-0.639237339	0.000973412
cg02099543	FBLN1	-0.730288031	0.00291219	cg02820309	OPN3	-0.81986274	7.86E-05	cg05057352	XYLT1	-0.465335289	0.003513306
cg04153551	FBLN5	-0.55625189	5.67E-05	cg04660147	OPRL1	-0.435576276	0.002694328	cg05105913	XYLT2	-0.357378971	0.001234298
cg13886554	FBLN7	-1.163421501	3.86E-05	cg13145528	OR2F2	-0.39297238	0.002400631	cg17701100	YIPF7	-0.403445598	0.000714337
cg19771626	FBRSL1	-0.521356821	0.003768576	cg23935054	OR4A5	-0.322519058	5.83E-05	cg17929479	YLPM1	-0.384576899	0.003667525
cg18108683	FBXL13	-0.5189828	0.00400056	cg16940501	ORC3L	-0.443249228	9.31E-05	cg13521620	YPEL2	-0.276903863	0.000809299
cg04005677	FBXL16	-0.299591567	0.008896993	cg18486906	OSBP2	-0.467822511	0.001890508	cg18449964	ZADH2	-0.738207792	0.000793358
cg06084952	FBXL19	-0.479773231	0.000163747	cg26055812	OSBPL9	-0.404336324	0.000256183	cg11821269	ZBTB10	-0.266785823	0.002112147
cg14286665	FBXO11	-0.281985525	0.007384751	cg24062706	OSM	-0.281030179	0.003734055	cg26334507	ZBTB17	-0.343951613	0.002771813
cg26470309	FBXO21	-0.438513813	0.00502656	cg22478121	OSR1	-0.829875186	0.001057357	cg10960375	ZBTB47	-0.556864745	0.007350523
cg24881202	FBXO6	-0.582000282	0.000671247	cg22920700	OSR2	-0.508258464	0.00184084	cg07828024	ZC3H12D	-0.340557874	0.007008371
cg20577477	FDFT1	-0.262522151	0.003813124	cg16537367	OTOR	-0.3650534	0.008529667	cg07376541	ZC3H13	-0.333697614	0.001003083
cg19730600	FER	-0.283963919	0.001333268	cg20405584	OXCT1	-0.735554149	0.000172492	cg12128483	ZC3HC1	-0.333067776	0.000323222
cg00664222	FER1L6	-0.556648673	0.007892342	cg09306606	OXR1	-0.679043245	1.78E-05	cg20618826	ZCCHC24	-0.270416463	0.001114678
cg05366909	FEZ1	-0.593930039	0.007004242	cg17285225	OXTR	-0.917500863	0.005536572	cg19426266	ZEB2	-0.580591852	0.00293083
cg20222926	FEZF1	-0.388782147	7.63E-05	cg25351996	P4HA2	-1.297694198	6.27E-05	cg08251499	ZFAND1	-0.315837817	0.008270605

cg25036456	FGD6	-0.301337402	0.004755573	cg09328228	PABPC1L	-0.39036805	0.005574837	cg25662926	ZFHX4	-0.459404204	0.00477743
cg01096381	FGF1	-0.377379121	0.001625208	cg08893575	PAK4	-0.264949709	0.00539586	cg27162196	ZFP1	-0.280925023	0.008885438
cg06127862	FGF12	-0.271122537	0.00120863	cg01965476	PAK6	-0.377035284	0.004001472	cg04920761	ZFP36L2	-0.491707377	0.003367519
cg18761450	FGF14	-0.370542687	0.000579069	cg18413025	PALLD	-0.488620146	0.009085532	cg11903133	ZFP64	-0.70824238	0.000751927
cg20321432	FGF17	-0.396717759	0.008320011	cg14695566	PALM	-0.499025988	0.000556764	cg27268840	ZFP90	-0.417518825	0.001470781
cg12004787	FGF19	-0.385135429	0.005111236	cg01642824	PAPL	-0.740130473	0.001978828	cg12797828	ZFPM2	-0.319677284	0.008625961
cg17808882	FGF20	-0.468624802	0.003102913	cg09636214	PAPLN	-0.485652064	0.00516838	cg01801603	ZHX2	-0.582459174	0.00104948
cg04495670	FGF3	-0.553437027	0.006626798	cg08784462	PAQR9	-0.781222739	0.002745972	cg02647941	ZIC1	-0.76544625	0.002727473
cg04223548	FGF9	-0.642212707	0.002176109	cg16404105	PARD3B	-0.279263768	0.009779808	cg23980740	ZIC4	-0.55299165	4.65E-05
cg14526525	FGFBP3	-0.632059469	0.005759645	cg04010446	PARK2	-0.266693179	0.009639425	cg15669196	ZIC5	-0.378165709	0.00409808
cg11547613	FGFR1	-0.372178948	0.001447499	cg04203587	PARM1	-0.531357154	0.000853604	cg25034155	ZMIZ1	-0.34037475	0.000381577
cg22633036	FGFR2	-0.306193397	0.006000798	cg03628000	PARN	-0.561421477	0.001111516	cg25987452	ZMYM2	-0.517579634	8.75E-07
cg27571329	FGGY	-0.269498727	0.002120526	cg11903790	PARP8	-0.309898439	0.001911243	cg21199093	ZMYM4	-0.417604666	0.000408257
cg14181576	FGR	-0.930275422	2.21E-05	cg12828018	PATL1	-0.580322282	0.001573642	cg17900689	ZMYND15	-0.603234029	9.97E-05
cg20366397	FHIT	-0.357386739	0.004978129	cg11118778	PAWR	-0.404333379	0.002646998	cg27002271	ZNF121	-0.569781727	0.005991974
cg08834401	FIGLA	-0.278839065	0.000310357	cg16616521	PAX6	-0.524947519	0.000746077	cg14858551	ZNF133	-0.276417149	0.001262586
cg15287594	FITM2	-0.474828837	0.001475853	cg10911990	PAX9	-0.413734918	0.000880081	cg24802771	ZNF141	-0.282371748	0.006959085
cg20346388	FKBP11	-0.35049555	0.009151041	cg02779948	PBLD	-0.281465299	0.00221306	cg03668763	ZNF143	-0.313636455	0.003442151
cg03591753	FKBP5	-0.309457178	0.002003593	cg06750897	PBX1	-0.858146137	0.000414062	cg02339392	ZNF187	-0.543046588	0.002707348
cg05098551	FKBP7	-0.606760284	0.008207347	cg20733761	PCBP3	-0.839401456	0.003535557	cg15407162	ZNF193	-0.436248023	0.000496876
cg08634012	FKRP	-0.57667175	0.007400685	cg15112032	PCDH17	-0.408108781	0.000448425	cg12869659	ZNF238	-0.502942576	0.006816705
cg00344445	FLI1	-0.905826414	0.000252039	cg00817501	PCDH18	-0.498492124	0.001802535	cg20662725	ZNF257	-0.54446593	0.006787842
cg14979609	FLJ10661	-0.296009617	0.00050988	cg16987900	PCDHA2	-0.90206691	9.83E-05	cg12575136	ZNF397	-0.521021121	4.50E-05
cg17283857	FLJ41350	-0.605948308	0.009865501	cg19596110	PCDHA6	-0.888550988	5.58E-06	cg04086531	ZNF423	-0.947517431	0.000879858
cg02637352	FLJ41603	-0.309573006	0.008099735	cg23356309	PCDHA7	-0.343723191	0.002560877	cg13584718	ZNF432	-0.621197777	0.00630079
cg04255278	FLJ42709	-0.286299221	0.000656597	cg21101631	PCDHGA4	-0.336142035	0.007242916	cg25888881	ZNF438	-0.394450294	0.003574999
cg14926717	FLJ43390	-0.329318089	0.002389225	cg13485809	PCGF3	-0.491235858	0.000250389	cg00711090	ZNF471	-0.608165755	0.00044879
cg16706751	FLJ43663	-0.265710341	0.003048186	cg25267304	PCOTH	-0.285441544	0.004657111	cg27213549	ZNF485	-0.347165481	0.00182877
cg27097438	FLJ44606	-0.943663917	0.008412638	cg10453419	PCSK6	-1.096843255	1.27E-05	cg01565690	ZNF510	-0.266838965	0.006267557
cg15330117	FLJ45983	-0.868388522	0.003306214	cg12850242	PCYOX1	-0.485971364	0.005225348	cg01094891	ZNF536	-0.720239591	1.99E-07
cg15733367	FLNB	-0.647169986	0.004023232	cg26780688	PDCL	-0.292686217	0.003333341	cg15495372	ZNF579	-0.543633593	1.10E-05
cg18760837	FLOT1	-0.394257254	0.002799304	cg20824867	PDDC1	-0.345865979	0.001738787	cg26916780	ZNF609	-0.59434567	0.007381583
cg02186409	FLT1	-0.329957006	0.007973753	cg16640865	PDE2A	-0.876039087	0.006620554	cg11981871	ZNF616	-0.260302939	0.006491319
cg26493188	FLYWCH1	-0.301203264	0.000557795	cg22999327	PDE3A	-0.376671553	0.003014708	cg03608000	ZNF69	-0.325810994	0.000960292
cg15748490	FMN2	-0.511098269	0.003556528	cg26817935	PDE4D	-0.425452324	0.002539427	cg01274826	ZNF709	-0.342086221	0.00452084
cg04953238	FMNL2	-0.389416917	0.005469432	cg23942789	PDE8B	-0.489673204	0.000550644	cg11638847	ZNF749	-0.280614656	0.002255226

cg20951350	FNDC1	-0.817407965	7.49E-10	cg18688704	PDGFC	-0.295735607	0.004557166	cg17850538	ZNF770	-0.318834385	0.000690741
cg25790298	FNDC3B	-0.475554051	0.00156092	cg23358564	PDLIM4	-0.332448503	0.00940115	cg01017773	ZNF772	-0.51941712	0.002372366
cg13702235	FNIP2	-0.439037458	0.001348156	cg07034563	PDLIM7	-0.369080483	0.005610711	cg00475260	ZNF800	-0.362667732	0.007230947
cg24397007	FOSL2	-0.58732716	0.002889233	cg04886857	PDPN	-0.403022363	0.0016855	cg25400396	ZNF814	-0.543845056	0.002929742
cg04510512	FOXC2	-0.539919393	0.00529433	cg01907098	PDXK	-0.490158504	0.00772997	cg09427605	ZNF827	-0.695148243	0.000213168
cg22796507	FOXE3	-0.718738225	0.000907195	cg18050520	PEBP4	-0.366943513	0.007106537	cg17132967	ZNF83	-0.456454798	0.007589815
cg17525102	FOXG1	-0.765718333	6.23E-05	cg04368094	PELI2	-0.378883098	0.005333416	cg19507256	ZNF862	-0.396857117	0.003313109
cg13491584	FOXI3	-0.457128402	0.000430387	cg23072629	PER2	-0.372179792	0.007621143	cg27662633	ZNRF2	-0.306256546	0.00016087
cg17815933	FOXJ2	-0.436301737	0.003298036	cg16699385	PERP	-0.629174639	0.000381222	cg13298682	ZNRF3	-0.749873401	0.00329929
cg25344401	FOXK1	-0.525625979	0.001262419	cg06622725	PEX16	-0.264129958	0.008658352	cg17237506	ZPBP	-0.38455586	0.002671509
cg25008263	FOXN3	-0.355441793	9.30E-05	cg26693553	PFKP	-0.414515994	0.000261957	cg16810031	ZPBP2	-0.504891132	0.000172964
cg01511742	FOXP1	-0.575004886	0.000445971	cg16754788	PGCP	-0.490606135	0.00199086	cg16325326	ZYG11B	-0.375681232	0.005905939
cg05232889	FOXP2	-0.879261406	0.000970376	cg13964726	PGM5	-0.511180707	0.005329159	cg03761471	ZYX	-0.409950967	0.00968965

Note: Chronic obstructive pulmonary disease, COPD. Methylation dataset of GSE111396 was reanalyzed in R using DESeq2 package. Samples from non-smokers and ex-smokers were selected and were grouped by COPD stages. The gene annotation for each probe was according to Illumina Human Methylation 450 Bead Chip (GPL13534). The criteria (Log2 foldchange was less than -0.26 and *p* value was less than 0.01) were used to identify hypomethylated genes, and the probes with the minimum Log2 foldchanges were retained. A total of 2085 hypomethylated genes (shown in this table) were identified in the lungs of COPD patients who belonged to COPD stage 1 to 2.

Table S9 Primers and probes sequences to amplify for HTR4 transcripts using TaqMan real-time qPCR.

Transcript		Sequence (5'-3')
HTR4-b	Forward	CGAATCTGCCAGGGCACCTC
	Reserve	CTCCTCAGAACTCACATTAGCATCAAG
	Probe	CCTCGCCTCTGGCAGCGGGAC
HTR4-c	Forward	GAGCGCTACCGAAGACCTTC
	Reserve	GGCATTTGGATGGTTTGGTCAATC
	Probe	CCAGACTGTCCCTTGTTCAACCACAACC
HTR4-i	Forward	TCCTCTGCTGTGATGATGAGC
	Reserve	GCTCAATGTGCCTGAGAATGG
	Probe	CCGCTCTGGCAGGCTTTGTCCAA
HTR4-d	Forward	CCTCTGCTGTGATGATGAGCGC
	Reserve	GTGTACAAAAACCTGTGTTGGGCAC
	Probe	ACCGAAGACCTTCCATTCTGGGCC
HTR4-a	Forward	ACTGTCCCTTGTTCAACCACAAC
	Reserve	CTGGGTCATTGTGTATGGGCAG
	Probe	CCACACATGTACTAAGGTACACCGTTCTGC
HTR4-g	Forward	CTTCCTCCTGCTCTTCTGCAAT
	Reserve	TGTGTATGGGCAGTTTCTCGAG
	Probe	ACCAGTTCCTGTCTAACTCTGAAAGTGCTC
HTR4	Forward	TGTGAGTTCTGAGGAGGGTTTCG
	Reserve	CGAAACCAGCAGATCCGCAA
	Probe	TGGTGCTGCTCACGTTTCTCTCGAC
GAPDH	Forward	CCAGGTGGTCTCCTCTGACTTC
	Reserve	TCATACCAGGAAATGAGCTTGACA
	Probe	CAGCGACACCCACTCCTCCACC

Table S10 sgRNA oligonucleotide sequences for HTR4 knockout in A549 cells.

sgRNA Oligonucleotide ID	Sequence
sgHTR4 F	5'-caccGAAATCGATGCCGTTGTGAGC
sgHTR4 R	5'-aaacGCTCACAACGGCATCGATTTc
sgNontargeting F	5'-caccGGCTCGGTCCCGCGTCGTCG
sgNontargeting R	5'-aaacCGACGACGCGGGACCGAGCC

Table S11 Three eQTLs of HTR4 were retrieved from GTEx database.

Variant ID	SNP ID	*p* Value	NES	Tissue
chr5_148735243_A_G_b38	rs2400642	0.000014	0.42	Testis
chr5_148735334_A_G_b38	rs2400643	0.000014	0.42	Testis
chr5_148736639_T_G_b38	rs1465405	0.000018	0.4	Testis

Note: Normalized effect size (NES) of the eQTLs is defined as the effect of the alternative (ALT) allele relative to the reference (REF) allele, when NES is positive, it means the effect of ALT allele is increasing expression of HTR4 relative to REF allele.

Table S12 Five SNPs of HTR4 were associated with human lung function or COPD morbidity in previous studies.

SNP ID	Effect	Position	Reference
rs7735184	decrease of FEV1	chr5:148464829	[22]
rs11168048	decrease of FEV1	chr5:148462790	
rs3995090	association with COPD morbidity; decrease of FEV1 and FEV1/FVC	chr5:148466252	[23, 24]
rs6889822	decrease of FEV1 and FEV1/FVC	chr5:148467144	[25]
rs7733088	decrease of FEV1 and FEV1/FVC	chr5:148476770	[26]

Table S13 Prevalence of COPD in different regions globally.

Region	COPD Prevalence (%)	Reference
China	15.0	[27]
Japan	13.6	[28]
India	7.7	[29]
USA	14.0	[10]
Spain	10.2	[30]
United Kingdom	5.4	[31]
Finland	6.0	[32]
Latin America	12.2	[33-35]
Africa	7.7	[36]
Global	11.7	[37]

Note: The COPD criterion use the fixed ratio based on FEV1/FVC < 70% with post-bronchodilator spirometry. The COPD prevalence in Latin America was the weighted average based on population sizes of the corresponding countries when the investigations in the reports were launched. The data of the population sizes were obtained from DataBank of the World Bank.

References

(1) Nielsen, G. D.; Larsen, S. T.; Wolkoff, P. Re-Evaluation of the Who (2010) Formaldehyde Indoor Air Quality Guideline for Cancer Risk Assessment. *Archives of Toxicology* **2017**, *91* (1), 35-61.

(2) Golden, R. Identifying an Indoor Air Exposure Limit for Formaldehyde Considering Both Irritation and Cancer Hazards. *Critical Reviews in Toxicology* **2011**, *41* (8), 672-721.

(3) Ashcroft, T.; Simpson, J. M.; Timbrell, V. Simple Method of Estimating Severity of Pulmonary Fibrosis on a Numerical Scale. *Journal of Clinical Pathology* **1988**, *41* (4), 467-470.

(4) Huebner, R.-H.; Gitter, W.; El Mokhtari, N. E.; Mathiak, M.; Both, M.; Bolte, H.; Freitag-Wolf, S.; Bewig, B. Standardized Quantification of Pulmonary Fibrosis in Histological Samples. *Biotechniques* **2008**, *44* (4), 507-+.

(5) Pinero, J.; Manuel Ramirez-Anguita, J.; Sauch-Pitarch, J.; Ronzano, F.; Centeno, E.; Sanz, F.; Furlong, L. I. The Disgenet Knowledge Platform for Disease Genomics: 2019 Update. *Nucleic Acids Research* **2020**, *48* (D1), D845-D855.

(6) Kim, V.; Criner, G. J. Chronic Bronchitis and Chronic Obstructive Pulmonary Disease. *American Journal of Respiratory and Critical Care Medicine* **2013**, *187* (3), 228-237.

(7) Sanchez, D.; Batet, M. Semantic Similarity Estimation in the Biomedical Domain: An Ontology-Based Information-Theoretic Perspective. *Journal of Biomedical Informatics* **2011**, *44* (5), 749-759.

(8) Clifford, R. L.; Fishbane, N.; Patel, J.; Macisaac, J. L.; Mcewen, L. M.; Fisher, A. J.; Brandsma, C.-A.; Nair, P.; Kobor, M. S.; Hackett, T.-L.; Knox, A. J. Altered DNA Methylation Is Associated with Aberrant Gene Expression in Parenchymal but Not Airway Fibroblasts Isolated from Individuals with Copd. *Clinical Epigenetics* **2018**, *10*.

(9) Love, M. I.; Huber, W.; Anders, S. Moderated Estimation of Fold Change and Dispersion for Rna-Seq Data with Deseq2. *Genome Biology* **2014**, *15* (12).

(10) Tilert, T.; Dillon, C.; Paulose-Ram, R.; Hnizdo, E.; Doney, B. Estimating the Us Prevalence of Chronic Obstructive Pulmonary Disease Using Pre- and Post-Bronchodilator Spirometry: The National Health and Nutrition Examination Survey (Nhanes) 2007-2010. *Respiratory Research* **2013**, *14*.

(11) Han, B.; Eskin, E. Interpreting Meta-Analyses of Genome-Wide Association Studies. *Plos Genetics* **2012**, *8* (3).

(12) Thun, G. A.; Imboden, M.; Ferrarotti, I.; Kumar, A.; Obeidat, M. E.; Zorzetto, M.; Haun, M.; Curjuric, I.; Alves, A. C.; Jackson, V. E.; Albrecht, E.; Ried, J. S.; Teumer, A.; Lopez, L. M.; Huffman, J. E.; Enroth, S.; Bosse, Y.; Hao, K.; Timens, W.; Gyllensten, U.; Polasek, O.; Wilson, J. F.; Rudan, I.; Hayward, C.; Sandford, A. J.; Deary, I. J.; Koch, B.; Reischl, E.; Schulz, H.; Hui, J.; James, A. L.; Rochat, T.; Russi, E. W.; Jarvelin, M.-R.; Strachan, D. P.; Hall, I. P.; Tobin, M. D.; Dahl, M.; Nielsen, S. F.; Nordestgaard, B. G.; Kronenberg, F.; Luisetti, M.; Probst-Hensch, N. M. Causal and Synthetic Associations of Variants in the Serpina Gene Cluster with Alpha1-Antitrypsin Serum Levels. *Plos Genetics* **2013**, *9* (8).

(13) Altshuler, D. M.; Durbin, R. M.; Abecasis, G. R.; Bentley, D. R.; Chakravarti, A.; Clark, A. G.; Donnelly, P.; Eichler, E. E.; Flicek, P.; Gabriel, S. B.; Gibbs, R. A.; Green, E. D.; Hurles, M. E.; Knoppers, B. M.; Korbel, J. O.; Lander, E. S.; Lee, C.; Lehrach, H.; Mardis, E. R.; Marth, G. T.; Mcvean, G. A.; Nickerson, D. A.; Schmidt, J. P.; Sherry, S. T.; Wang, J.; Wilson, R. K.; Gibbs, R. A.; Boerwinkle, E.; Doddapaneni, H.; Han, Y.; Korchina, V.; Kovar, C.; Lee, S.; Muzny, D.; Reid, J. G.; Zhu, Y.; Wang, J.; Chang, Y.; Feng, Q.; Fang, X.; Guo, X.; Jian, M.; Jiang, H.; Jin, X.; Lan, T.; Li, G.; Li, J.; Li, Y.; Liu, S.; Liu, X.; Lu, Y.; Ma, X.; Tang, M.; Wang, B.; Wang, G.; Wu, H.; Wu, R.; Xu, X.; Yin, Y.; Zhang, D.; Zhang, W.; Zhao, J.; Zhao, M.; Zheng, X.; Lander, E. S.; Altshuler, D. M.; Gabriel, S. B.; Gupta, N.;

Gharani, N.; Toji, L. H.; Gerry, N. P.; Resch, A. M.; Flicek, P.; Barker, J.; Clarke, L.; Gil, L.; Hunt, S. E.; Kelman, G.; Kulesha, E.; Leinonen, R.; Mclaren, W. M.; Radhakrishnan, R.; Roa, A.; Smirnov, D.; Smith, R. E.; Streeter, I.; Thormann, A.; Toneva, I.; Vaughan, B.; Zheng-Bradley, X.; Bentley, D. R.; Grocock, R.; Humphray, S.; James, T.; Kingsbury, Z.; Lehrach, H.; Sudbrak, R.; Albrecht, M. W.; Amstislavskiy, V. S.; Borodina, T. A.; Lienhard, M.; Mertes, F.; Sultan, M.; Timmermann, B.; Yaspo, M.-L.; Mardis, E. R.; Wilson, R. K.; Fulton, L.; Fulton, R.; Sherry, S. T.; Ananiev, V.; Belaia, Z.; Beloslyudtsev, D.; Bouk, N.; Chen, C.; Church, D.; Cohen, R.; Cook, C.; Garner, J.; Hefferon, T.; Kimelman, M.; Liu, C.; Lopez, J.; Meric, P.; O'sullivan, C.; Ostapchuk, Y.; Phan, L.; Ponomarov, S.; Schneider, V.; Shekhtman, E.; Sirotkin, K.; Slotta, D.; Zhang, H.; Mcvean, G. A.; Durbin, R. M.; Balasubramaniam, S.; Burton, J.; Danecek, P.; Keane, T. M.; Kolb-Kokocinski, A.; Mccarthy, S.; Stalker, J.; Quail, M.; Schmidt, J. P.; Davies, C. J.; Gollub, J.; Webster, T.; Wong, B.; Zhan, Y.; Auton, A.; Campbell, C. L.; Kong, Y.; Marcketta, A.; Gibbs, R. A.; Yu, F.; Antunes, L.; Bainbridge, M.; Muzny, D.; Sabo, A.; Huang, Z.; Wang, J.; Coin, L. J. M.; Fang, L.; Guo, X.; Jin, X.; Li, G.; Li, Q.; Li, Y.; Li, Z.; Lin, H.; Liu, B.; Luo, R.; Shao, H.; Xie, Y.; Ye, C.; Yu, C.; Zhang, F.; Zheng, H.; Zhu, H.; Alkan, C.; Dal, E.; Kahveci, F.; Marth, G. T.; Garrison, E. P.; Kural, D.; Lee, W.-P.; Leong, W. F.; Stromberg, M.; Ward, A. N.; Wu, J.; Zhang, M.; Daly, M. J.; Depristo, M. A.; Handsaker, R. E.; Altshuler, D. M.; Banks, E.; Bhatia, G.; Del Angel, G.; Gabriel, S. B.; Genovese, G.; Gupta, N.; Li, H.; Kashin, S.; Lander, E. S.; Mccarroll, S. A.; Nemesh, J. C.; Poplin, R. E.; Yoon, S. C.; Lihm, J.; Makarov, V.; Clark, A. G.; Gottipati, S.; Keinan, A.; Rodriguez-Flores, J. L.; Korbel, J. O.; Rausch, T.; Fritz, M. H.; Stuetz, A. M.; Flicek, P.; Beal, K.; Clarke, L.; Datta, A.; Herrero, J.; Mclaren, W. M.; Ritchie, G. R. S.; Smith, R. E.; Zerbino, D.; Zheng-Bradley, X.; Sabeti, P. C.; Shlyakhter, I.; Schaffner, S. F.; Vitti, J.; Cooper, D. N.; Ball, E. V.; Stenson, P. D.; Bentley, D. R.; Barnes, B.; Bauer, M.; Cheetham, R. K.; Cox, A.; Eberle, M.; Humphray, S.; Kahn, S.; Murray, L.; Peden, J.; Shaw, R.; Kenny, E. E.; Batzer, M. A.; Konkel, M. K.; Walker, J. A.; Macarthur, D. G.; Lek, M.; Sudbrak, R.; Amstislavskiy, V. S.; Herwig, R.; Mardis, E. R.; Ding, L.; Koboldt, D. C.; Larson, D.; Ye, K.; Gravel, S.; Swaroop, A.; Chew, E.; Lappalainen, T.; Erlich, Y.; Gymrek, M.; Willems, T. F.; Simpson, J. T.; Shriver, M. D.; Rosenfeld, J. A.; Bustamante, C. D.; Montgomery, S. B.; De La Vega, F. M.; Byrnes, J. K.; Carroll, A. W.; Degorter, M. K.; Lacroute, P.; Maples, B. K.; Martin, A. R.; Moreno-Estrada, A.; Shringarpure, S. S.; Zakharia, F.; Halperin, E.; Baran, Y.; Lee, C.; Cerveira, E.; Hwang, J.; Malhotra, A.; Plewczynski, D.; Radew, K.; Romanovitch, M.; Zhang, C.; Hyland, F. C. L.; Craig, D. W.; Christoforides, A.; Homer, N.; Izatt, T.; Kurdoglu, A. A.; Sinari, S. A.; Squire, K.; Sherry, S. T.; Xiao, C.; Sebat, J.; Antaki, D.; Gujral, M.; Noor, A.; Ye, K.; Burchard, E. G.; Hernandez, R. D.; Gignoux, C. R.; Haussler, D.; Katzman, S. J.; Kent, W. J.; Howie, B.; Ruiz-Linares, A.; Dermitzakis, E. T.; Devine, S. E.; Goncalo, R. A.; Kang, H. M.; Kidd, J. M.; Blackwell, T.; Caron, S.; Chen, W.; Emery, S.; Fritsche, L.; Fuchsberger, C.; Jun, G.; Li, B.; Lyons, R.; Scheller, C.; Sidore, C.; Song, S.; Sliwerska, E.; Taliun, D.; Tan, A.; Welch, R.; Wing, M. K.; Zhan, X.; Awadalla, P.; Hodgkinson, A.; Li, Y.; Shi, X.; Quitadamo, A.; Lunter, G.; Mcvean, G. A.; Marchini, J. L.; Myers, S.; Churchhouse, C.; Delaneau, O.; Gupta-Hinch, A.; Kretzschmar, W.; Iqbal, Z.; Mathieson, I.; Menelaou, A.; Rimmer, A.; Xifara, D. K.; Oleksyk, T. K.; Fu, Y.; Liu, X.; Xiong, M.; Jorde, L.; Witherspoon, D.; Xing, J.; Eichler, E. E.; Browning, B. L.; Browning, S. R.; Hormozdiari, F.; Sudmant, P. H.; Khurana, E.; Durbin, R. M.; Hurles, M. E.; Tyler-Smith, C.; Albers, C. A.; Ayub, Q.; Balasubramaniam, S.; Chen, Y.; Colonna, V.; Danecek, P.; Jostins, L.; Keane, T. M.; Mccarthy, S.; Walter, K.; Xue, Y.; Gerstein, M. B.; Abyzov, A.; Balasubramanian, S.; Chen, J.; Clarke, D.; Fu, Y.; Harmanci, A. O.; Jin, M.; Lee, D.; Liu, J.; Mu, X. J.; Zhang, J.; Zhang, Y.; Li, Y.; Luo, R.; Zhu, H.; Alkan, C.; Dal, E.; Kahveci, F.; Marth, G. T.; Garrison, E. P.; Kural, D.; Lee, W.-P.; Ward, A. N.; Wu, J.; Zhang, M.; Mccarroll, S. A.;

Handsaker, R. E.; Altshuler, D. M.; Banks, E.; Del Angel, G.; Genovese, G.; Hartl, C.; Li, H.; Kashin, S.; Nemesh, J. C.; Shakir, K.; Yoon, S. C.; Lihm, J.; Makarov, V.; Degenhardt, J.; Korbel, J. O.; Fritz, M. H.; Meiers, S.; Raeder, B.; Rausch, T.; Stuetz, A. M.; Flicek, P.; Casale, F. P.; Clarke, L.; Smith, R. E.; Stegle, O.; Zheng-Bradley, X.; Bentley, D. R.; Barnes, B.; Cheetham, R. K.; Eberle, M.; Humphray, S.; Kahn, S.; Murray, L.; Shaw, R.; Lameijer, E.-W.; Batzer, M. A.; Konkel, M. K.; Walker, J. A.; Ding, L.; Hall, I.; Ye, K.; Lacroute, P.; Lee, C.; Cerveira, E.; Malhotra, A.; Hwang, J.; Plewczynski, D.; Radew, K.; Romanovitch, M.; Zhang, C.; Craig, D. W.; Homer, N.; Church, D.; Xiao, C.; Sebat, J.; Antaki, D.; Bafna, V.; Michaelson, J.; Ye, K.; Devine, S. E.; Gardner, E. J.; Abecasis, G. R.; Kidd, J. M.; Mills, R. E.; Dayama, G.; Emery, S.; Jun, G.; Shi, X.; Quitadamo, A.; Lunter, G.; Mcvean, G. A.; Chen, K.; Fan, X.; Chong, Z.; Chen, T.; Witherspoon, D.; Xing, J.; Eichler, E. E.; Chaisson, M. J.; Hormozdiari, F.; Huddleston, J.; Malig, M.; Nelson, B. J.; Sudmant, P. H.; Parrish, N. F.; Khurana, E.; Hurles, M. E.; Blackburne, B.; Lindsay, S. J.; Ning, Z.; Walter, K.; Zhang, Y.; Gerstein, M. B.; Abyzov, A.; Chen, J.; Clarke, D.; Lam, H.; Mu, X. J.; Sisu, C.; Zhang, J.; Zhang, Y.; Gibbs, R. A.; Yu, F.; Bainbridge, M.; Challis, D.; Evani, U. S.; Kovar, C.; Lu, J.; Muzny, D.; Nagaswamy, U.; Reid, J. G.; Sabo, A.; Yu, J.; Guo, X.; Li, W.; Li, Y.; Wu, R.; Marth, G. T.; Garrison, E. P.; Leong, W. F.; Ward, A. N.; Del Angel, G.; Depristo, M. A.; Gabriel, S. B.; Gupta, N.; Hartl, C.; Poplin, R. E.; Clark, A. G.; Rodriguez-Flores, J. L.; Flicek, P.; Clarke, L.; Smith, R. E.; Zheng-Bradley, X.; Macarthur, D. G.; Mardis, E. R.; Fulton, R.; Koboldt, D. C.; Gravel, S.; Bustamante, C. D.; Craig, D. W.; Christoforides, A.; Homer, N.; Izatt, T.; Sherry, S. T.; Xiao, C.; Dermitzakis, E. T.; Abecasis, G. R.; Kang, H. M.; Mcvean, G. A.; Gerstein, M. B.; Balasubramanian, S.; Habegger, L.; Yu, H.; Flicek, P.; Clarke, L.; Cunningham, F.; Dunham, I.; Zerbino, D.; Zheng-Bradley, X.; Lage, K.; Jespersen, J. B.; Horn, H.; Montgomery, S. B.; Degorter, M. K.; Khurana, E.; Tyler-Smith, C.; Chen, Y.; Colonna, V.; Xue, Y.; Gerstein, M. B.; Balasubramanian, S.; Fu, Y.; Kim, D.; Auton, A.; Marcketta, A.; Desalle, R.; Narechania, A.; Sayres, M. a. W.; Garrison, E. P.; Handsaker, R. E.; Kashin, S.; Mccarroll, S. A.; Rodriguez-Flores, J. L.; Flicek, P.; Clarke, L.; Zheng-Bradley, X.; Erlich, Y.; Gymrek, M.; Willems, T. F.; Bustamante, C. D.; Mendez, F. L.; Poznik, G. D.; Underhill, P. A.; Lee, C.; Cerveira, E.; Malhotra, A.; Romanovitch, M.; Zhang, C.; Abecasis, G. R.; Coin, L.; Shao, H.; Mittelman, D.; Tyler-Smith, C.; Ayub, Q.; Banerjee, R.; Cerezo, M.; Chen, Y.; Fitzgerald, T.; Louzada, S.; Massaia, A.; Mccarthy, S.; Ritchie, G. R.; Xue, Y.; Yang, F.; Gibbs, R. A.; Kovar, C.; Kalra, D.; Hale, W.; Muzny, D.; Reid, J. G.; Wang, J.; Dan, X.; Guo, X.; Li, G.; Li, Y.; Ye, C.; Zheng, X.; Altshuler, D. M.; Flicek, P.; Clarke, L.; Zheng-Bradley, X.; Bentley, D. R.; Cox, A.; Humphray, S.; Kahn, S.; Sudbrak, R.; Albrecht, M. W.; Lienhard, M.; Larson, D.; Craig, D. W.; Izatt, T.; Kurdoglu, A. A.; Sherry, S. T.; Xiao, C.; Haussler, D.; Abecasis, G. R.; Mcvean, G. A.; Durbin, R. M.; Balasubramaniam, S.; Keane, T. M.; Mccarthy, S.; Stalker, J.; Chakravarti, A.; Knoppers, B. M.; Abecasis, G. R.; Barnes, K. C.; Beiswanger, C.; Burchard, E. G.; Bustamante, C. D.; Cai, H.; Cao, H.; Durbin, R. M.; Gerry, N. P.; Gharani, N.; Gibbs, R. A.; Gignoux, C. R.; Gravel, S.; Henn, B.; Jones, D.; Jorde, L.; Kaye, J. S.; Keinan, A.; Kent, A.; Kerasidou, A.; Li, Y.; Mathias, R.; Mcvean, G. A.; Moreno-Estrada, A.; Ossorio, P. N.; Parker, M.; Resch, A. M.; Rotimi, C. N.; Royal, C. D.; Sandoval, K.; Su, Y.; Sudbrak, R.; Tian, Z.; Tishkoff, S.; Toji, L. H.; Tyler-Smith, C.; Via, M.; Wang, Y.; Yang, H.; Yang, L.; Zhu, J.; Bodmer, W.; Bedoya, G.; Ruiz-Linares, A.; Cai, Z.; Gao, Y.; Chu, J.; Peltonen, L.; Garcia-Montero, A.; Orfao, A.; Dutil, J.; Martinez-Cruzado, J. C.; Oleksyk, T. K.; Barnes, K. C.; Mathias, R. A.; Hennis, A.; Watson, H.; Mckenzie, C.; Qadri, F.; Larocque, R.; Sabeti, P. C.; Zhu, J.; Deng, X.; Sabeti, P. C.; Asogun, D.; Folarin, O.; Happi, C.; Omoniwa, O.; Stremlau, M.; Tariyal, R.; Jallow, M.; Joof, F. S.; Corrah, T.; Rockett, K.; Kwiatkowski, D.; Kooner, J.; Tran Tinh, H.; Dunstan, S. J.; Nguyen Thuy, H.; Fonnie, R.; Garry, R.; Kanneh, L.; Moses, L.; Sabeti, P. C.; Schieffelin, J.; Grant, D. S.; Gallo,

C.; Poletti, G.; Saleheen, D.; Rasheed, A.; Brook, L. D.; Felsenfeld, A.; Mcewen, J. E.; Vaydylevich, Y.; Green, E. D.; Duncanson, A.; Dunn, M.; Schloss, J. A.; Wang, J.; Yang, H.; Auton, A.; Brooks, L. D.; Durbin, R. M.; Garrison, E. P.; Kang, H. M.; Korbel, J. O.; Marchini, J. L.; Mccarthy, S.; Mcvean, G. A.; Abecasis, G. R.; Genomes Project, C. A Global Reference for Human Genetic Variation. *Nature* **2015**, *526* (7571), 68-+.

(14) Xia, P.; Zhang, X.; Xie, Y.; Guan, M.; Villeneuve, D. L.; Yu, H. Functional Toxicogenomic Assessment of Triclosan in Human Hepg2 Cells Using Genome-Wide Crispr-Cas9 Screening. *Environmental Science & Technology* **2016**, *50* (19), 10682-10692.

(15) Shalem, O.; Sanjana, N. E.; Hartenian, E.; Shi, X.; Scott, D. A.; Mikkelsen, T. S.; Heckl, D.; Ebert, B. L.; Root, D. E.; Doench, J. G.; Zhang, F. Genome-Scale Crispr-Cas9 Knockout Screening in Human Cells. *Science* **2014**, *343* (6166), 84-87.

(16) Shen, H.; Mchale, C. M.; Smith, M. T.; Zhang, L. Functional Genomic Screening Approaches in Mechanistic Toxicology and Potential Future Applications of Crispr-Cas9. *Mutation Research-Reviews in Mutation Research* **2015**, *764*, 31-42.

(17) Lujan, H.; Romer, E.; Salisbury, R.; Hussain, S.; Sayes, C. Determining the Biological Mechanisms of Action for Environmental Exposures: Applying Crispr/Cas9 to Toxicological Assessments. *Toxicological Sciences* **2020**, *175* (1), 5-18.

(18) Castriconi, F.; Paolino, M.; Donati, A.; Giuliani, G.; Anzini, M.; Mennuni, L.; Sabatini, C.; Lanza, M.; Caselli, G.; Makovec, F.; Sbraccia, M.; Molinari, P.; Costa, T.; Cappelli, A. Multivalent Ligands for the Serotonin 5-Ht4 Receptor. *Medchemcomm* **2017**, *8* (3), 647-651.

(19) Gaven, F.; Pellissier, L. P.; Queffeulou, E.; Cochet, M.; Bockaert, J.; Dumuis, A.; Claeysen, S. Pharmacological Profile of Engineered 5-Ht4 Receptors and Identification of 5-Ht4 Receptor-Biased Ligands. *Brain Research* **2013**, *1511*, 65-72.

(20) Kim, M. O.; Lee, Y. J.; Park, J. H.; Ryu, J. M.; Yun, S. P.; Han, H. J. Pka and Camp Stimulate Proliferation of Mouse Embryonic Stem Cells by Elevating Glut1 Expression Mediated by the Nf-Kappa B and Creb/Cbp Signaling Pathways. *Biochimica Et Biophysica Acta-General Subjects* **2012**, *1820* (10), 1636-1646.

(21) Zhong, H. H.; Suyang, H.; Erdjumentbromage, H.; Tempst, P.; Ghosh, S. The Transcriptional Activity of Nf-Kappa B Is Regulated by the I Kappa B-Associated Pkac Subunit through a Cyclic Amp-Independent Mechanism. *Cell* **1997**, *89* (3), 413-424.

(22) Hancock, D. B.; Eijgelsheim, M.; Wilk, J. B.; Gharib, S. A.; Loehr, L. R.; Marciante, K. D.; Franceschini, N.; Van Durme, Y. M. T. A.; Chen, T.-H.; Barr, R. G.; Schabath, M. B.; Couper, D. J.; Brusselle, G. G.; Psaty, B. M.; Van Duijn, C. M.; Rotter, J. I.; Uitterlinden, A. G.; Hofman, A.; Punjabi, N. M.; Rivadeneira, F.; Morrison, A. C.; Enright, P. L.; North, K. E.; Heckbert, S. R.; Lumley, T.; Stricker, B. H. C.; O'connor, G. T.; London, S. J. Meta-Analyses of Genome-Wide Association Studies Identify Multiple Loci Associated with Pulmonary Function. *Nature Genetics* **2010**, *42* (1), 45-U61.

(23) Artigas, M. S.; Wain, L. V.; Repapi, E.; Obeidat, M. E.; Sayers, I.; Burton, P. R.; Johnson, T.; Zhao, J. H.; Albrecht, E.; Dominiczak, A. F.; Kerr, S. M.; Smith, B. H.; Cadby, G.; Hui, J.; Palmer, L. J.; Hingorani, A. D.; Wannamethee, S. G.; Whincup, P. H.; Ebrahim, S.; Smith, G. D.; Barroso, I.; Loos, R. J. F.; Wareham, N. J.; Cooper, C.; Dennison, E.; Shaheen, S. O.; Liu, J. Z.; Marchini, J.; Dahgam, S.; Naluai, A. T.; Olin, A.-C.; Karrasch, S.; Heinrich, J.; Schulz, H.; Mckeever, T. M.; Pavord, I. D.; Heliovaara, M.; Ripatti, S.; Surakka, I.; Blakey, J. D.; Kahonen, M.; Britton, J. R.; Nyberg, F.; Holloway, J. W.; Lawlor, D. A.; Morris, R. W.; James, A. L.; Jackson, C. M.; Hall, I. P.; Tobin, M. D.; Med Res Council Natl Survey Hlth, D.; Spirometa, C. Effect of Five Genetic Variants Associated with Lung

Function on the Risk of Chronic Obstructive Lung Disease, and Their Joint Effects on Lung Function. *American Journal of Respiratory and Critical Care Medicine* **2011**, *184* (7), 786-795.
(24) Yang, J.; Zhou, H.; Liang, B.; Xiao, J.; Su, Z.; Chen, H.; Ma, C.; Li, D.; Feng, Y.; Ou, X. Association of Five Genetic Variants with Chronic Obstructive Pulmonary Disease Susceptibility and Spirometric Phenotypes in a Chinese Han Population. *Respirology* **2014**, *19* (2), 262-268.
(25) Repapi, E.; Sayers, I.; Wain, L. V.; Burton, P. R.; Johnson, T.; Obeidat, M. E.; Zhao, J. H.; Ramasamy, A.; Zhai, G.; Vitart, V.; Huffman, J. E.; Igl, W.; Albrecht, E.; Deloukas, P.; Henderson, J.; Granell, R.; Mcardle, W. L.; Rudnicka, A. R.; Barroso, I.; Loos, R. J. F.; Wareham, N. J.; Mustelin, L.; Rantanen, T.; Surakka, I.; Imboden, M.; Wichmann, H. E.; Grkovic, I.; Jankovic, S.; Zgaga, L.; Hartikainen, A.-L.; Peltonen, L.; Gyllensten, U.; Johansson, A.; Zaboli, G.; Campbell, H.; Wild, S. H.; Wilson, J. F.; Glaeser, S.; Homuth, G.; Voelzke, H.; Mangino, M.; Soranzo, N.; Spector, T. D.; Polasek, O.; Rudan, I.; Wright, A. F.; Heliovaara, M.; Ripatti, S.; Pouta, A.; Naluai, A. T.; Olin, A.-C.; Toren, K.; Cooper, M. N.; James, A. L.; Palmer, L. J.; Hingorani, A. D.; Wannamethee, S. G.; Whincup, P. H.; Smith, G. D.; Ebrahim, S.; Mckeever, T. M.; Pavord, I. D.; Macleod, A. K.; Morris, A. D.; Porteous, D. J.; Cooper, C.; Dennison, E.; Shaheen, S.; Karrasch, S.; Schnabel, E.; Schulz, H.; Grallert, H.; Bouatia-Naji, N.; Delplanque, J.; Froguel, P.; Blakey, J. D.; Britton, J. R.; Morris, R. W.; Holloway, J. W.; Lawlor, D. A.; Hui, J.; Nyberg, F.; Jarvelin, M.-R.; Jackson, C.; Kahonen, M.; Kaprio, J.; Probst-Hensch, N. M.; Koch, B.; Hayward, C.; Evans, D. M.; Elliott, P.; Strachan, D. P.; Hall, I. P.; Tobin, M. D.; Wellcome Trust Case Control, C.; Team, N. R. S. Genome-Wide Association Study Identifies Five Loci Associated with Lung Function. *Nature Genetics* **2010**, *42* (1), 36-U51.
(26) Wilk, J. B.; Shrine, N. R. G.; Loehr, L. R.; Zhao, J. H.; Manichaikul, A.; Lopez, L. M.; Smith, A. V.; Heckbert, S. R.; Smolonska, J.; Tang, W.; Loth, D. W.; Curjuric, I.; Hui, J.; Cho, M. H.; Latourelle, J. C.; Henry, A. P.; Aldrich, M.; Bakke, P.; Beaty, T. H.; Bentley, A. R.; Borecki, I. B.; Brusselle, G. G.; Burkart, K. M.; Chen, T.-H.; Couper, D.; Crapo, J. D.; Davies, G.; Dupuis, J.; Franceschini, N.; Gulsvik, A.; Hancock, D. B.; Harris, T. B.; Hofman, A.; Imboden, M.; James, A. L.; Khaw, K.-T.; Lahousse, L.; Launer, L. J.; Litonjua, A.; Liu, Y.; Lohman, K. K.; Lomas, D. A.; Lumley, T.; Marciante, K. D.; Mcardle, W. L.; Meibohm, B.; Morrison, A. C.; Musk, A. W.; Myers, R. H.; North, K. E.; Postma, D. S.; Psaty, B. M.; Rich, S. S.; Rivadeneira, F.; Rochat, T.; Rotter, J. I.; Artigas, M. S.; Starr, J. M.; Uitterlinden, A. G.; Wareham, N. J.; Wijmenga, C.; Zanen, P.; Province, M. A.; Silverman, E. K.; Deary, I. J.; Palmer, L. J.; Cassano, P. A.; Gudnason, V.; Barr, R. G.; Loos, R. J. F.; Strachan, D. P.; London, S. J.; Boezen, H. M.; Probst-Hensch, N.; Gharib, S. A.; Hall, I. P.; O'connor, G. T.; Tobin, M. D.; Stricker, B. H. Genome-Wide Association Studies Identify Chrna5/3 and Htr4 in the Development of Airflow Obstruction. *American Journal of Respiratory and Critical Care Medicine* **2012**, *186* (7), 622-632.
(27) Fang, L.; Gao, P.; Bao, H.; Tang, X.; Wang, B.; Feng, Y.; Cong, S.; Juan, J.; Fan, J.; Lu, K.; Wang, N.; Hu, Y.; Wang, L. Chronic Obstructive Pulmonary Disease in China: A Nationwide Prevalence Study. *Lancet Respiratory Medicine* **2018**, *6* (6), 421-430.
(28) Fukahori, S.; Matsuse, H.; Takamura, N.; Hirose, H.; Tsuchida, T.; Kawano, T.; Fukushima, C.; Mizuta, Y.; Kohno, S. Prevalence of Chronic Obstructive Pulmonary Diseases in General Clinics in Terms of Fev1/Fvc. *International Journal of Clinical Practice* **2009**, *63* (2), 269-274.
(29) Mckay, A. J.; Mahesh, P. A.; Fordham, J. Z.; Majeed, A. Prevalence of Copd in India: A Systematic Review. *Primary Care Respiratory Journal* **2012**, *21* (3), 313-321.
(30) Soriano, J. B.; Ancochea, J.; Miravitlles, M.; Garcia-Rio, F.; Duran-Tauleria, E.; Munoz, L.; Jimenez-Ruiz, C. A.; Masa, J. F.; Viejo, J. L.; Villasante, C.; Fernandez-Fau, L.; Sanchez, G.; Sobradillo-Pena, V. Recent Trends in Copd Prevalence in Spain: A Repeated Cross-Sectional Survey 1997-2007.

European Respiratory Journal **2010**, *36* (4), 758-765.
(31) Rayner, L.; Sherlock, J.; Creagh-Brown, B.; Williams, J.; Delusignan, S. The Prevalence of Copd in England: An Ontological Approach to Case Detection in Primary Care. *Respiratory Medicine* **2017**, *132*, 217-225.
(32) Kainu, A.; Timonen, K.; Lindqvist, A.; Piirila, P. Gold Criteria Overestimate Airflow Limitation in One-Third of Cases in the General Finnish Population. *ERJ open research* **2016**, *2* (4).
(33) Caballero, A.; Torres-Duque, C. A.; Jaramillo, C.; Bolivar, F.; Sanabria, F.; Osorio, P.; Orduz, C.; Guevara, D. P.; Maldonado, D. Prevalence of Copd in Five Colombian Cities Situated at Low, Medium, and High Altitude (Prepocol Study). *Chest* **2008**, *133* (2), 343-349.
(34) Jaganath, D.; Miranda, J. J.; Gilman, R. H.; Wise, R. A.; Diette, G. B.; Miele, C. H.; Bernabe-Ortiz, A.; Checkley, W.; Grp, C. C. S. Prevalence of Chronic Obstructive Pulmonary Disease and Variation in Risk Factors across Four Geographically Diverse Resource-Limited Settings in Peru. *Respiratory Research* **2015**, *16*.
(35) Menezes, A. M. B.; Perez-Padilla, R.; Jardim, J. R. B.; Muino, A.; Lopez, M. V.; Valdivia, G.; De Oca, M. M.; Talamo, C.; Hallal, P. C.; Victora, C. G.; Team, P. Chronic Obstructive Pulmonary Disease in Five Latin American Cities (the Platino Study): A Prevalence Study. *Lancet* **2005**, *366* (9500), 1875-1881.
(36) Obaseki, D. O.; Erhabor, G. E.; Gnatiuc, L.; Adewole, O. O.; Buist, S. A.; Burney, P. G. Chronic Airflow Obstruction in a Black African Population: Results of Bold Study, Ile-Ife, Nigeria. *Copd-Journal of Chronic Obstructive Pulmonary Disease* **2016**, *13* (1), 42-49.
(37) Ko, F. W. S.; Wong, G. W. K. Drug Treatment for Early-Stage Copd. *New England Journal of Medicine* **2017**, *377* (10), 988-989.